Doctoral Dissertation

Development of a general strategy for formulation optimization of therapeutic monoclonal antibodies

Shuntaro Saito

July 2013

Department of Biotechnology
Graduate School of Engineering,
Osaka University

Table of contents

ABBREVIATIONS

ADA	anti-drug antibody
AUC-SE	analytical ultracentrifugation sedimentation equilibrium
B_2	second virial coefficient
B_{22}	osmotic second virial coefficient
BC	B-cell
CDR	complementarity determining region
DC	dendritic cell
DI	developability index
DLS	dynamic light scattering
DSC	differential scanning calorimetry
ΔG_{FU}	free energy difference between the folded and unfolded states
EMA	European Medicines Agency
FDA	Food and Drug Administration
k_D	interaction parameter
MAb	monoclonal antibody
PDB	protein databank
SAP	spatial aggregation propensity
SEC	size exclusion chromatography
SIC	self-interaction chromatography
SLS	static light scattering
T_m (T_{max})	apparent unfolding temperature
T_{agg}	apparent aggregation temperature
TC	T-cell

Chapter 1
General introduction

1.1 Therapeutic antibodies

Several different therapeutic monoclonal antibodies (MAbs) have recently entered into the market with many more under clinical trials for treatment of diseases such as cancer, infectious diseases, allergies, autoimmune diseases, cardiovascular diseases, and inflammation (Reichert et al., 2005). Development of therapeutic MAbs, however, remains challenging because of their unique characteristics arising from their large size (approximately 150 kDa) and complex higher-order structures. Aggregation is one of the crucial issues in therapeutic proteins because they potentially impact on protein activity, pharmacokinetics and safety due to immunogenicity. Regulatory agencies such as the Food and Drug Administration (FDA) and European Medicines Agency (EMA) have posed safety and efficacy concerns of aggregates, and have recommended appropriate control of aggregates in the therapeutic proteins (EMA guideline, 2007, FDA guidance, 2013). Aggregates cover a large variety of heterogeneous species composed of folded and/or unfolded monomers ranging in size from dimer in a few nanometers to visible particulates in the hundreds of microns. In addition, there are reversible and irreversible aggregates formed by non-covalent and covalent bonds, respectively. Various stresses (heat, freeze-thawing, and agitation) are known as factors that induce aggregation, although the mechanism of aggregation formation by these stress factors remains elusive. Thereby, aggregation of therapeutic MAbs can be promoted anytime in their life cycle, including the period of manufacturing, storage, transportation, and administration

to patients. High viscosity at a highly concentrated solution is also a crucial issue for therapeutic MAbs because it prevents effective manufacturing and limits the route and mode of administration to patients.

MAbs in the same subclass have similar primary structures composed of variable and constant regions. The constant region occupies more than 75% of their primary structure, in which the amino acid sequences determine the subclass of antibodies and are identical in the antibodies of the same subclass. On the other hand, the variable regions, which occupy less than 25% of the primary structure, are composed of different amino acid sequences and play an essential role in the recognition and binding to antigens. It is known that individual MAbs show different physical properties, i.e. aggregation propensity and viscosity, even though most of their amino acid sequences are identical (Yadav et al., 2010b, Sahin et al., 2010). In addition, various environmental factors such as pH, ionic strength and excipients in the formulation contribute differently to the physical properties of MAb solutions. Optimization of the formulation should be conducted for each MAb, which is essential to produce superior therapeutic MAbs with a longer shelf life, higher manufacturability and ability for more effective administration.

1.2 Immunogenicity risk of aggregates

Immunogenicity of therapeutic proteins is an increasing problem with serious clinical consequences and safety concerns (Rosenberg, 2006). Therapeutic proteins can potentially induce an early innate immune response through cells that defend the host from infection in an immediate and nonspecific manner that is not associated with long term memory. An innate response can lead to a late stage T-cell mediated adaptive response (Matzinger, 2002, 2007), resulting in the breaking

of tolerance and induction of T-cell dependent and B-cell mediated anti-drug antibody (ADA) responses (Fig. 1.1). These innate and adaptive immune responses to therapeutic proteins imply safety risks inducing serious side effects such as anaphylaxis and infusion reactions in patients. In addition, ADAs potentially alter the pharmacokinetic/pharmacodynamic profile of proteins by enhancing the clearance of prolonging systemic exposure. Furthermore, ADAs neutralize the function of therapeutic proteins by disrupting their ability to bind to the target, resulting in lower biological activity (Singh, 2010). In worst-case scenarios, formation of ADAs can be life-threatening as in the cases of pure red cell aplasia (PRCA) after administration of Eprex (synthetic erythropoietin), where Eprex developed ADAs neutralizing the endogenous erythropoietin (Peces et al., 1996). Even in the case of therapeutic MAbs, including fully human MAbs such as adalimumab and panitumumab, the formation of ADAs is commonly observed (Singh, 2010). In the case of adalimumab, ADA response is associated with loss of clinical responses (Bender et al., 2007). Thus, the development of ADA potentially impacts the safety and efficacy of the therapeutic protein.

Many product-related factors are considered to contribute to the immunogenicity of therapeutic proteins, including primary structure and impurities. Aggregation has been, in particular, considered as the most important structural change (Hermeling et al., 2004). Multiple publications have implied potential risk of protein aggregates that induce adverse immunogenic responses as shown in Table 1.1 (Rosenberg, 2006, Sauerborn et al., 2010, Wang et al., 2012). For example, administration of heavily aggregated human interferon α2β induced significant formation of ADAs relative to fresh sample in both wild-type and transgenic mice (Hermeling et al., 2006). A relevant clinical observation was also reported where the administration of aggregates containing recombinant human IL-2 induced the high level of ADA formation (Prummer, 1997). A widely accepted theory for immunogenicity enhancement by protein aggregates is the T-cell independent

activation of B-cells through cross-linking mechanisms owing to presenting the multiple and repetitive epitopes in protein aggregates, which are analogues to bacterial antigens (Vos et al., 2000) (Fig. 1.1). Another obvious mechanism for enhancing immunogenicity of aggregates is aggregation-induced structural changes toward more foreignness. Even in the cases of therapeutic MAbs, a potential linkage between protein aggregation and enhanced immunogenicity has been reported. Wright et al. (1980) reported that oligomers of immunoglobulin activated the complement fixation, which may induce serious adverse effects such as hemolytic anemia. Joubert et al. (2012) reported that aggregated antibodies prepared by various stresses, such as stirring and heating, enhanced the in vitro innate and adaptive T-cell immune responses. Notably, this immune response depended on the aggregate type, inherent immunogenicity of the monomer, and donor responsiveness, and required a high number of particles. Filipe et al. (2012) investigated the immunogenicity response by the administration of differently stressed MAbs (IgGs) to both wild-type and transgenic mice containing human genes. Herein, the stress induced aggregation of MAb led to enhanced immunogenicity, but not all aggregates posed the same immunogenic risk. Under such circumstances, regulatory agencies have recently highlighted the subvisible particulates in the 0.1-10 μm range due to the uncertainty around the potential immunogenicity risk, and have recommended to monitor these particles and to assess their immunogenicity risks during the non-clinical study (Carpenter et al., 2009, Singh et al., 2010). In spite of these recognized risks of aggregates, the assessment of immunogenicity in non-clinical study remains difficult because the appropriate animal model reflecting the immunogenicity in humans does not exist (Singh, 2010). Therefore, the reduction of aggregation has been claimed to reduce the immunogenicity risk of therapeutic MAbs.

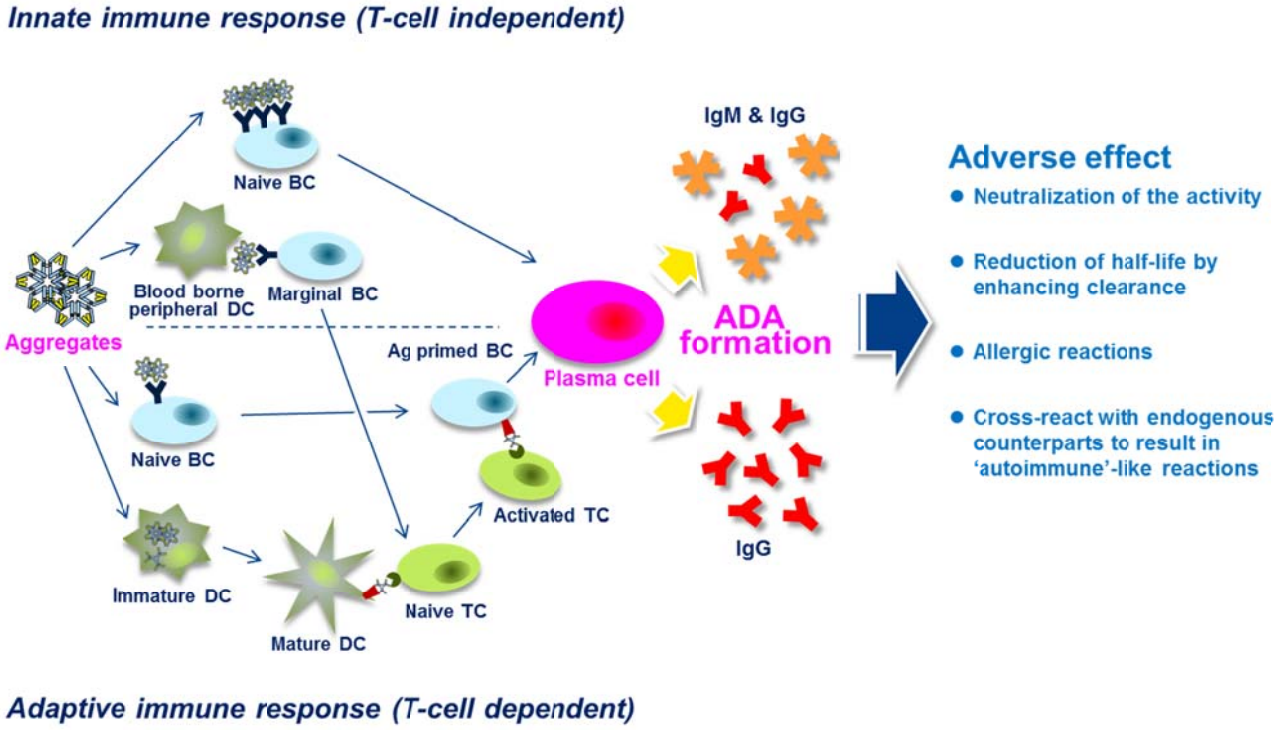

Figure 1.1. Immunogenicity responses by protein aggregates

T-cell (TC)-dependent and independent pathways involved in an immunogenic response resulting in the formation of anti-drug antibodies (ADAs). The TC-dependent pathway involves the uptake of protein (aggregates) by antigen-presenting cells such as immature dendritic cells (DC) and B-cells (BCs). DSs process the protein into peptides and present them to naive TCs to activate and proliferate TCs. BCs also take up the protein aggregates, process and present antigenic peptides to activated TCs. Activated TCs stimulate Antigen (Ag) primed BCs resulting in the generation of antigen specific IgG antibody secreting plasma cells. The TC-independent pathway involves the direct stimulation of BCs by an aggregated form of proteins. Marginal zone BCs can be stimulated by blood borne peripheral DCs. This pathway leads to a generation of plasma cells that predominantly secrete IgM antibodies.

Table 1.1. Examples of protein aggregates linked to enhanced immunogenicity

Protein	Aggregate level and type	Dose and administration	Test model	Reference
Soluble aggregates				
Epoetin α	Low amount of dimers and other aggregates induced by tungsten	25 IU/kg 3 times per week or 75 IU/kg weekly; SC	Anemic patients	Seidl et al., 2011
Human γ-globulin	Variable levels of aggregates by heating at 63◦C for 15 min	5 mg; IV	Rabbits	Biro and Garcia, 1965
Human γ-globulin	Variable levels of aggregates by heating at 63◦C for 30 min	100 μg; IP	A/J mice; IP	Gamble, 1966
Human growth hormone	Variable levels of aggregates	0.1-2U 3 times per week; SC	Children	Moore and Leppert, 1980
Human interferon-α2	50% dimer and very small amount of oligomers	0.3 μg weekly for 5 weeks; IP	Balb/C and transgenic mice	Braun et al., 1997
Human interferon-α2b	Variable levels of oxidized aggregates	10 μg repeated dose; SC	Wild-type and transgenic mice	Hermeling et al., 2006
Human interferon-β1a	~80% oligomeric or large aggregates formed by metal catalysis	5 μg repeated dose; IP	Transgenic mice	van Beers et al., 2011
Human interferon-β1a	Small amount of mainly non-covalent aggregates	5 μg repeated dose; IP	Transgenic mice	van Beers et al., 2010a
IFN-α2b-HSA fusion protein	20% to 42% dimers and aggregates by shaking	100 μg twice per week for 4 weeks; SC	Mice	Zhao et al., 2009
Insoluble aggregates or mixtures				
Bovine γ-globulin	Insoluble aggregates by centrifugation	2 mg adsorbed on Bentonite; IP	CBA mice	Claman, 1963
Murine growth hormone	1.2% subvisible particles (based MFI) vs control	2 μg repeated dose; SC	Mice	Fradkin et al., 2011a
Human growth hormone (product A & B)	5% soluble and 72% insoluble (A) and 31% soluble through F/T	10 μg weekly for 2 weeks; SC	Naive and primed mice	Fradkin et al., 2009
Human interferon-α2b	17% large aggregates and 10% insoluble formed by metal catalysis	10 μg repeated dose; IP	Wild-type & transgenic mice	Hermeling et al., 2005
Human interferon-β1a	More aggregates as monitored by light scattering	0.25 μg (SC) or 0.5 μg (IN); 3 days/week for 4 or 5 weeks	C57BL/6 mice	Rifkin et al., 2011
Protein aggregates as vaccines				
Bacterial needle protein $MxiH^{\Delta 5}$	Multimers, induced with a full length	10 μg on Days 0, 14, 28; IM	Balb/c mice	Barrett et al., 2010
Hemagglutinin	Trimers, induced via trimeric motif	3 μg on Days 0 and 14; SC	Balb/c mice	Weldon et al., 2010
Hepatitis B peptide antigen	Multimers, derivatized with dipalmityl-lysine	200 μg twice with Freund's adjuvant; SC	Rabbits	Hopp, 1984
HIV Tat101 protein derivative	Disulfide bonded dimers	5 μg twice; SC	Balb/c mice	Kittiworakarn et al., 2006
HIV envelope protein GP120	Trimers, induced via a trimeric motif	7-9 μg 3 times with 1X Ribi adjuvant; SC	Balb/c mice	Yang et al., 2001
Horse heart cytochrome c	Aggregates induced by glutaraldehyde	5 mg per animal with Freund's adjuvant; IV	Rabbits	Reichlin et al., 1970
Human muscle creatine kinase	Aggregates induced by glutaraldehyde	150 μg per animal with Freund's adjuvant; IP	Balb/c mice	Man et al., 1989
γ^{KEI} polypeptide	Oligomerized by PEGylation	100 μg with a 50 μg boost at week 4; SC	C57BL/6 mice	Rudra et al., 2010

This table is cited from Wang et al., 2012.

1.3 Colloidal and conformational stabilities

Appropriate control of aggregation is a considerable challenge because of the contributions of multiple aggregation pathways (Chi et al., 2003a, Hawe et al., 2009, Mahler et al., 2009). Knowledge of aggregation mechanisms has accumulated, and models of the aggregation pathways have been proposed, as shown in Fig. 1.2 (Chi et al., 2003a, Chi et al., 2003b, Goldberg et al., 2011, Chou et al., 2012). Two types of stability, colloidal and conformational, are related to the formation of aggregates in these models. Colloidal stability is a measure of molecular dispersity and predominantly affects pathway I (Zhang and Liu, 2003, Saluja et al., 2008), which is determined by the marginal balance of attractive and repulsive intermolecular interactions among protein molecules. The Derjaguin–Landau–Verwey–Overbeek (DLVO) theory states that for a solution with high colloidal stability, the repulsive forces arising from electrostatic interactions among molecules are greater than the attractive forces attributed to van der Waals interactions (Verwey and Overbeck, 1948). A pathway to enhance the viscosity has been also explained in terms of colloidal stability, where enhancement of viscosity is attributed to network formations among monomers by weak attractive interactions, however the presence of this pathway has not been fully evidenced (Guo et al., 2012, Yadav et al., 2012). In contrast, the conformational stability is defined as the free energy difference between the folded and unfolded states (ΔG_{FU}) (Chi et al., 2003a, Garber and Demarest, 2007, Zhang et al., 2012). A higher ΔG_{FU} indicates greater conformational stability, because the population of unfolded states is smaller (Fig. 1.2, pathway II). Unfolded states consist of an ensemble of various structures. For example, hydrophobic residues that are buried in the native structure are exposed, making them prone to aggregate. A protein with higher conformational stability is therefore expected to possess a lower aggregation propensity. In practice, multiple pathways independently, additively, or synergistically contribute to the aggregation.

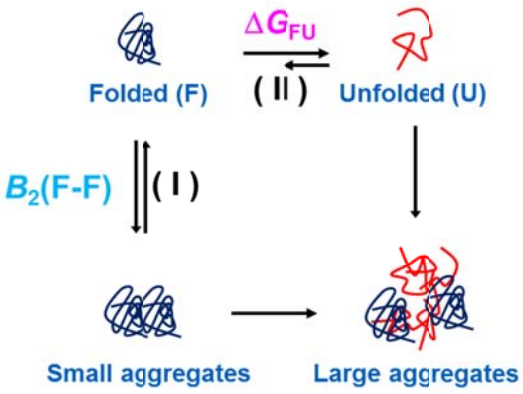

Figure 1.2. A model of protein aggregation

B_2(F-F) is the second virial coefficient for MAbs in the folded state. ΔG_{FU} is the free energy difference between MAbs in the folded and unfolded states.

Colloidal and conformational stabilities have been assessed for optimizing formulations, stabilizing proteins, and determining the mechanisms of aggregation (Neal et al., 1998, Liu et al., 2005, Goldberg et al., 2011, Chou et al., 2012, Saito et al., 2012). In these studies, several parameters were used as indicators of colloidal and conformational stabilities. The osmotic second virial coefficient (B_{22}) is one of the parameters that represents the degree of intermolecular interactions in relatively dilute solutions and can be used to assess colloidal stability (Holde et al., 2006). It is generally understood that a positive B_{22} value implies the presence of repulsive intermolecular interactions, whereas a negative B_{22} value indicates the presence of attractive intermolecular interactions (Neal et al., 1998, Holde et al., 2006). The second virial coefficient, B_2 ($B_2 = B_{22}/M_W^2$), can be determined experimentally using static light scattering (SLS), self-interaction chromatography (SIC), or analytical ultracentrifugation sedimentation equilibrium (AUC-SE). The interaction parameter (k_D), which relates to B_2, can be derived from dynamic light

scattering (DLS). SLS and DLS are used most frequently for the evaluation of B_2 and k_D, respectively (Narayanan et al., 2003, Zhang et al., 2003, Attri and Minton, 2005, Alford et al., 2008). SIC provides values of B_2 comparable to those determined using SLS in a shorter time and with a smaller amount of samples (Tessier et al., 2002, Brun et al. 2010a, Sule et al., 2012). AUC-SE is a conventional but powerful method for the determination of B_2 from the concentration dependence of the apparent molecular weight ($M_{W,app}$) of a protein in solution (Fujita, 1962, Liu et al., 2005, Jiménez et al., 2007). This method is applicable to samples over a wide range of concentrations and of various solvent compositions (Liu J et al., 2005, Jiménez et al., 2007). Winzor et al. (2007) reported that B_2 values evaluated from AUC-SE data represent specificintermolecular interactions, whereas light scattering techniques such as DLS and SLS provide an indication of both solute-solute interactions and solute-solvent interactions.

The conformational stability of a protein is evaluated using several approaches, including differential scanning calorimetry (DSC), DLS, circular dichroism spectroscopy (Vermeer et al., 2000, Harn et al., 2007), and differential scanning fluorimetry. The apparent unfolding temperature (T_m), the temperature at which unfolding begins (T_{onset}), or aggregation temperature (T_{agg}), partly reflects ΔG_{FU} at temperatures not far from the unfolding temperature. DSC, in particular, enables direct thermodynamic assessment of the conformational stability per domain based on the endothermic reaction accompanying unfolding. DLS enables the monitoring of the increase of the hydrodynamic radius with an elevating temperature and provides the T_{agg} representing the temperature at which aggregation begins. Generally, indicators of colloidal and conformational stabilities such as B_2 or T_m, T_{onset} and/or T_{agg} provide good correlation with aggregation propensities and/or viscosity, although exceptions have been frequently observed (Goldberg et al., 2011, Saito et al., 2012).

1.4 Objectives of the present study

The relationship between colloidal or conformational stabilities, and long-term storage stability or viscosity remains uncertain. Nevertheless, in practice, the assessment of long-term storage stability and direct viscosity measurement, which are time consuming and requires a large amount of samples, have been conducted taken for evaluating aggregation propensity and viscosity. In this context, further understanding of the relationship between colloidal or conformational stabilities, and aggregation propensity or viscosity are urgently needed to develop alternative techniques for long-term storage stability and direct viscosity measurement. The goal of this study is to understand the mechanisms of aggregation and viscosity enhancement in MAbs and to develop a general strategy for optimizing MAb formulations without the direct assessment of long-term stability and viscosity. Throughout the present studies, we focused on B_2 obtained from AUC-SE as a technique to determine the type and degree of colloidal stability.

This thesis is composed of five chapters. In Chapter 1, the objectives and background of this thesis are mentioned in the general introduction.

In Chapter 2, the relationships between B_2 obtained at low concentration, and the viscosity and aggregation propensity of highly concentrated MAbs solutions were investigated. Herein, we evaluated B_2 obtained from our optimized AUC-SE method as an indicator of aggregation propensity and viscosity. The pH dependencies of B_2 were qualitatively correlated with the aggregation propensity and viscosity of the three MAbs, indicating that increases in aggregation and viscosity can be attributed to a reduction in colloidal stability, and that B_2 can be used as an effective indicator of the viscosity and aggregation propensity of highly concentrated MAb solutions. However, the correlation became insignificant in particular between different MAbs when the B_2 values were negative.

In Chapter 3, we further evaluated the B_2 from AUC-SE for the general purpose of investigating the influence of pH, salt and sugars, which are representative formulation parameters for therapeutic MAb, on aggregation propensity under different stresses. In addition, we investigated the contribution of conformational stability to aggregation. We found that assessment of colloidal stability at the lowest ionic strength is particularly effective for the optimization of formulations. If necessary, salts were added to enhance the colloidal stability. Sugars further improved aggregation propensities by enhancing conformational stability. These behaviors are rationally predictable according to the surface potentials of MAbs. On the basis of these findings, we presented the aggregation and viscosity enhancement model.

In Chapter 4, we presented a strategy for optimizing MAb formulation in terms of colloidal and conformational stabilities and confirmed that our strategy enables optimization of the formulation with smaller sample requirements and a shorter assessment time compared to the conventional strategy on the basis of direct assessments of stability and viscosity, and *in-silico* strategy using the IgG_1 structural model.

In Chapter 5, we summarized our studies in the general conclusion.

Chapter 2

Predictions of aggregation propensity and viscosity at high concentrations based on the second virial coefficient (B_2) at low concentrations

2.1 Introduction

Antibody treatment generally involves administration of high doses of antibodies. Therefore, intravenous (IV) administration is often the first choice for an administration route. IV administration, however, requires a significant amount of time, and sufficient care needs to be provided by skilled healthcare professionals. Therefore, patients must receive treatments at clinics specializing in antibody treatment. More convenient administration routes such as subcutaneous (SC) and intramuscular (IM) routes are favorable because they would reduce the burden on patients. In both routes, the maximum injection volume should be below approximately 1.5 mL per dose in a single injection. To achieve a therapeutic effect, an antibody solution with a concentration as high as 100 mg/mL needs to be administered.

Development of high-concentration MAb solutions is challenging because unfavorable phenomena such as increased viscosity and aggregates formation are frequently induced by increases in the concentration of MAb solutions (Treuheit et al., 2002, Shire et al., 2004). These properties pose challenges in effective manufacturing, formulation development, analytical characterization, and administration of therapeutic MAbs. Although direct measurements of the viscosity and aggregation propensity using high-concentration solutions provide useful information, the preparation of such solutions itself remains challenging, even on a small scale. In addition, it is technically difficult to measure the very weak intermolecular interactions (K_d ~mM) that become

dominant at concentrations above 100 mg/mL (Liu J et al., 2005, Jiménez et al., 2007). Furthermore, even in cases where successful measurements have been made, interpretation of the data is extremely difficult since no concrete theory regarding the intermolecular interactions at high concentrations has yet been established. For example, the contribution of the repulsive interactions due to the excluded volume effects becomes more significant (Minton, 2001, Minton, 2005) and the shorter interactive intermolecular distances change the short-range intermolecular interactions as the concentration increases. This causes the intermolecular interaction profile to become more complicated (Harn et al., 2007, Kamerzell et al., 2009). In practice, an analytical technique for estimating potential risks involved in developing high-concentration antibody solutions is strongly required.

Reversible self-association of MAbs is thought to induce high viscosity (Liu J et al., 2005, Kanai et al., 2008, Yadav et al., 2010a) and aggregation at high concentrations (Zhang et al., 2003, Saluja et al., 2007a, Alford et al., 2008). The mechanism of self-association at the molecular level is complicated. Different types of intermolecular forces are involved in reversible intermolecular interactions, such as electrostatic interactions, van der Waals forces, and hydrophobic interactions (Chari et al., 2009). Environmental factors such as pH, ionic strength, and additives can alter the intermolecular interaction profile drastically (Chi et al., 2003a, Alford et al., 2008a, Gokarn et al., 2009, Mahler et al., 2009). In our recent study, we reported that ionic strength has a significant effect on the reversible self-association of an MAb, leading to liquid-liquid phase separation and an increase in viscosity at low ionic conditions (Nishi et al., 2010). These studies indicate that the selected formulation is critical for reducing viscosity (Liu J et al., 2005, Salinas et al., 2010). As for the relationship between self-association and aggregation, Wu et al. (2010a) reported that hydrophobic patches on the surface of MAb molecules cause low solubility and induce aggregation due to self-association. Primary and higher-order structures of MAbs are also important factors,

and different types of self-association have been reported such as Fab-Fab and Fc-Fc interactions (Nezlin, 2010). Kanai et al. (2008) reported that self-association between Fab fragments is responsible for high viscosity at high concentrations where electrostatic interactions are a major driving force for self-association. However, this is not always true for all MAbs. The types and strength of interactions are highly dependent on the amino acid sequence of the MAbs.

In this chapter, we first carried out AUC-SE of three MAbs at nine different concentrations to determine a concentration range suitable for the estimation of B_2. Then, B_2 was determined in solutions of varying pH for three different MAbs. We also measured the viscosity and aggregation propensity of MAb solutions at high concentrations. All MAbs showed a marked B_2 trend as a function of pH, and this is in good qualitative agreement with both the viscosity and the aggregation propensity. Our study demonstrates that B_2 values derived from AUC-SE using MAb solutions below 10 mg/mL as the initial loading concentration can be a reliable, qualitative indicator of MAb behaviors at high concentrations.

2.2 Materials and methods

2.2.1 Materials

The humanized monoclonal antibody A (IgG_1 subclass, MAb-A), B (IgG_1 subclass, MAb-B), and C (IgG_1 subclass, MAb-C) were produced and highly purified at Daiichi Sankyo Co., Ltd., Tokyo, Japan. All MAbs are humanized IgG_1, but recognize different antigens. The theoretical isoelectric points (pIs) of MAb-A, MAb-B, and MAb-C are 6.7, 8.9, and 8.8, respectively. The selected three MAbs cover pI ranges of general therapeutic MAbs on the market, which ranges from 6 to 9 (Fig. 2.1). The molecular weights (M_Ws) of MAb-A, MAb-B, and MAb-C calculated

from amino acid sequences with two oligosaccharide chains ($M_{W,cal}$) are 150, 147, and 148 kDa, respectively. All MAbs were stocked at -80°C in 10 mM sodium citrate buffer and 140 mM sodium chloride (pH 6). MAbs were dialyzed against the desired buffers (pH 5, 6, 7, and 8) before use, and the concentrations were determined based on the absorbance at 280 nm. MAbs were diluted to adjust the desired concentration prior to each experiment. Sodium chloride was purchased from Wako Pure Chemical Industries, Ltd. (Osaka, Japan), and sodium phosphate and sodium acetate were purchased from Kanto Chemical Co. (Tokyo, Japan). Four buffers of different pH were prepared. The composition at pH 5 was 10 mM sodium acetate buffer containing 140 mM NaCl, and those at pH 6, 7, and 8 were 10 mM sodium phosphate buffer containing 140 mM NaCl.

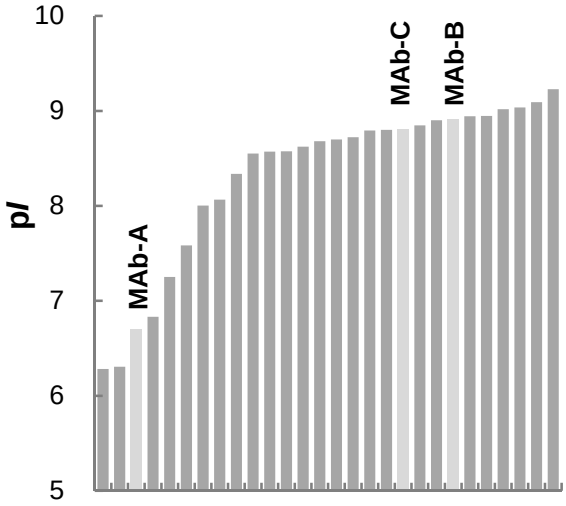

Figure 2.1. Theoretical pIs of therapeutic MAbs

The theoretical pIs were calculated based on the amino acid sequences for 25 therapeutic MAbs on the market, MAb-A, MAb-B and MAb-C.

2.2.2 Analytical ultracentrifugation sedimentation equilibrium (AUC-SE) studies

Sedimentation equilibrium was carried out using XL-I (Beckman Coulter, Inc. Brea, CA). A volume of 100 μL of each solution was applied into the sample sectors of 6 holes, a charcoal-filled epon centerpiece (1.2 cm) with sapphire windows, and 100 μL of reference solutions were applied into the reference sectors. The runs were carried out at 11,000 rpm at 20°C by using the An-60Ti rotor. The concentration gradient was acquired by Rayleigh interference (IF) optics. The concentration gradients were acquired at 2-hour intervals, and were judged to be at equilibrium when the 3 successive gradients were completely superimposed. $M_{W,app}$ was estimated by nonlinear least-squares fitting of data according to Eq. 2.1 using the OriginLab software, ver 4.1 or 6.04 (OriginLab Co., Northampton, MA):

$$c(r) = c_0 \exp\left[\frac{M_{W,app}(1-\bar{\nu}\rho)\omega^2}{2RT}(r^2 - r_o^2)\right] + \text{Baseline} \qquad (2.1)$$

,where $c(r)$ (mg/mL) is the protein concentration at the radial position r (cm), c_0 is the protein concentration at the reference radial position r_0, $\bar{\nu}$ (cm^3/g) is the partial specific volume of solute defined as the change in volume of a solution by the addition of the solute divided by the mass of the solute, ρ (g/cm^3) is the solvent density, ω (rad/s) is the angular velocity, T (K) is the absolute temperature, and R is the gas constant. The partial specific volume and solvent density were calculated using the Sednterp software (Laue et al., 1992). The partial specific volumes of MAb-A, MAb-B, and MAb-C, according to their amino acid compositions, were 0.7261, 0.7272, and 0.7275 cm^3/g, respectively.

B_2 was obtained from the slope of the plot of the inverse of $M_{W,app}$ against the concentration, according to Eq. 2.2:

$$\frac{1}{M_{W,app}} = \frac{1}{M_W} + 2B_2c \quad (2.2)$$

$$B_{22} = B_2 \times M_W{}^2 \quad (2.3)$$

,where M_W is the weight-average molecular weight at infinite dilution and c is the initial loading concentration (mg/mL). B_{22} was obtained using Eq. 2.3 (Winzor et al., 2007).

2.2.3 Estimation of concentration dependence of diffusion coefficient by dynamic light scattering (DLS)

A 20 μL volume of 1.0, 2.0, 4.0, 6.0, 8.0, and 10 mg/mL sample solutions (after filtration with a 0.22-μm filter) were applied to 384-well optically clear-bottom microtiter plates. From the following centrifugation at ×50 *g* for 3 min to remove bubbles, the diffusion coefficient was measured from time dependent fluctuation of scattered light using a DynaPro Plate Reader (Wyatt Technology Co., Santa Barbara, CA) at 20°C. The interaction parameter (k_D) was calculated using Eq. 2.4, where D_m is the measured diffusion coefficient, D_S, is the diffusion coefficient at infinite dilution, and c is the concentration of MAb (mg/mL) (Narayanan et al., 2003, Zhang et al., 2003).

$$D_m = D_S(1 + k_D c) \quad (2.4)$$

k_D represents the thermodynamic term of B_2 and the hydrodynamic term of ($\xi_1 + \bar{\nu}$) as shown in the following equation:

$$k_D = 2B_2M_W - (\xi_1 + \bar{\nu}) \quad (2.5)$$

,where ξ_1 is the coefficient of the linear term in the virial expansion of the frictional coefficient as a function of solute concentration (Chari et al., 2009).

2.2.4 Viscosity measurement

Concentrated samples for viscosity measurement were prepared followed by the buffer exchange using a Vivapore-2 concentrator device (Sartorius AG, Goettingen, Germany). Following centrifugal filtration (filter size: 0.45 μm), samples were adjusted to a concentration of 150 mg/mL. The concentrations of the sample were determined by size exclusion chromatography (SEC) using reference solutions for the respective MAbs; the concentrations of these solutions were calculated based on the absorbance at 280 nm. SEC analysis was conducted with a TSK gel G3000SW_{XL} (TOSOH Co., Tokyo, Japan) column using the mobile phase of 30 mM sodium phosphate buffer and 300 mM NaCl (pH 6.7) at a flow rate of 1.0 mL/min and a column temperature of 20°C. The sample solution was diluted to approximately 1.0 mg/mL, and 50 μL of each solution was injected for analysis. The peak area was monitored at 280 nm using a UV detector. Viscosity was measured by VROC (RheoSense, Inc., San Ramon, CA) at the controlled temperature of 20°C (Nishi et al., 2010).

2.2.5 Stability study

Volumes of 100 μL of 100 mg/mL MAb solutions were applied in triplicate to a 96-well polypropylene polymerase chain reaction (PCR) plate with cap. Plates were stored at 40°C for 2 or 4 weeks. Each sample was diluted to 1.0 mg/mL, and their aggregation profiles were analyzed by SEC, DLS, and turbidity analyses. It was confirmed that there was no change in concentration during storage.

2.2.6 Size exclusion chromatography (SEC)

Diluted samples of 1.0 mg/mL were filtered using 96-well filtration plates (0.45 μm). The SEC analysis was carried out with a TSK gel G3000SW$_{XL}$ (Tosoh Co.) column, using 30 mM phosphate buffer and 300 mM NaCl (pH 6.7) as the mobile phase at a flow rate of 1.0 mL/min and a column temperature of 25°C. A 50 μL volume of each solution was injected into the column. The elution was monitored at 280 nm by a UV detector. The percentage of aggregates, determined from the sum of peaks eluted in front of the monomer peak, was estimated by dividing the aggregate peak area by the total peak area. The rate of increase in the aggregates, the aggregation rate (% per month), was estimated from least-squares fitting of the time dependence of the percentage of aggregates.

2.2.7 DLS

Volumes of 20 μL of samples were applied to 384-well optical clear-bottom microtiter plates. Following centrifugation at ×50 *g* for 3 min to remove the large particulates and bubbles, the average hydrodynamic diameter was measured at 20°C using a DynaPro Plate Reader (Wyatt Technology Co.). Herein, hydrodynamic diameter was calculated from the diffusion coefficient on the assumption that the solute molecule is spherical in shape.

2.2.8 Turbidity measurement

Volumes of 200 μL of samples were applied to 96-well optical clear-bottom microtiter plates. The turbidity was monitored at 350 nm by a SpectraMax M2 plate reader (Molecular

Devices, Sunnyvale, CA). The optical path length d was determined experimentally based on the published method (McGown and Hafeman, 1998). The turbidity of the solution was calculated according to the following equation:

$$\text{Turbidity(AU/cm)} = \frac{A_{350}}{d} \quad (2.6)$$

,where A_{350} is the absorbance at 350 nm.

2.2.9 Thermal stability assessment by DLS

Samples were diluted with buffers to a concentration of 1.0 mg/mL. Volumes of 20 μL of sample solutions after filtration (0.22 μm) were applied to 384-well optical clear-bottom microtiter plates. Following centrifugation at ×50 *g* for 3 min to remove bubbles, samples were covered with 10 μL of mineral oil to prevent evaporation. Thermal stability assessments were performed using a DynaPro Plate Reader (Wyatt Technology Co.). The average hydrodynamic diameter (d_H) was acquired by Dynamics Ver. 7.0.2 (Wyatt Technology Co.) The plate temperature was increased from 50°C to 75°C at a temperature increment of 1°C. The plate temperature was monitored during the assay. The d_H at each temperature was measured after the plate temperature became stable at the set temperatures. Consequently, the average heating rate was approximately 0.032°C/min ± 0.005°C/min. T_{agg} was defined as the temperature where the average d_H drastically jumps from the value of the MAb monomer (approximately 10 nm) to over 200 nm, which corresponds to a large aggregate.

2.3 Results

2.3.1 B_2 measurement by AUC-SE

Fig. 2.2 shows the concentration dependence of $1/M_{W,app}$, from which B_2 could be estimated for all MAbs. As described in Section 2.2.2, a positive B_2 value is obtained from an increase in $1/M_{W,app}$ with an increase in concentration. This indicates the presence of repulsive intermolecular interactions. Negative B_2 values obtained from concentration-dependent decrease in $1/M_{W,app}$ indicate the presence of attractive intermolecular interactions (Neal et al., 1998, Holde et al., 2006). Three MAbs showed significant differences in the concentration dependencies of $1/M_{W,app}$. The $1/M_{W,app}$ of MAb-A decreased as the concentration increased, indicating the presence of attractive intermolecular interactions. On the other hand, $1/M_{W,app}$ of MAb-C increased as the concentration increased, indicating the presence of repulsive intermolecular interactions. The concentration dependencies of $1/M_{W,app}$ were successfully fitted using a linear model for MAb-A and MAb-C with the correlation coefficients (R) of $R > 0.95$ in the tested concentration range from 1 to 12 mg/mL. The concentration dependence of $1/M_{W,app}$ of MAb-B was different from that of MAb-A and MAb-C; $1/M_{W,app}$ of MAb-B was observed to increase in the concentration range of 1 to 3 mg/mL and decrease in the higher concentration range of 4 to 12 mg/mL. Obviously, a linear model could not be applied to MAb-B over the entire concentration range examined. Thus, the concentration range was divided into 2 ranges, and linear regressions were calculated for each concentration range. The lower range was defined as 0 to 3 mg/mL, at which the fitting was successful as confirmed by $R = 1.00$. The higher range was defined as 4 to 12 mg/mL. The linear fitting using the data at a higher concentration range provided a slope that is clearly different from the slope obtained for the lower range. Thus, two B_2 values were obtained from the different

concentration ranges. The M_W values of MAb-A, MAb-B, and MAb-C at infinite dilution obtained by AUC-SE according to Eq. 2.2 were 150, 147, and 147 kDa, respectively. As for MAb-B, the B_2 value obtained for the lower concentration range was employed because B_2 is estimated from the lower concentration range by definition. All M_W values were in good accordance with the $M_{W,cal}$ values (150, 147, and 148 kDa). These results indicate that concentration dependencies of $1/M_{W,app}$ for all MAbs are represented as linear models and that reliable B_2 values can be obtained for the concentrations examined.

Thus, in our study in this chapter, subsequent AUC-SE measurements of MAb-A and MAb-C were carried out at 1, 5, and 10 mg/mL, from which $1/M_{W,app}$ values for B_2 were estimated. AUC-SE measurements of MAb-B were performed at 1, 2, 3, 5, 7.5, and 10 mg/mL. B_2 values of MAb-B were estimated from the concentration dependence of $1/M_{W,app}$ values at 1, 2, and 3 mg/mL, and/or the concentration dependence of $1/M_{W,app}$ values at 5, 7.5, and 10 mg/mL in order to investigate the influence of the concentration for B_2 estimation.

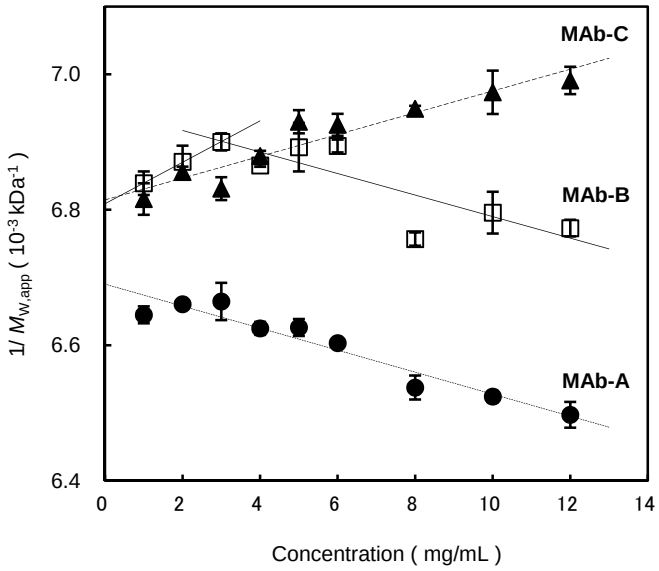

Figure 2.2. Concentration dependence of $1/M_{W,app}$ obtained from AUC-SE

The results of MAb-A (●), MAb-B(□), and MAb-C (▲) in 10 mM citrate buffer containing 140 mM NaCl (pH6) are shown. Regression lines are generated from the least-squares fitting of the concentration dependence of $1/M_{W,app}$. The data obtained over the entire concentration range of 1 to 12 mg/mL are used for MAb-A and MAb-C. Those with lower concentrations of 1 to 3 mg/mL or higher concentrations of 4 to 12 mg/mL are used for MAb-B. The error bars were estimated from 3 independent experiments under the same conditions. The intercepts of the regression line is $1/M_W$ according to Eq. 2.2, and the values of MAb-A, MAb-B, and MAb -C were 6.69, 6.81, and 6.81 × 10^{-6} kDa^{-1}, respectively, corresponding to M_W values of 150, 147, and 147 kDa, respectively.

2.3.2 pH dependence of B_2

B_2 and k_D have been investigated as a function of solution pH because pH is recognized as an important parameter influencing intermolecular interactions by changing the electrostatic environment of proteins. In fact, B_2 and k_D are known to vary according to pH (Saluja et al., 2007a, Sahin et al., 2010, Yadav et al., 2010a). In this chapter, we investigated the effect of pH on the

intermolecular interactions of MAbs. Ionic strength also slightly varies according to pH, however its influence to intermolecular interaction can be negligible in the presence of 140 mM NaCl. B_2 determined by AUC-SE at different pH values is shown in Fig. 2.3. All three MAbs clearly show remarkable pH dependencies of B_2 values with only small standard deviations estimated from three repeated experiments. B_2 values of MAb-A increased with an increase in pH; being negative at pH 5 and 6 and positive at pH 7 and 8. These results indicate that attractive intermolecular interactions dominate at pH 5 and 6 while repulsive intermolecular interactions dominate at pH 7 and 8. In contrast, B_2 values of MAb-C decreased as the pH increased. As for MAb-B, the B_2 values were estimated from two concentration ranges. Obviously, the pH dependencies of both B_2 values were qualitatively comparable: both B_2 values were observed to decrease with an increase in pH. On the other hand, the absolute magnitudes of B_2 values from the two different concentration ranges were different from each other at all pH values examined. This indicates that the magnitude of the intermolecular interactions depends upon the concentration. These results indicate that attractive intermolecular interactions of MAb-B and MAb-C become dominant at high pH.

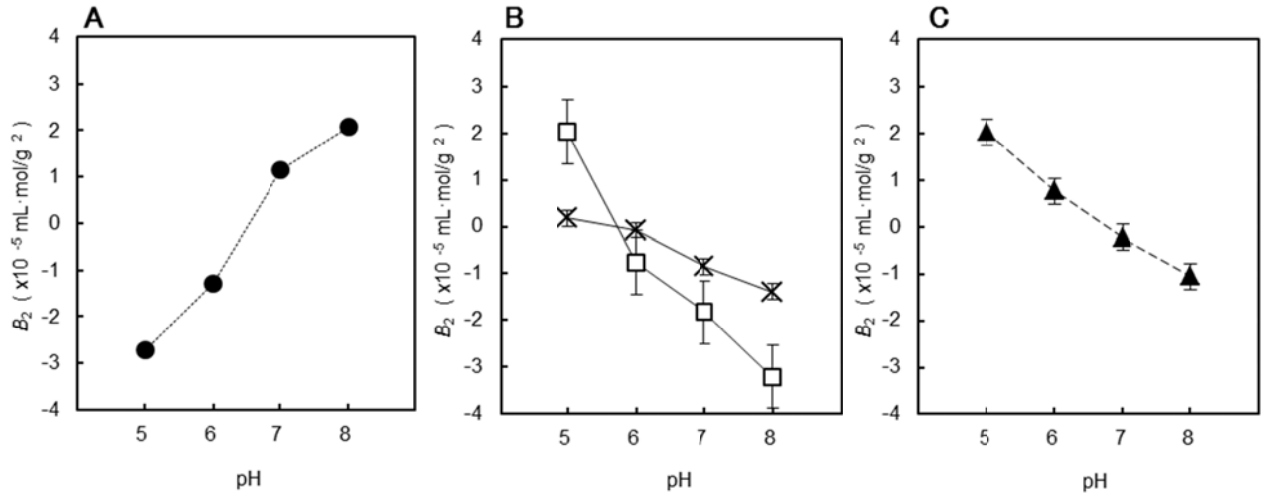

Figure 2.3. pH dependence of B_2

The second virial coefficient (B_2) for MAb-A (**A**), MAb-B (**B**), and MAb-C (**C**) were obtained from the concentration dependence of $M_{W,app}$ at 3 different concentrations in 10 mM sodium acetate buffer containing 140 mM NaCl (pH 5) or 10 mM phosphate buffer containing 140 mM NaCl (pH 6, 7, and 8). B_2 of MAb-A and MAb-C were obtained from concentration range at 1, 5, and 10 mg/mL. B_2 of MAb-B were obtained from the 2 concentration ranges at 1, 2, and 3 mg/mL (×) and 5, 7.5, and 10 mg/mL (□).

2.3.3 k_D measurement by DLS

DLS is widely used to estimate intermolecular interactions. It has the advantages of high throughput and operability. DLS has been employed to investigate k_D based on the concentration dependence of the diffusion constant using Eq. 2.4. k_D is regarded as a factor that reflects the extent of intermolecular interactions (Narayanan et al., 2003, Zhang et al., 2003).

The results indicate that all MAbs show decreases in D_m with increasing concentrations under all pH conditions, indicating negative k_D values. As shown in Fig. 2.4, MAb-A has a more

negative k_D value as the pH decreases. In contrast, k_D values of MAb-B and MAb-C become gradually less negative as the pH decreases, except for the k_D of MAb-C at pH 8. Consequently, the k_D value of MAb-C was minimal at pH 7.

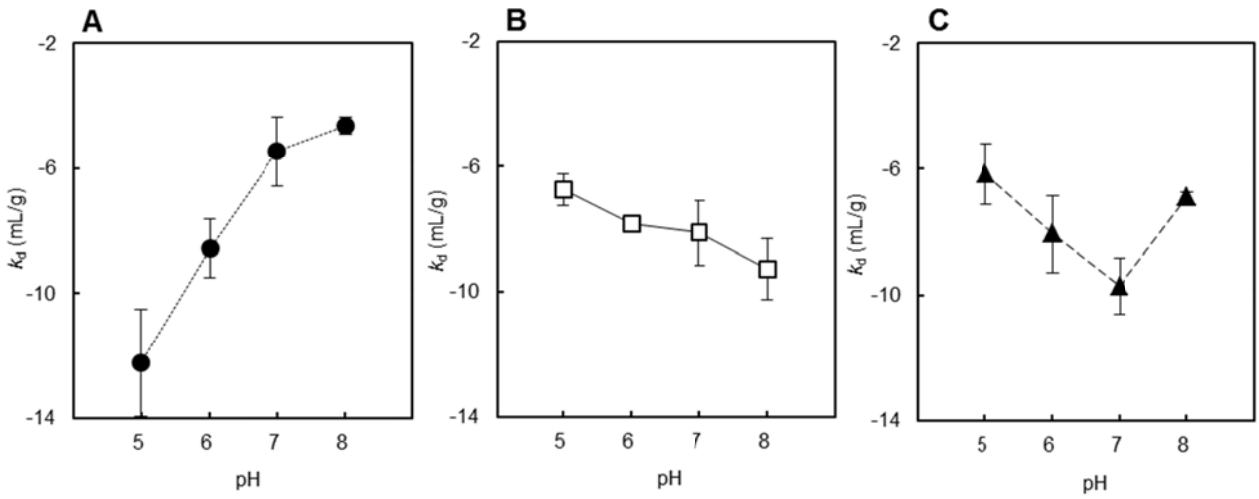

Figure 2.4. pH dependence of k_D based on DLS

The k_D values were obtained from 6 different concentrations—1.0, 2.0, 4.0, 6.0, 8.0, and 10.0 mg/mL for 3 MAbs. MAb-A (**A**), MAb-B (**B**), and MAb-C (**C**) were formulated in 10 mM sodium acetate buffer containing 140 mM NaCl (pH 5) and 10 mM phosphate buffer containing 140 mM NaCl (pH 6, 7, and 8). The error bars were estimated from 3 independent experiments performed under the same conditions.

2.3.4 Thermal stability assessment by DLS

Aggregation induced by thermal unfolding can be monitored by measuring the average d_H value with elevated temperatures. The diameter of an MAb monomer is approximately 10 nm while above the T_{agg}, the observed diameter is greater than several hundred nm, indicating the formation

of large aggregates. Figs. 2.5A–C illustrate the average d_H with elevated temperatures for three MAbs with different pH values. The T_{agg} of MAb-A is clearly dependent on pH (Fig. 2.5D). The lowest thermal stability was confirmed at pH 5 and was found to be enhanced according to the following trend: pH 5 < pH 6 < pH 7 = pH 8. Herein, MAb-A showed unique behavior at pH 7 and 8, where d_H was observed to first increase to approximately 100 nm with a subsequent jump to more than 200 nm at higher temperature. The higher temperature was defined as T_{agg} of MAb-A. No significant difference among T_{agg} values was confirmed in either MAb-B or MAb-C for all pH values investigated.

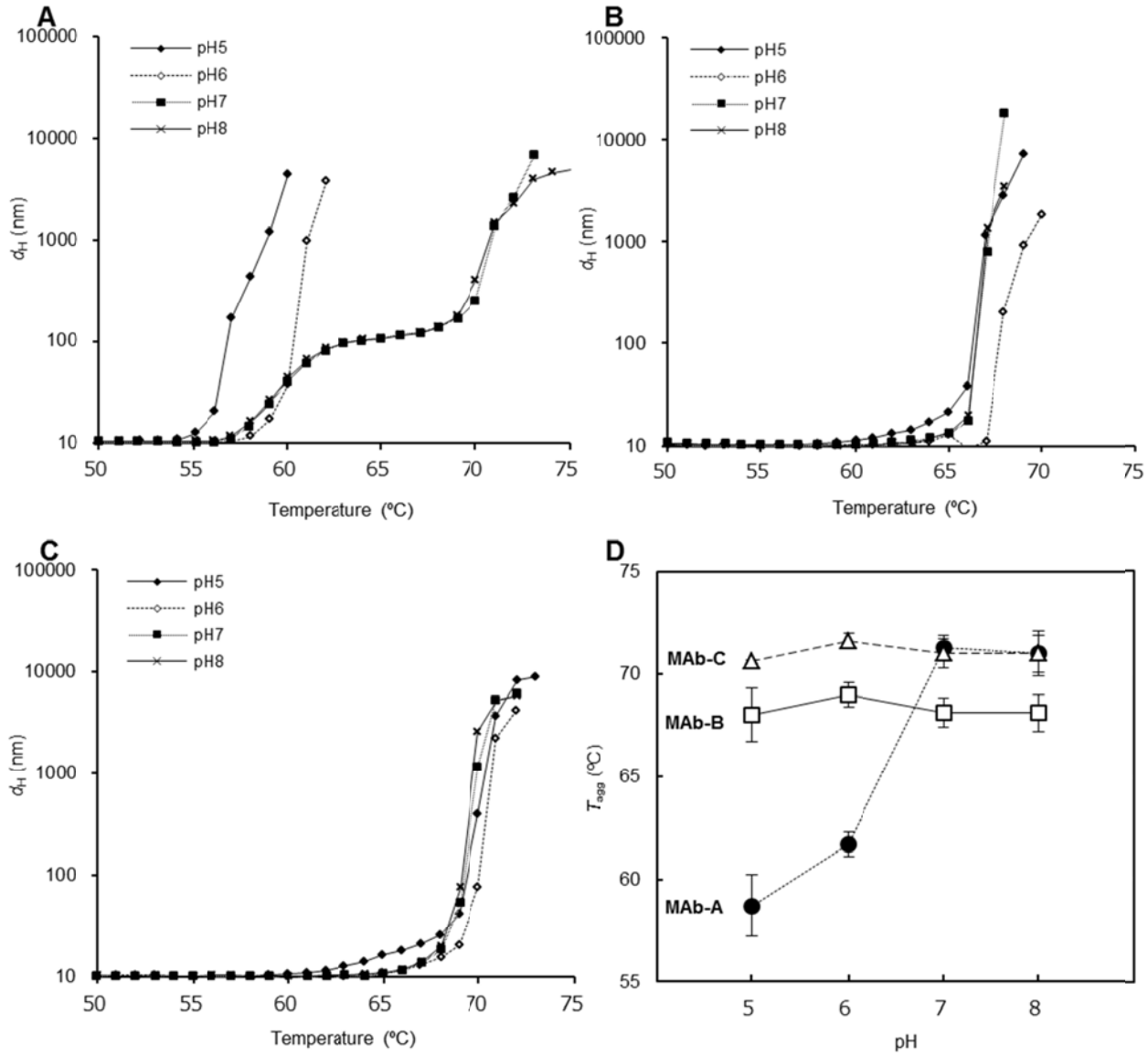

Figure 2.5. pH dependence of thermal stability based on DLS

The hydrodynamic diameters d_H were obtained by elevating the temperature from 50°C to 75°C. MAb-A (**A**), MAb-B (**B**), and MAb-C (**C**) were formulated in 10 mM sodium acetate buffer containing 140 mM NaCl (pH 5) and 10 mM phosphate buffer of 140 mM NaCl (pH 6, 7, and 8). T_{agg} values are plotted as a function of pH for MAb-A (●), MAb-B(□), and MAb-C (Δ) (**D**). The error bars were estimated from 3 independent experiments performed under the same conditions.

2.3.5 Viscosity of monoclonal antibody (MAb) solutions at high concentrations

The viscosities of the three MAbs at a concentration of 150 mg/mL were measured at different pH values. Fig. 2.6 indicates that the viscosities of all MAb solutions are clearly dependent upon the pH of the solution. The viscosity of the MAb-A solution is higher at low pH (pH 5 and 6). In contrast, the pH dependencies of MAb-B and MAb-C are different from that of MAb-A, where viscosity is markedly increased at high pH. In all cases, the quantities of aggregates were unchanged when observed by SEC (data not shown), indicating that the differences in viscosity cannot be attributed to differences in the aggregate content.

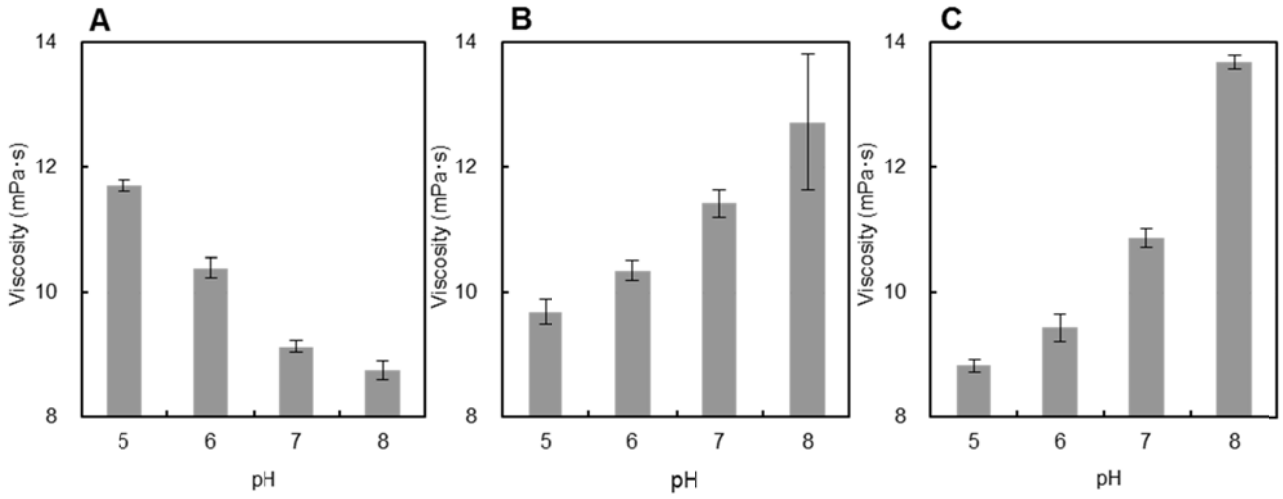

Figure 2.6. pH dependencies of viscosity

Viscosities were measured using MAb solutions with a concentration of 150 mg/mL. MAb-A (**A**), MAb-B (**B**), and MAb-C (**C**) were formulated in 10 mM sodium acetate buffer containing 140 mM NaCl (pH 5) and 10 mM phosphate buffer containing 140 mM NaCl (pH 6, 7, and 8). The error bars were estimated from three independent experiments performed under the same conditions.

2.3.6 Aggregation propensities of highly concentrated MAbs during storage

Stability assessment under accelerated conditions (40°C) was carried out for highly concentrated solutions (100 mg/mL) of all three MAbs. In this study, changes in the aggregate profile during storage were evaluated by SEC, DLS, and turbidity in order to monitor the wide ranges of aggregates in terms of size (Engelsman et al., 2011). SEC is widely used for the evaluation of small soluble aggregates that pass through the SEC column (invisible aggregates of sizes less than 0.1 μm). DLS is suitable for the detection of sub-micron (subvisible aggregates of sizes between 0.1 to 1 μm: subvisible) particles, and turbidity measurements can detect insoluble aggregates (visible aggregates of sizes greater than 1 μm).

Fig. 2.7 illustrates the amounts of soluble aggregates obtained and the rates of aggregation increases per month as estimated from SEC measurements. The increase in amounts of small soluble aggregates was observed for all MAbs at 40°C. MAb-A clearly shows pH dependence where the aggregation rate accelerates as the pH decreases. In contrast, the pH dependencies of the aggregation rates for MAb-B and MAb-C accelerate as the pH increases.

The results of turbidity measurements are summarized in Table 2.1. The absorbance increase due to particulate formation was not observed for all MAbs. The formation of submicron-sized particles represented by d_H on DLS is also shown in Table 2.1. No significant change in d_H was observed during storage. These results indicate that neither submicron particulates nor insoluble aggregates are formed under any pH conditions.

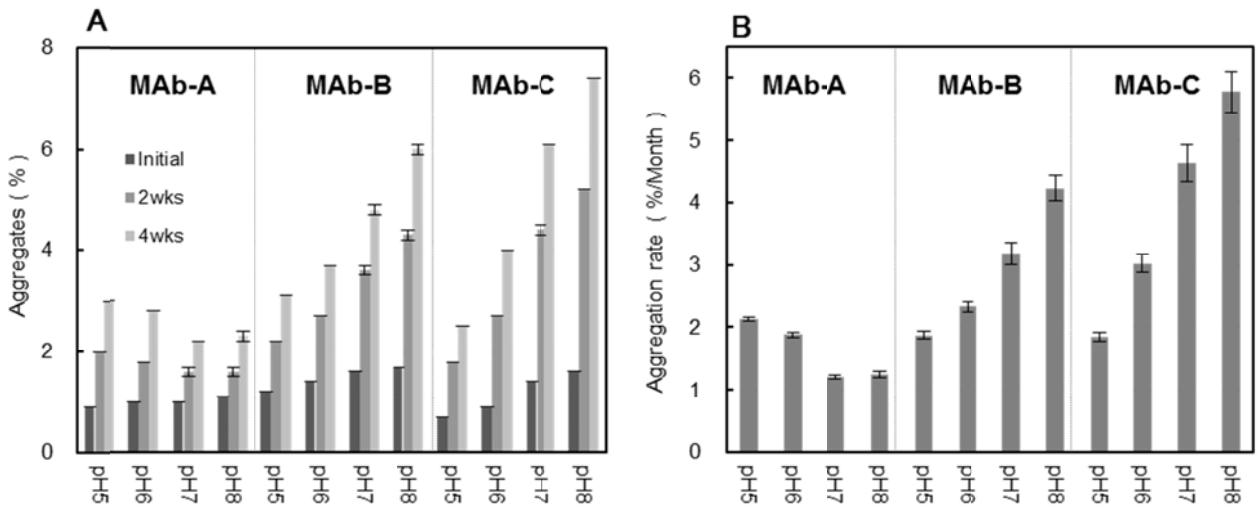

Figure 2.7. Quantification of aggregates by SEC

MAbs were stored at 40°C at 4 different pHs. (**A**) Aggregates (%) were measured after 0, 2, and 4 weeks of storage. (**B**) The increases in the rate of aggregation were estimated from the increase in the population of aggregates (%) per month. The error bars were estimated from 3 independent experiments performed under the same conditions.

Table 2.1. Stability assessments based on turbidity and the hydrodynamic diameter

		Turbidity (AU/cm)		d_H (nm)	
		Initial	40°C	Initial	40°C
MAb-A	pH 5	0.14 ± 0.01	0.12 ± 0.00	10.6 ± 0.1	10.9 ± 0.1
	pH 6	0.14 ± 0.00	0.13 ± 0.00	10.6 ± 0.1	10.7 ± 0.0
	pH 7	0.14 ± 0.00	0.12 ± 0.00	10.7 ± 0.2	11.0 ± 0.0
	pH 8	0.14 ± 0.01	0.13 ± 0.00	10.5 ± 0.1	11.6 ± 0.4
MAb-B	pH 5	0.14 ± 0.01	0.13 ± 0.00	10.4 ± 0.0	10.5 ± 0.1
	pH 6	0.13 ± 0.01	0.13 ± 0.00	10.4 ± 0.1	10.5 ± 0.0
	pH 7	0.13 ± 0.00	0.13 ± 0.00	10.5 ± 0.1	10.7 ± 0.1
	pH 8	0.13 ± 0.00	0.13 ± 0.00	10.5 ± 0.1	11.1 ± 0.1
MAb-C	pH 5	0.14 ± 0.01	0.13 ± 0.00	10.4 ± 0.0	10.8 ± 0.2
	pH 6	0.13 ± 0.00	0.13 ± 0.00	10.4 ± 0.1	10.8 ± 0.5
	pH 7	0.13 ± 0.00	0.13 ± 0.00	10.6 ± 0.1	10.6 ± 0.2
	pH 8	0.13 ± 0.01	0.13 ± 0.00	10.5 ± 0.0	11.3 ± 0.5

MAbs were stored at 40°C for 4 weeks at 4 different pH values. The hydrodynamic diameters d_H were obtained from DLS. The error values were estimated from 3 independent experiments performed under the same conditions.

2.4 Discussion

2.4.1 Evaluation of B_2 from AUC-SE for characterizing the intermolecular interactions of MAbs

The purpose of the study in this chapter was to investigate whether B_2 determined at low concentrations of MAbs can be correlated with viscosity or aggregation propensity so that one can select MAbs with superior physical properties such as low viscosity and low aggregation propensity in the final product. Although direct measurements of viscosity and aggregation propensity using highly concentrated solutions are desirable, it is difficult to prepare highly concentrated solutions, and large amounts of samples are required for the measurements. These drawbacks reduce the numbers of candidate MAbs and formulation parameters such as type and concentration of excipients for comprehensive characterization, and cause MAbs to be selected in the context of specific formulations for further development without sufficient data on the physical properties of the MAbs. Instead of direct measurements, predictions of viscosity and aggregation at high concentrations from the solution properties of diluted solutions can be an effective approach.

In this chapter, the relationships between intermolecular interactions at low concentrations reflected by B_2 values and viscosity/aggregation propensity at high concentrations were investigated. As the first step to estimate B_2 values under different conditions, the concentration dependencies of $1/M_{W,app}$ were precisely measured at concentrations ranging from 1 to 12 mg/mL. In the cases of MAb-A and MAb-C, the $1/M_{W,app}$ values changed linearly with the increase of concentrations, which is consistent with linear-regression fitting having high R values. In contrast, it was unexpected that MAb-B showed two phases with different slopes and intercepts. Concentrations ranging from 1 to 3 mg/mL and from 4 to 12 mg/mL gave two different B_2 values suggesting that repulsive interactions are dominant within the concentration range of 1 to 3 mg/mL,

and attractive interactions become gradually dominant above 4 mg/mL. This change in the type of intermolecular interactions with increasing concentrations leads to the unique concentration dependence of $1/M_{W,app}$. Importantly, although the two B_2 values of MAb-B differ from each other under all pH conditions, they similarly vary as the solution pH changes (Fig. 2.3B). Hence, the relationship of B_2 with pH showed similar patterns in the concentration ranges 1 to 3 mg/mL and 4 to 12 mg/mL (Fig. 2.3B). In addition, the two B_2 values of MAb-B, which are either positive or negative, coincide with each other under all pH conditions. Our study demonstrated that B_2 values as a function of pH at concentrations lower than 10 mg/mL are in good qualitative agreement with measurements of viscosity and aggregation propensity at concentrations higher than 100 mg/mL for all three MAbs as detailed in Sections 2.4.2 and 2.4.3. Each MAb used in this study recognizes different antigens and has a different primary structure. Therefore, all MAbs have different pI values and amino acid compositions (Fig. 2.1). This suggests that our approach could be applicable to other MAbs. Thus, for MAb solutions under physiological conditions, we can infer that there is qualitative consistency of intermolecular interactions at low and high concentrations.

The k_D from DLS has been successfully used as an indicator of intermolecular interaction (Yadav et al., 2010b). However, it should be noted that an exceptional relation in the pH dependence of MAb-C between k_D and B_2 was observed in the present study where k_D reached its minimum value at pH 7 but B_2 did so at pH 8 (Figs. 2.3C and 2.4C). Herein, the pH dependencies of viscosity and aggregation propensities are in good qualitative agreement with that of B_2 but not that of k_D as shown in Fig. 2.8, where k_D deviated from the linear correlation with aggregation propensity, indicating that k_D did not accurately reflect the aggregation propensity. Thus, the k_D value obtained by DLS may be misleading with respect to the magnitude of intermolecular interactions because k_D is related not only to B_2, but also to ξ_1, which depends upon the shape and hydration state of the MAb as described in Eq. 2.5 (Yamakawa et al., 1962, Frost et al., 1976,

Lehermayr et al., 2011). If the shape and size of the molecule change depends on the concentration, the k_D value does not reflect only that type of intermolecular interaction. On the contrary, AUC-SE directly provides a B_2 value based on the concentration dependence of $M_{W,app}$. In addition, light scattering techniques such as DLS and SLS provide an indication of both solute-solute interactions and solute-solvent interactions, whereas AUC-SE and osmometry only indicate solute-solute interactions (Deszczynski et al., 2006, Winzor et al., 2007). Therefore, proper estimation of intermolecular interactions can be established by AUC-SE. The relationship between k_D and B_2 are further discussed in Chapter 4.

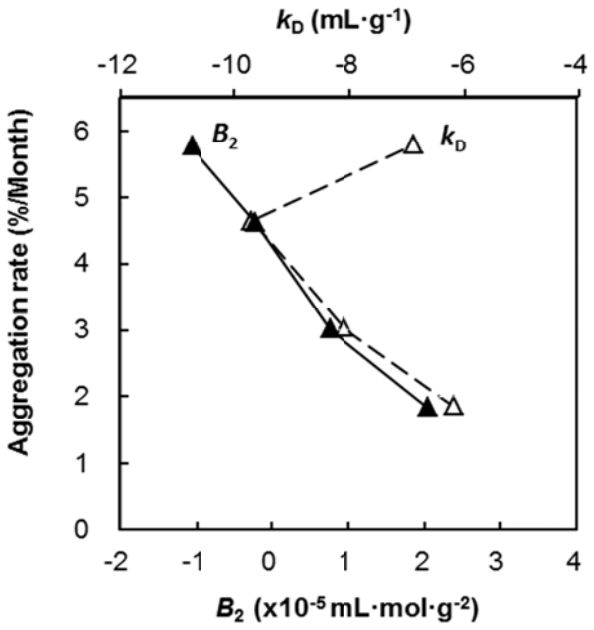

Figure 2.8. Relationship between aggregation propensity and B_2 or k_D for MAb-C
B_2 values (▲) were obtained from AUC-SE and k_D (△) values were obtained from DLS for MAb-C. Aggregation rates were estimated from SEC in storage at 40°C.

2.4.2 Relationship between viscosity and B_2

Fig. 2.9 describes a model of MAb viscosity enhancement. In this pathway, high viscosity would be induced at high concentrations due to transiently cross-linked networks among MAbs formed via weak reversible self-association. The relationship between self-association of antibodies and the viscosity of antibody solutions has been investigated by Liu et al. (2005) who showed that viscosity is enhanced at around its own pI and at low ionic conditions for specific IgG_1 via reversible self-association. Yadav et al. (2010a) evaluated the self-association of the same IgG_1 based on the ultrasonic storage module, and suggested that short-range electrostatic interactions such as dipole-dipole and dipole-charge interactions play significant roles in highly concentrated solutions. A similar case was reported by Chari et al. (2009) for an IgG_2. These intermolecular interactions causing the high viscosity can be evaluated by B_2 estimated from MAb solutions in the native state at a relatively low concentration, as indicated in the present study. Higher viscosities were observed at the pH levels where MAbs have lower B_2 values for all of the MAbs, as indicated in Fig. 2.10A (generated from the values described in Fig. 2.6 and Table 2.2). These results support the contribution of the pathway in Fig. 2.9 and indicate that B_2 (determined by AUC-SE at low concentrations) could be a reliable predictor of the viscosity of the highly concentrated MAb solution. The viscosities of three MAbs vary significantly with respect to conditions that provide larger negative B_2 values indicating the presence of stronger attractive interactions. This variation in viscosity is attributed to the type of attractive interactions contributing to the viscosity enhancement. There are various types of attractive interactions, such as dipole-dipole and hydrophobic interactions, the magnitudes of which are largely dependent on the state of the protein surface. The profile of attractive intermolecular interactions is largely dependent on the MAbs because each MAb has primary and higher order structures, which provide specific functions

including binding to its specific antigen. On the other hand, the viscosities of the three MAb solutions were found to have similar values as B_2 increased and finally converged under conditions that provide positive B_2 values. This behavior could be explained by the relationship between the intermolecular forces and the enhancement of viscosity. The major contributors of repulsive interactions of proteins are charge-charge repulsion and the excluded volume effect. In general, charge-charge repulsion is negligible in the presence of high concentrations of salt. The excluded volume is dependent on the size of the molecules and its magnitude is essentially constant for all MAbs. Thus, the viscosities of MAbs are expected to be similar values in the absence of any attractive interactions.

In the case of MAb-B, two B_2 values were obtained in the low and high concentrations. The viscosity vs. B_2 relationships for the three MAbs converge well when B_2 is from the concentration range of 5 to 10 mg/mL, when B_2 was positive. On the other hand, the exceptional point (B_2, 2.03 × 10^{-5} (mL·mol)/g^{-2} and viscosity, 9.7 mPas) was confirmed for MAb-B in the plot of B_2 vs. viscosity, when B_2 was estimated in the lower concentration range of 1 to 3 mg/mL, as shown in Fig. 2.10A. These results suggest that B_2 values estimated from rather high concentrations are suitable for predicting the viscosity at high concentrations.

Figure 2.9. Model of viscosity enhancement

B_2(F-F) is the second virial coefficient for MAbs in the folded state. Viscosity is enhanced due to the transient cross-linked networks formed via weak reversible self-association.

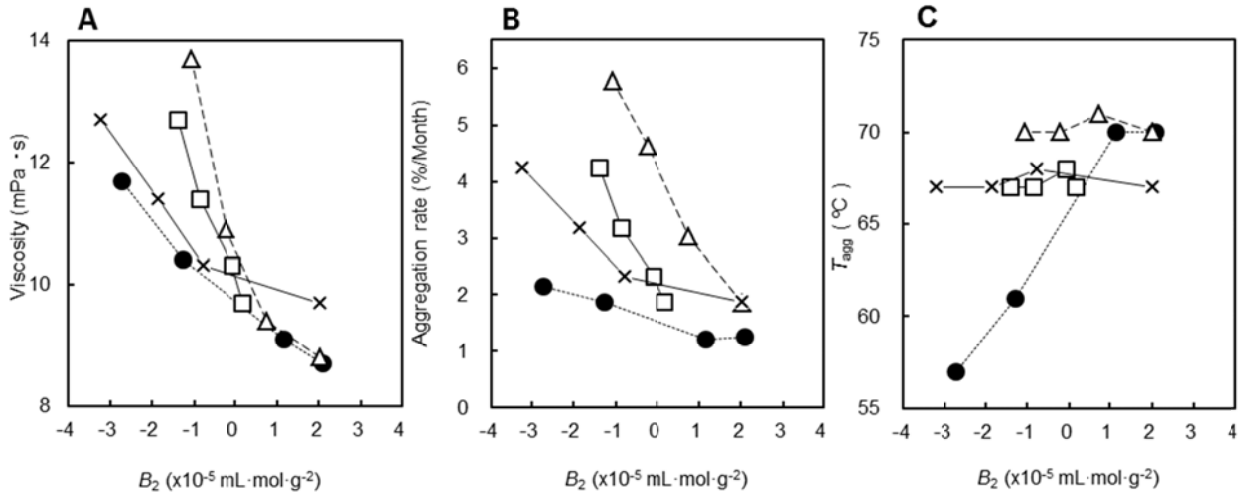

Figure 2.10. Correlation of B_2 with viscosity (A), aggregation propensity (B), and thermal stability (C): MAb-A (●), MAb-B (×: 1-3 mg/mL, □: 5-10 mg/mL), and MAb-C (Δ)

B_2 values were obtained from AUC-SE. T_{agg} values were obtained from DLS. Viscosities were obtained at a concentration of 150 mg/mL, and aggregation rates were estimated based on SEC.

Table 2.2 Summary of physical parameters

	pI	pH	B_2 (× 10^{-5}・mL・mol・g^{-2})	k_D (mL/g)	T_{agg} (ºC)	Viscosity (mPs・s)	Aggregation rate (%/Month)
MAb-A	6.7	5	-2.71	-12.2 ± 1.7	57	11.7	2.14 ± 0.03
		6	-1.28	-8.6 ± 0.9	61	10.4	1.88 ± 0.04
		7	1.15	-5.5 ± 1.1	70	9.1	1.21 ± 0.03
		8	2.08	-4.6 ± 0.3	70	8.7	1.25 ± 0.05
MAb-B	8.9	5	0.34 (2.03)	-6.7 ± 0.5	67	9.7	1.87 ± 0.05
		6	-0.72 (-0.77)	-7.8 ± 0.2	68	10.3	2.33 ± 0.07
		7	-1.15 (-1.83)	-8.1 ± 1.0	67	11.4	3.18 ± 0.18
		8	-1.49 (-3.21)	-9.3 ± 1.0	67	12.7	4.23 ± 0.20
MAb-C	8.8	5	2.03	-6.2 ± 1.0	70	8.8	1.84 ± 0.08
		6	0.76	-8.1 ± 1.2	71	9.4	3.02 ± 0.14
		7	-0.22	-9.7 ± 0.9	70	10.9	4.63 ± 0.30
		8	-1.06	-6.9 ± 0.2	70	13.7	5.77 ± 0.33

B_2 values were obtained from AUC-SE. For MAb-B, B_2 values were obtained from the concentrations of 1, 2, and 3 mg/mL (in parenthesis), and 5, 7.5, and 10 mg/mL. k_D and T_{agg} values were obtained from DLS. Viscosities were obtained at a concentration of 150 mg/mL, and aggregation rates were estimated from SEC.

2.4.3 Relationship between aggregation propensity and B_2

To predict the aggregation propensity of MAb solutions, the physical properties of the MAbs must be assessed in terms of colloidal and conformational stabilities. Colloidal stability is attributed to intermolecular interactions. On the other hand, conformational stability is attributed to a free energy difference, ΔG_{FU}, between folded (F) and unfolded (U) states of protein. Each aspect of stability is related to aggregation via different pathways, as shown in Fig. 2.11 (Chi et al., 2003a, Chi et al., 2003b, Hawe et al., 2009, Saito et al., 2012). One major pathway related to colloidal stability is initiated by reversible self-association of a MAb in the folded state (Fig. 2.11, pathway I). The other pathway related to conformational stability is initiated by structural changes resulting in the accumulation of a MAb in the unfolded state, followed by the successive formation of large aggregates via the formation of small aggregates (Fig. 2.11, pathway II). In the present study, it was found that aggregation was accelerated under conditions that give a large negative B_2 attributable to the presence of attractive intermolecular interactions in all MAbs (Fig. 2.10B). Thus, colloidal stability is related to the formation of aggregates as previously mentioned (Chi et al., 2003a, Chi et al., 2003b) and B_2, estimated from AUC-SE of MAbs solutions at low concentrations, is an effective indicator of stability for highly concentrated solutions.

Conformational stability by pathway II, in which the difference in free energy between folded and unfolded states contributes to aggregation at higher temperatures, was investigated based on the thermal stability using DLS (Fig. 2.5 and Table 2.2). In this pathway, intermolecular interactions among MAbs in the folded state (represented as B_2(F-F)) do not contribute to the formation of aggregates, whereas intermolecular interactions between unfolded states (represented as B_2(U-U)) contribute to the formation of aggregates (Fig. 2.11). B_2 values determined by AUC-SE at ambient temperatures do not reflect aggregation occurring via pathway II. In fact, there is no

significant correlation observed between B_2 and T_{agg} (Fig. 2.10C). In one exception, B_2 showed good qualitative agreement with T_{agg} in MAb-A. In this case, intermolecular interactions between MAbs in the unfolded state could be attributed to B_2 because the population in the unfolded state should be larger in MAbs with smaller T_{agg} values.

In conclusion, B_2 determined by AUC-SE is a qualitative indicator for aggregation via the pathway I initiated by the self-association of MAbs. This pathway is considered to contribute to the formation of aggregates during storage. This is not a stressing condition where unfolding is slightly induced. Therefore, it is useful to select formulations of MAbs that have promising stability. On the other hand, aggregation via the pathway II initiated by unfolding did not necessarily correlate with B_2 because aggregation is mainly attributed to conformational stability. In this case, a combination of B_2 and T_{agg} determined by DLS and/or other techniques, such as DSC, will provide effective information for estimating the aggregation propensity.

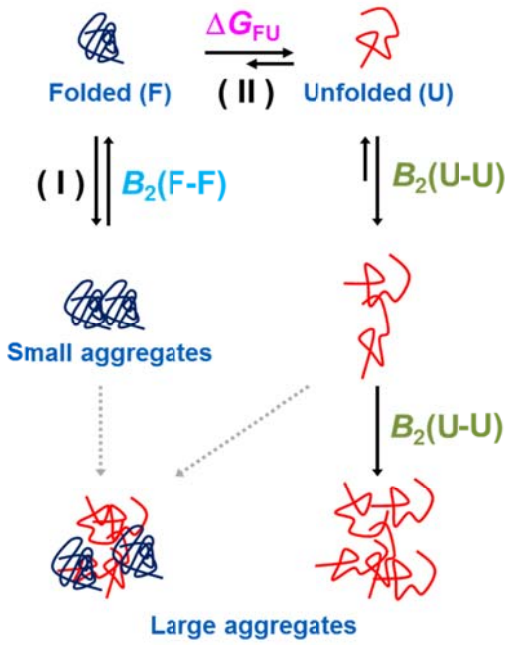

Figure 2.11. Model of aggregation

B_2(F-F) is the second virial coefficient for MAbs in the folded state and B_2(U-U) is the second

virial coefficient for MAbs in the unfolded state. ΔG_{FU} is the free energy difference between MAbs in the folded and unfolded states.

2.5 Conclusion

Aggregation and viscosity are difficult problems to overcome in the development of therapeutic MAbs. Therefore, a reliable strategy to predict viscosity and aggregation propensity is an important requirement. In this study, we investigated the intermolecular interaction of MAbs by determining B_2 using AUC-SE measurements. As a whole, we ensured that the intermolecular interactions at low concentrations are qualitatively comparable to those determined at high concentrations. In fact, B_2 determined by AUC-SE was in good qualitative accordance with viscosity and aggregation propensity for all the MAb solutions studied. In particular, the better correlation was confirmed when B_2 values are positive. However, the relationship was found to be only qualitative in the presence of attractive interactions that are presented as negative B_2 values. We also determined based on the comparison of AUC-SE data with DLS data, that AUC-SE provides B_2 values that are qualitatively consistent with viscosity and aggregation propensity. A good relationship was confirmed between B_2 determined from AUC-SE and k_D determined from DLS. AUC-SE and DLS have been widely used to evaluate dispersion in protein solutions. An exception was observed in the correlation of k_D with viscosity and aggregation propensity. These results indicate that B_2 determined from AUC-SE is a better indicator for the estimation of the viscosity and aggregation propensity of highly concentrated solutions. Although AUC-SE is recognized as a low throughput technique, the information obtained from this technique is highly valuable and can provide useful details about the type of dominant intermolecular interactions and the critical physical parameters of target therapeutic proteins.

Chapter 3

Exploration of a predictive indicator for aggregation propensity of monoclonal antibodies in terms of colloidal and conformational stabilities

3.1 Introduction

Multiple pathways independently, additively, or synergistically contribute to the formation of aggregates. Various factors in solution such as pH, ionic strength and the presence of sugars and surfactants impact each pathway, resulting in different aggregation propensity. Likewise, different stress factors such as heat, freeze-thawing and agitation differently impact these multiple pathways. Thus, deeper understanding of the role and impact of these factors from the aspect of the aggregation pathway is necessary to accurately predict the aggregation propensity of MAb solutions. In Chapter 2, we focused on the colloidal stability and investigated the correlations between B_2 from AUC-SE and aggregation propensity for three different MAbs (Saito et al., 2012). The pH dependencies of B_2 were qualitatively correlated with the aggregation propensity of the three MAbs, indicating that aggregation is attributed to the colloidal stability regulating pathway (Fig. 2.11, pathway I). However, the correlations were limited in qualitative manner and became insignificant when the B_2 values were negative. Thus, the attribution of the colloidal stability to aggregation has not been fully elucidated. In addition, the contribution of other pathways to aggregation remains uncertain.

In this chapter, we aimed to develop a general strategy for the development of MAb formulation through the proper assessment of colloidal and conformational stabilities. To assess these stabilities, we studied four MAbs, namely, MAb-A, MAb-B, MAb-C, and MAb-D, which

differ in the amino acid sequences of their variable regions. The colloidal stabilities were assessed in terms of B_2 from AUC-SE, k_D from DLS, and zeta potential and net charge from electrophoretic light scattering. Zeta potential and/or net charge have been evaluated to characterize the electrostatic potential of proteins. The electrostatic interaction is a major attribution to repulsive interaction according to the well-known DLVO theory, therefore the electrostatic potential has been regarded as an indicator of colloidal stability. Zeta potential is estimated from electrophoretic mobility measured under an applied electric field using the Henry equation (Jachimska et al., 2008, Lehermayr et al., 2011), and the zeta potentials of several MAbs were reported (Salinas et al., 2010, Nishi et al., 2011). The effective net charge of a protein is derived from its electrophoretic mobility and diffusion constant, from which the protein net charge is calculated based on the Debye-Hückel-Henry model (Moody et al., 2005). The electrostatic properties of a protein can be accurately determined by its net charge (Durant et al., 2002, Moody et al., 2005). As the net charge of a protein is a global attribute which depends on the properties of protein, the properties of the counter ion and co-ions, and the behavior of ions in the vicinity of proteins, this parameter is highly complex. Therefore, it is necessary to determine the actual charge of the protein (Moody et al., 2005, Chase et al., 2008). On the other hand, the conformational stability can be assessed based on the T_m obtained from DSC. DSC enables direct assessment of the conformational stability per domain, and provides more accurate information than other techniques, such as DLS which provides T_{agg}.

We focused first on the effect of salts on the intermolecular interaction in terms of the electrostatic interaction, which have recently received much attention (Nishi et al., 2010, Saluja et al., 2010, Yadav et al., 2010b, Yadav et al., 2012), because colloidal stability is largely modulated by ionic strength and the species of ion. An increased ionic strength will suppress the electrostatic interactions among molecules and lead to reduced repulsive forces, resulting in promotion of

aggregation, as predicted by the DLVO theory of colloidal stability. Our findings emphasize the great importance of measuring the type of electrostatic interaction. Furthermore, electrostatic repulsion and attraction were determined from electrostatic potential surfaces simulated according to the Poisson–Boltzmann equation using the structure of IgG_1 as a model. Second, we assessed the effect of sugars which are representative excipients in protein pharmaceutics. Sugars enhance conformational stability through a preferential solvation mechanism in solution (Timasheff, 2002, Thakkar et al., 2012). Finally, we confirmed the contribution of colloidal and conformational stabilities to aggregation propensities in the presence of different stress factors.

3.2 Materials and methods

3.2.1 Materials

Humanized monoclonal antibody A (IgG_1 subclass, MAb-A), B (IgG_1 subclass, MAb-B), C (IgG_1 subclass, MAb-C), and D (IgG_1 subclass, MAb-D) were produced and highly purified at Daiichi Sankyo Co. Ltd. All the MAbs were humanized IgG_1. The theoretical isoelectric points (p*I*s) of MAb-A, MAb-B, MAb-C, and MAb-D were 6.7, 8.9, 8.8, and 9.0 respectively. The molecular weights (M_Ws) of MAb-A, MAb-B, MAb-C, and MAb-D, calculated from amino acid sequences with two oligosaccharide chains, were 150, 147, 148, and 151 kDa, respectively. All the MAbs were dialyzed against appropriate initial buffers (pH 5, 6, 7, and 8) before use, and the concentrations were determined based on the absorbance at 280 nm. The MAbs were diluted to adjust the concentration to 20 mg/mL for storage. Each MAb in the initial buffer was diluted two-fold with the necessary buffer to give a solution concentration of 10 mg/mL prior to each experiment. NaCl was purchased from Wako Pure Chemical Industries, Ltd., and sodium phosphate

and sodium acetate were purchased from Kanto Chemical Co. Sucrose, sorbitol, and trehalose were purchased from Merck (Darmstadt, Germany), Roquette Co. (Lestern, France) and Hayashibara Co. (Okayama, Japan), respectively.

3.2.2 Formulations

The initial buffer at pH 5 was 10 mM sodium acetate buffer. The initial buffers at pH 6, pH 7, and pH 8 were 10 mM sodium phosphate buffer. The initial buffers for MAb-A additionally contained 30 mM NaCl because the solution become opaque at an NaCl concentration of less than 30 mM. These initial buffers correspond to the lowest ionic strength. Buffers designated as +70, +140, and +300 mM NaCl each contained the indicated concentration of NaCl. The buffers represented as +Sorbitol, +Sucrose, and +Trehalose contained 5% sorbitol, 10% sucrose, and 10% trehalose, respectively under the lowest ionic strengths.

3.2.3 AUC-SE studies

AUC-SE was conducted using a Proteome XL-I (Beckman Coulter, Inc.). A volume of 60 μL of each solution at 1, 5, or 10 mg/mL, was placed in sample sectors with six holes, a charcoal-filled epon centerpiece (1.2 cm) with sapphire windows, and 60 μL of reference solutions were added to the reference sectors. Measurement and B_2 determination were carried out according to the method already mentioned in Section 2.2.2. The partial specific volumes of MAb-A, MAb-B, MAb-C, and MAb-D, according to their amino acid compositions, were 0.7261, 0.7272, 0.7275, and 0.7287 cm^3/g, respectively.

3.2.4 Estimation of concentration dependence of diffusion coefficient by DLS

Samples of volume 15 μL of 2.0, 4.0, 6.0, 8.0, and 10 mg/mL sample solutions (after filtration with a 0.22-μm filter) were applied to 384-well optical clear-bottomed microtiter plates. Following centrifugation at ×135 *g* for 3 min to remove bubbles, the diffusion coefficient was measured using a DynaPro Plate Reader (Wyatt Technology Co.) at 20°C. The interaction parameter (k_D) was calculated using Eq. 2.4

3.2.5 Determination of zeta potential and net charge

Approximately 600 μL of 2.0 mg/mL sample solution (after filtration through a 0.22-μm filter) was injected using a syringe pump. The zeta potential, ζ, was measured using a Mobius mobility instrument (Wyatt Technology Co.) at 20°C equipped with an ATRAS N_2 gas pressure device (Wyatt Technology Co.). The ATRAS device prevents the generation of air bubbles by pressurizing the solution and enables ζ measurements in the presence of high concentrations of salts. The solution state was monitored by DLS during the ζ measurements to confirm that aggregation and precipitation did not occur.

The zeta potential is calculated using the following equation (Jachimska et al., 2011, Yadav et al., 2011):

$$\zeta = \frac{3\eta}{2\varepsilon f(\kappa R_h)}\mu \qquad (3.1)$$

,where μ [m^2/(V s)] is the measured electrophoretic mobility, η (mPa) is the solvent viscosity at 20°C, calculated based on the buffer components using Sednterp software, ε [(A^2 $s^{4)}$/(kg m^3)] is the

absolute dielectric constant of water, and $f(\kappa R_h)$ is Henry's function.

The net charge z was estimated using the following equation (Chase et al., 2008):

$$z = \frac{\mu k_B T}{D_S e} \times \frac{(1 + \kappa R_h)}{f(\kappa R_h)} \quad (3.2)$$

,where k_B is the Boltzmann constant (1.3807×10^{-23} J/K), T is the temperature (293 K), D_S is the self-diffusion coefficient (m^2/s) determined from the extrapolation of diffusion coefficients obtained from DLS to zero concentration at different concentrations, e is the elementary charge ($1.6 \times e^{-19}$ C), κ is the inverse Debye length, R_h is the sum of the Stokes radii for the protein and its counter ion in the solution. The product κR_h has values near 2 and $f(\kappa R_h)$ is ~1. Hence, as a rough approximation, the net charge can be estimated according to the following equation:

$$z = \frac{\mu k_B T}{D_S e} \times 3 \quad (3.3)$$

3.2.6 Conformational stability assessment by differential scanning calorimetry (DSC)

DSC studies were performed using a VP capillary DSC system (GE Healthcare, Little Chalfont, UK). Samples of volume 400 µL of 1.0 mg/mL solutions were injected. Changes in the heat capacity (C_p) were measured as the samples were heated from 20 to 100°C at a scanning rate of 60°C/h and a filtering period of 10 s. Data analysis was performed using the OriginLab software (OriginLab Co.). For each sample, a relevant buffer composed of the same composition as the sample was subtracted as a reference. Normalized C_p data were corrected for the buffer baseline. An apparent transition midpoint (T_{max}) was determined from the exothermic peak providing the highest C_p.

3.2.7 Stability studies

Antibody solutions (150 μL, 10 mg/mL) were applied in triplicate to a 96-well polypropylene PCR plate with cap. One plate was analyzed immediately after preparation. Other plates were stored at 40°C for 1, 2, and 4 weeks. Another plate was frozen at -40°C and then thawed at 25°C using an aluminum block matching the shape of the storage plate. This freeze-thaw procedure was repeated 10 times. The aggregation profiles before and after stressing (40°C for 1, 2, and 4 weeks or 10-times freeze-thaw) were analyzed using SEC, DLS, and turbidity measurements. There was no detectable change in concentration during storage.

3.2.8 SEC

Samples were filtered without dilution using 96-well filtration plates (0.45 μm). SEC analysis was conducted according to the method mentioned in Section 2.2.6. A 20-μL sample of each solution was injected into the column. The rate of increase in the amount of aggregates, the aggregation rate (percentage per month or percentage per 10-times freeze-thaw cycles), was estimated from least-squares fitting of the aggregation percentages to a linear function.

3.2.9 DLS

The samples were diluted to 1 mg/mL with the corresponding formulation buffers and filtered using 96-well filtration plates (0.45 μm). Samples of volume 15 μL were applied to 384-well optical clear-bottomed microtiter plates. Following centrifugation at ×135 *g* for 3 min to remove large particulates and bubbles, the average hydrodynamic diameter was measured at 20°C

using a DynaPro Plate Reader (Wyatt Technology Co.).

3.2.10 Turbidity measurements

Samples of volume 20 μL were applied to 384-well optical clear-bottomed microtiter plates without dilution. The turbidity of the solution was obtained according to the procedure previously mentioned in Section 2.2.8.

3.2.11 Calculation of electrostatic potential surface

Full-length IgG_1 model structures of MAb-A and MAb-B were generated using Discovery Studio software (Accelrys Inc., San Diego, CA). The crystal structure of Anti-HIV-1 GP 120 IgG_1 was used as a template (PDB id: 1HZH). The electrostatic potential surfaces were determined according to the Poisson–Boltzmann equation at different pHs and ionic strengths, and +1 and -1 k_BT/e isovalue surfaces were mapped on the model structures.

3.3 Results

3.3.1 Influence of pH, NaCl concentration and type of sugars on B_2

The B_2 values of MAb-A and MAb-B were measured using AUC-SE in the formulations containing different concentrations of NaCl or sorbitol, sucrose, or trehalose to investigate their influence on intermolecular interactions. Evaluations of B_2 values were conducted at two different

pHs, at pH 5 and pH 7, where both MAbs showed distinct B_2 values at low ionic strength (Figs 3.1A and C); MAb-A showed negative at pH 5 and small negative at pH 7 and MAb-B showed large positive at pH 5 and small negative at pH 7, indicating the presence of different types of intermolecular interactions. This enabled the evaluation of the influence of salt and sugars on the different types of intermolecular interactions.

At the lowest NaCl concentration, negative B_2 values of MAb-A at pH 5 and pH 7 showed the presence of attractive intermolecular interactions. The B_2 values increased as the NaCl concentration increased and inverted from negative to positive values at 300 mM (pH 5) and 70 mM (pH 7). Such dependencies of B_2 on NaCl concentrations for MAb-A were similarly confirmed at pH 5 and pH 7; however, the B_2 values determined in each salt concentration at pH 7 were higher than those at pH 5, suggesting increased attractive intermolecular interactions at pH 5 than at pH 7. The addition of sugars did not significantly alter the B_2 values, although slight increases in B_2 were observed at pH 7 in the presence of sucrose and trehalose (Fig. 3.1B).

Figs. 3.1C and D show the B_2 values of MAb-B. The dependence of B_2 on the NaCl concentration was similar to that for MAb-A at pH 7, at which the B_2 values were negative in solutions of the lowest ionic strength. The B_2 values increased as the NaCl concentration increased and inverted to positive values in the presence of NaCl greater than 70 mM. In contrast, the B_2 value of MAb-B at pH 5 was high and positive, indicating the presence of strong repulsive intermolecular interactions. The B_2 values of MAb-B decreased strikingly by increasing the NaCl concentration, suggesting that NaCl greatly suppressed the repulsive intermolecular interactions. Sucrose enhanced the value of B_2, while sorbitol and trehalose did not.

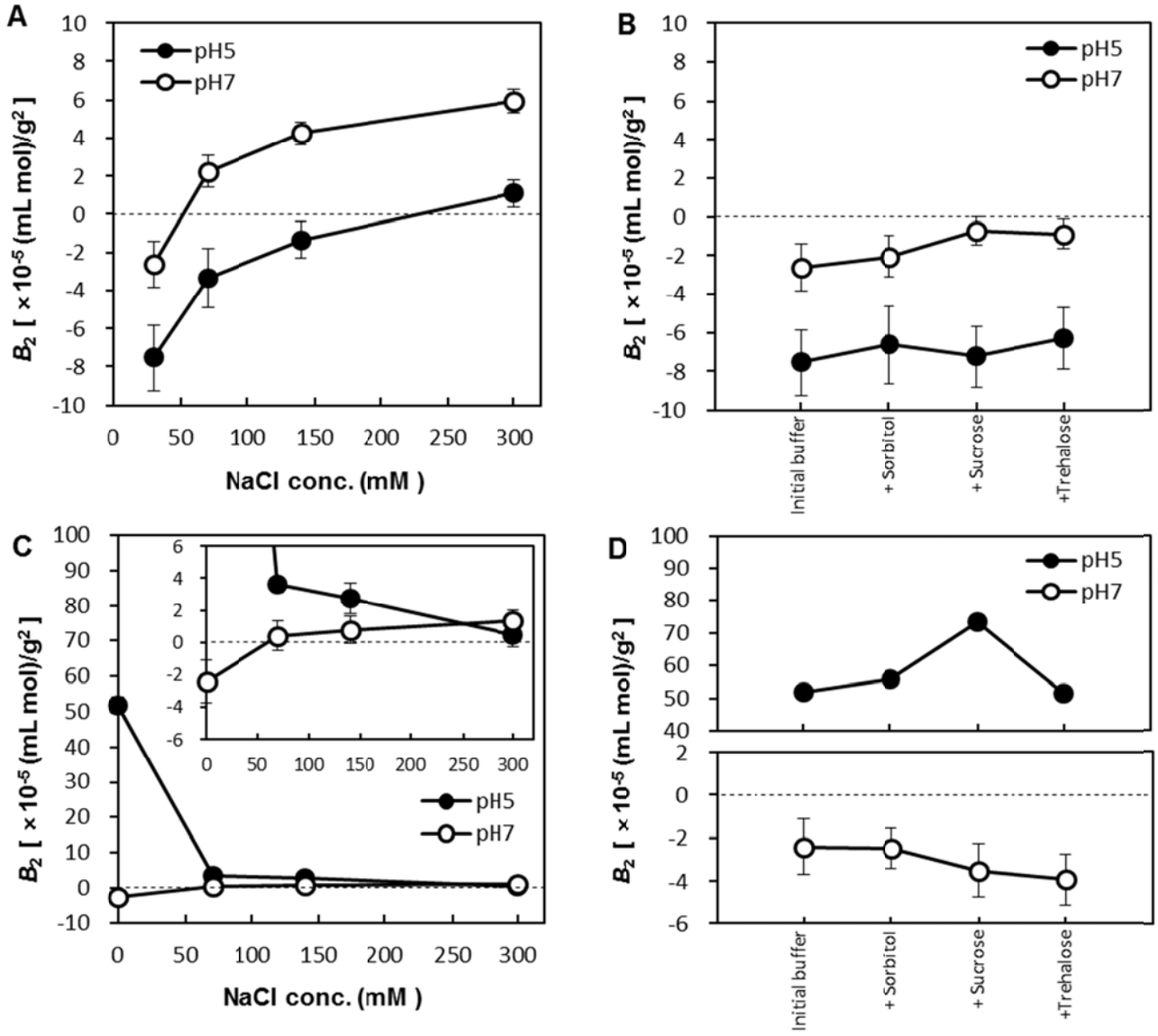

Figure 3.1. B_2 for MAbs in the different formulations

B_2 for MAb-A (**A** and **B**) and MAb-B (**C** and **D**) in formulations containing different concentrations of NaCl and different sugars were measured by AUC-SE. B_2 was obtained from the concentration dependence of $M_{W,app}$ at three different concentrations, i.e., 1, 5, and 10 mg/mL, in 10 mM AcONa (pH 5) (●) and 10 mM sodium phosphate buffer (pH 7) (○) containing NaCl or sugars as indicated in the figures. The inset in **C** is an expanded figure. The lowest ionic strength buffer (initial buffer) contained 30 mM NaCl for MAb-A and no NaCl for MAb-B. The error bars were estimated from three independent experiments under the same conditions.

3.3.2 B_2 measurements at low and high ionic strengths

The effects on B_2 of changes in the ionic strength were further investigated for four different MAbs (MAb-A, MAb-B, MAb-C, and MAb-D) at pH 5, pH 6, pH 7, and pH 8 at low ionic strength (30 mM NaCl for MAb-A, no NaCl for MAb-B, MAb-C, and MAb-D) or high ionic strength (300 mM NaCl for all MAbs). As shown in Figs. 3.2A–D, the B_2 values of all the MAbs were affected to some extent as the ionic strength changed, except for MAb-D at pH 7. The negative B_2 values for MAb-A at all pHs, MAb-B and MAb-C at pH 7 and pH 8, and MAb-D at pH 8 indicate the presence of weak attractive interactions at low ionic strength. Importantly, negative B_2 values were all inverted to positive values by the addition of 300 mM NaCl. Positive B_2 values were obtained at low ionic strength for MAb-B and MAb-C at pH 5 and pH 6, and MAb-D at pH 5, pH 6, and pH 7. These positive B_2 values were significantly reduced by the addition of 300 mM NaCl, except for MAb-D at pH 7.

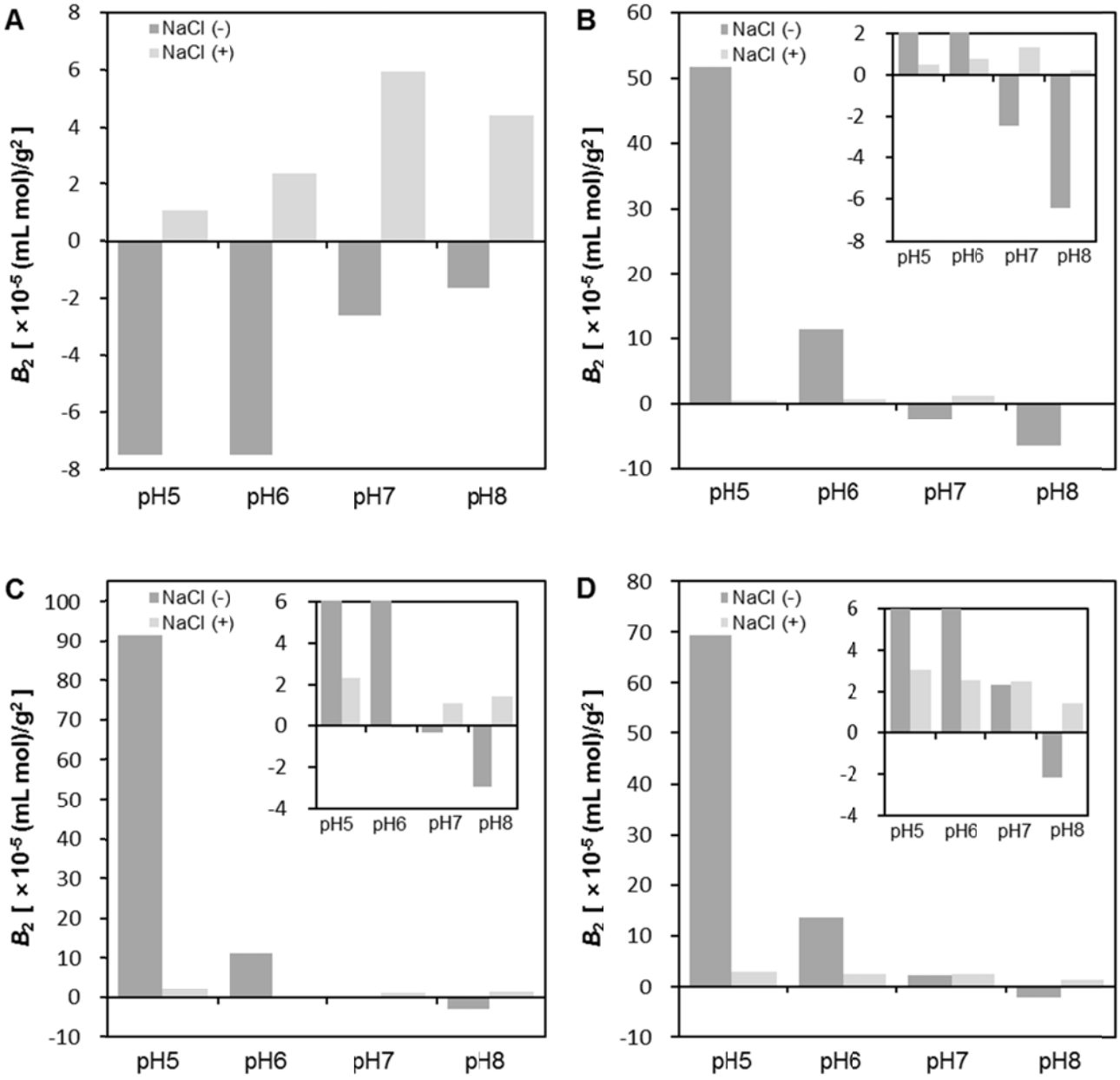

Figure 3.2. Influence of ionic strength on B_2

B_2 for MAb-A (**A**), MAb-B (**B**), MAb-C (**C**), and MAb-D (**D**) were measured at four pHs. B_2 was obtained from the concentration dependence of $M_{W,app}$ obtained by AUC-SE at three different concentrations, i.e., 1, 5, and 10 mg/mL, in 10 mM AcONa (pH 5) and 10 mM sodium phosphate buffer (pH 6, pH 7, and pH 8) at the lowest ionic strength (30 mM NaCl for MAb-A and no NaCl for MAb-B, MAb-C, and MAb-D) or at the highest ionic strength (300 mM NaCl).

3.3.3 Zeta potential and net charge determination

The values for zeta potential, ζ, and the net charge, z, were determined in the presence of different buffer conditions to assess the relationship of the electric potential surface with B_2. Figs. 3.3A-B and Table 3.1 show that MAb-A is positively charged at pH 5 in the presence of the lowest ionic strengths, which is consistent with our previous study (Nishi et al., 2011) and is reasonable when the pI of the MAb-A is considered (pI = 6.7). The charge decreased with increasing NaCl concentration and ultimately changed to a negative value in the presence of high ionic strengths. MAb-A was negatively charged at pH 7 in the presence of the lowest ionic strengths. The negative charge, as was the case at pH 5, decreased as the NaCl concentration increased.

When sugars were added, similar effects on reducing the net charger were observed. Sorbitol, sucrose, and trehalose reduced positive and negative charges at pH 5 and pH 7, respectively. For MAb-B, a positive value was observed in the presence of the lowest ionic strengths at pH 5 and pH 7 (Fig. 3.3C). The charges decreased as the NaCl concentration increased. The trends in net charge as a function of NaCl concentration were similar at pH 5 and pH 7, but the magnitudes of the positive charges at each NaCl concentration were slightly larger at pH 5 than those at pH 7. The decreases in the net charge of MAb-B observed upon the addition of sugars was not significant (Fig. 3.3D). The net charge is estimated from the observed electrophoretic mobility of a protein, which is also influenced by the diffusion coefficient, D_S (Eq. 3.2). In MAb-A at pH 5, D_S decreased while k_D was unchanged in the presence of sucrose and trehalose, implying that protein molecules are more hydrated and become bulky by the addition of these sugars (Table 3.1). The reduction of electrophoretic mobility by sugars, however, cannot be explained only by the reduction of D_S, because D_S was reduced by only one-fifth in the presence of sugars, whereas electrophoretic mobility was reduced to approximately one-fifth, indicating that the addition of sugars reduced the

net charge.

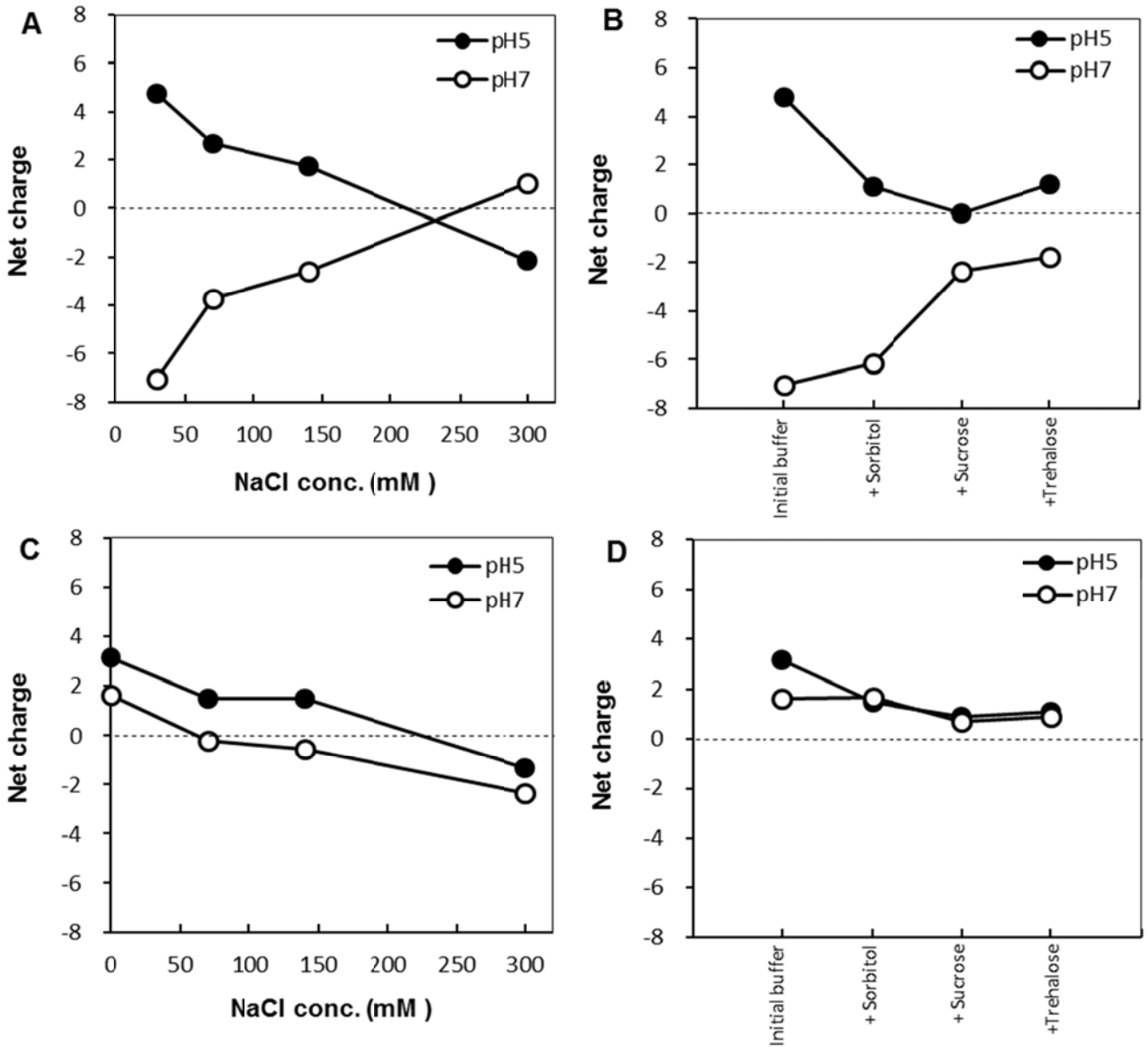

Figure 3.3. Net charge for MAbs in the different formulations

Net charges for MAb-A (**A** and **B**) and MAb-B (**C** and **D**) in different formulations were calculated from electrophoretic mobility measured at a concentration of 2 mg/mL in **1**0 mM AcONa (pH 5) (●) and 10 mM sodium phosphate buffer (pH 7) (○) containing NaCl or sugars as indicated in the figures. The lowest ionic strength buffer (initial buffer) contained 30 mM NaCl for MAb-A and no NaCl for MAb-B.

Table 3.1 Influence of formulations on the physical parameters of MAbs

MAb	pH	Formulation	B_2 ($\times 10^{-5}$·(mL·mol)/g^2)	k_D (mL/g)	D_S ($\times 10^{-7}$cm^2/sec)	Zeta potential (mV)	Net charge
MAb-A	5	Initial buffer	-7.53±1.69	-30.5±0.8	4.0±0.0	4.8	4.8
		+70 mM NaCl	-3.35±1.53	-18.7±0.8	3.9±0.0	2.7	2.7
		+140 mM NaCl	-1.36±0.95	-12.8±0.7	4.0±0.0	1.7	1.7
		+300 mM NaCl	1.09±0.73	-7.5±0.9	3.9±0.0	-2.1	-2.1
		Initial buffer	-7.53±1.69	-30.5±0.8	4.0±0.0	4.8	4.8
		+Sorbitol	-6.62±1.97	-26.9±1.5	3.4±0.0	1.2	1.1
		+Sucrose	-7.24±1.57	-30.4±0.6	3.2±0.1	0.0	0.0
		+Trehalose	-6.27±1.58	-29.7±0.1	3.2±0.0	1.3	1.2
	7	Initial buffer	-2.63±1.23	-14.3±0.9	3.9±0.1	-6.8	-7.0
		+70 mM NaCl	2.24±0.84	-7.8±1.0	3.9±0.0	-3.5	-3.7
		+140 mM NaCl	4.26±0.60	-3.7±0.2	3.8±0.0	-2.6	-2.6
		+300 mM NaCl	5.94±0.64	-3.1±0.6	3.7±0.1	1.1	1.0
		Initial buffer	-2.63±1.23	-14.3±0.9	3.9±0.1	-6.8	-7.0
		+Sorbitol	-2.05±1.06	-13.1±1.6	3.3±0.0	-5.9	-6.2
		+Sucrose	-0.73±0.73	-18.3±1.8	2.9±0.1	-2.1	-2.3
		+Trehalose	-0.88±0.78	-17.1±3.5	3.0±0.1	-1.8	-1.7
MAb-B	5	Initial buffer	51.83±2.39	19.6±2.3	4.1±0.0	3.2	3.2
		+70 mM NaCl	3.61±0.47	-6.2±1.2	4.1±0.0	1.5	1.5
		+140 mM NaCl	2.72±0.96	-8.5±0.7	4.1±0.0	1.6	1.5
		+300 mM NaCl	0.47±0.72	-8.8±1.0	4.0±0.0	-1.4	-1.3
		Initial buffer	51.83±2.39	19.6±2.3	4.1±0.0	3.2	3.2
		+Sorbitol	56.02±3.00	18.2±2.2	3.6±0.0	1.5	1.5
		+Sucrose	73.34±3.30	13.3±0.3	3.3±0.0	0.9	0.9
		+Trehalose	51.63±3.72	5.0±1.5	3.4±0.0	1.2	1.1
	7	Initial buffer	-2.41±1.29	-16.0±1.4	4.2±0.0	1.7	1.6
		+70 mM NaCl	0.42±0.89	-8.3±0.7	4.0±0.0	-0.3	-0.2
		+140 mM NaCl	0.76±0.85	-8.6±0.1	4.0±0.0	-0.6	-0.6
		+300 mM NaCl	1.30±0.67	-6.6±1.5	3.9±0.0	-2.3	-2.4
		Initial buffer	-2.41±1.29	-16.0±1.4	4.2±0.0	1.7	1.6
		+Sorbitol	-2.48±0.92	-17.7±1.0	3.6±0.0	1.4	1.7
		+Sucrose	-3.53±1.24	-23.1±0.4	3.3±0.0	0.7	0.7
		+Trehalose	-3.93±1.19	-23.6±1.8	3.3±0.0	1.1	0.9

The lowest ionic strength buffers (initial buffers) contained 30 mM NaCl for MAb-A and no NaCl for MAb-B.
The standard deviation of Z potential and Net charge was approximately less than 2.5 mV and 2.5, respectively

3.3.4 Aggregation propensities of MAbs during storage under accelerated conditions at 40°C or under freeze-thaw stress

Stability assessments under accelerated storage conditions at 40°C or freeze-thaw cycles were conducted for MAb-A and MAb-B at pH 5 and pH 7. In the present study, changes in the aggregate profile were evaluated by SEC, DLS, and turbidity in order to monitor the wide range of aggregates in terms of size (Engelsman et al., 2011).

Fig. 3.4 shows the aggregation rates of MAb-A and MAb-B at pH 5 and pH 7. The aggregation rates during storage at 40°C decreased as the NaCl concentration increased for MAb-A at pH 5 (Fig. 3.4A) and pH 7 (Fig. 3.4B), and MAb-B at pH 7 (Fig. 3.4D). These results suggested that NaCl effectively improved the solution stability at 40°C. In contrast, the aggregation rate of MAb-B increased with increasing the NaCl concentration at pH 5 (Fig. 3.4C), indicating a destabilizing effect of NaCl. Under freeze-thaw stress, aggregation was suppressed in MAb-A at pH 7 (Fig. 3.4B) but accelerated in MAb-B at pH 5 (Fig. 3.4C) as the NaCl concentration increased. The trends in aggregation rates as a function of the NaCl concentration under freeze-thaw stress were in good qualitative agreement with those for storage at 40°C. MAb-A at pH 5 showed the opposite trend in aggregation rates under freeze-thaw stress to those for storage at 40°C. In this case, aggregation was accelerated by freeze-thaw stress but was suppressed for storage at 40°C as the NaCl concentration increased (Fig. 3.4A). MAb-B at pH 7 showed unique aggregation rate behavior under freeze-thaw stress. The aggregation rates slightly decreased with increasing the NaCl concentration from 70 mM to 300 mM, which was the same trend as those for storage at 40°C (Fig. 3.4D). However, different from the storage at 40°C, the aggregation rate was well suppressed significantly in the absence of NaCl, which was out of line in terms of the relation between the aggregation rate and NaCl concentration.

The addition of sugars slightly improved the aggregation propensities under storage at 40°C

for MAb-A at pH 5 and pH 7 (Figs. 3.4A and B). No significant differences were observed for MAb-B, and the aggregation rates in formulations containing sugars were identical to those under the lowest ionic strength conditions in the absence of sugars (Figs. 3.4C and D).

In this stability assessment, the initial level of the small soluble aggregates at each pH for MAb-A and MAb-B were almost equivalent regardless of the buffer composition (Table 3.2). Both the DLS and turbidity measurements showed that neither submicron particulates nor insoluble aggregates were formed in any of the buffers before or after the acceleration test at 40°C and under freeze-thaw stress.

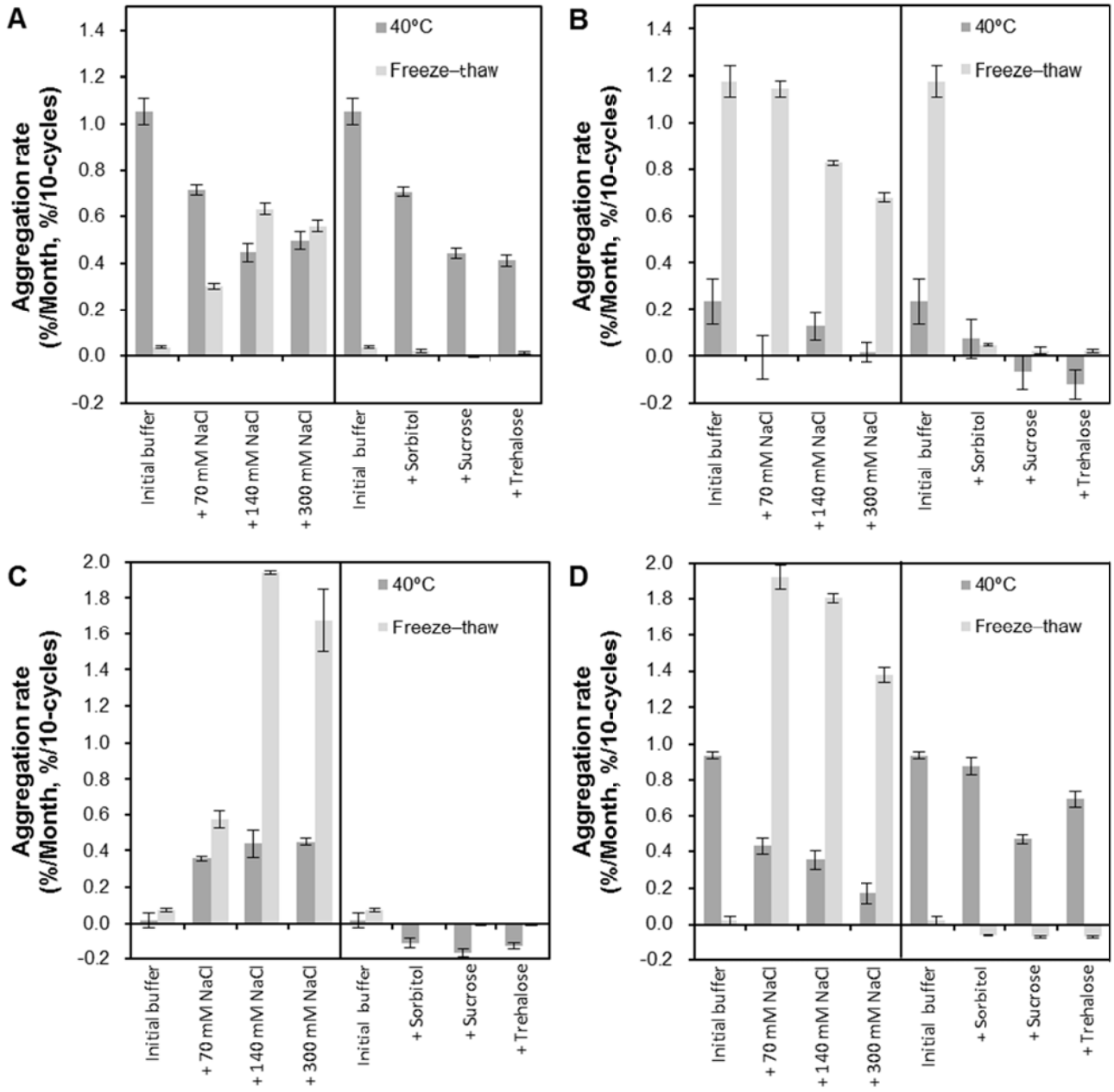

Figure 3.4. Quantification of aggregates by SEC

MAbs were degraded by storing them at 40°C for one month and 10 freeze-thaw cycles. The increase in the rate of aggregation was estimated from the increase in the population of aggregates after storage at 40°C (%/Month) and freeze-thawing (%/10-cycles) (**A**: MAb-A at pH 5, **B**: MAb-A at pH 7, **C**: MAb-B at pH 5, **D**: MAb-B at pH 7). A negative aggregation ratio indicates a decrease in aggregates compared with the initial measurement. The error bars were estimated from three independent experiments performed under the same conditions.

Table 3.2 Influence of formulations on the aggregation propensity

	pH	Formulation	Starting level of aggregates (%)	Aggregation rate		
				40ºC (%/Month)	25ºC (%/Month)	Freeze-thaw (%/10-cycles)
MAb-A	5	Initial buffer	1.71±0.03	1.06±0.06	0.18±0.00	0.04±0.01
		70 mM NaCl	1.74±0.01	0.72±0.02	0.10±0.00	0.30±0.01
		140 mM NaCl	1.72±0.02	0.45±0.04	0.04±0.00	0.63±0.02
		300 mM NaCl	1.73±0.01	0.50±0.04	0.00±0.00	0.56±0.02
		Initial buffer	1.71±0.03	1.06±0.06	0.18±0.00	0.04±0.01
		+Sorbitol	1.73±0.02	0.71±0.02	0.07±0.00	0.02±0.01
		+Sucrose	1.74±0.02	0.45±0.02	0.04±0.00	0.00±0.01
		+Trehalose	1.75±0.02	0.41±0.03	0.06±0.00	0.01±0.01
	7	Initial buffer	1.80±0.01	0.24±0.10	0.08±0.01	1.17±0.07
		70 mM NaCl	1.94±0.00	-0.01±0.09	-0.02±0.00	1.14±0.03
		140 mM NaCl	1.91±0.00	0.13±0.06	-0.04±0.00	0.83±0.01
		300 mM NaCl	1.89±0.01	0.02±0.04	-0.04±0.00	0.68±0.02
		Initial buffer	1.80±0.01	0.24±0.10	0.08±0.01	1.17±0.07
		+Sorbitol	1.85±0.01	0.07±0.08	0.04±0.01	0.05±0.01
		+Sucrose	1.88±0.01	-0.07±0.07	-0.04±0.01	0.02±0.01
		+Trehalose	1.89±0.00	-0.12±0.06	-0.05±0.00	0.02±0.01
MAb-B	5	Initial buffer	1.30±0.00	0.02±0.04	0.00±0.00	0.07±0.01
		70 mM NaCl	1.36±0.00	0.36±0.01	0.12±0.00	0.57±0.05
		140 mM NaCl	1.38±0.00	0.44±0.08	0.13±0.00	1.94±0.01
		300 mM NaCl	1.38±0.00	0.45±0.02	0.13±0.00	1.68±0.18
		Initial buffer	1.30±0.00	0.02±0.04	0.00±0.00	0.07±0.01
		+Sorbitol	1.29±0.00	-0.11±0.03	-0.04±0.00	-0.01±0.00
		+Sucrose	1.29±0.00	-0.17±0.02	-0.06±0.00	-0.01±0.00
		+Trehalose	1.30±0.00	-0.13±0.02	-0.04±0.00	-0.01±0.00
	7	Initial buffer	2.45±0.00	0.94±0.02	0.36±0.01	0.02±0.02
		70 mM NaCl	2.31±0.00	0.43±0.04	0.12±0.03	1.92±0.07
		140 mM NaCl	2.29±0.00	0.36±0.05	0.12±0.01	1.81±0.03
		300 mM NaCl	2.23±0.00	0.17±0.05	0.10±0.01	1.38±0.04
		Initial buffer	2.45±0.00	0.94±0.02	0.36±0.01	0.02±0.02
		+Sorbitol	2.36±0.00	0.88±0.05	0.41±0.02	-0.06±0.00
		+Sucrose	2.34±0.00	0.47±0.02	0.35±0.01	-0.07±0.00
		+Trehalose	2.37±0.00	0.69±0.05	0.28±0.00	-0.07±0.01

The lowest ionic strength buffers (initial buffers) contained 30 mM NaCl for MAb-A and no NaCl for MAb-B.

3.3.5 Conformational stability assessment by DSC

DSC was performed to investigate the contribution of the conformational stability to aggregation propensities in the presence and absence of sugars. T_{max} values, which were defined as the transition temperature of the highest endothermic peak, are summarized in Table 3.3, and their heat capacity curves are shown in Fig. 3.5. Both MAb-A and MAb-B had higher T_{max} values in the presence of sugars under the lowest ionic strength conditions, indicating that sugars improved the thermal stabilities of MAbs.

Table 3.3 Effect of sugars on conformational stability assessed by DSC

pH	Formulation	T_{max} (°C)	
		MAb-A	MAb-B
5	Initial buffer	68.6	76.9
	+Sorbitol	69.7	77.7
	+Sucrose	70.1	78.0
	+Trehalose	70.6	77.9
7	Initial buffer	68.5	67.7
	+Sorbitol	69.2	74.4
	+Sucrose	69.6	74.8
	+Trehalose	69.6	74.8

The lowest ionic strength buffers (initial buffers) contained 30 mM NaCl for MAb-A and no NaCl for MAb-B.
The standard deviation of T_{max} was approximately less than 0.1ºC.

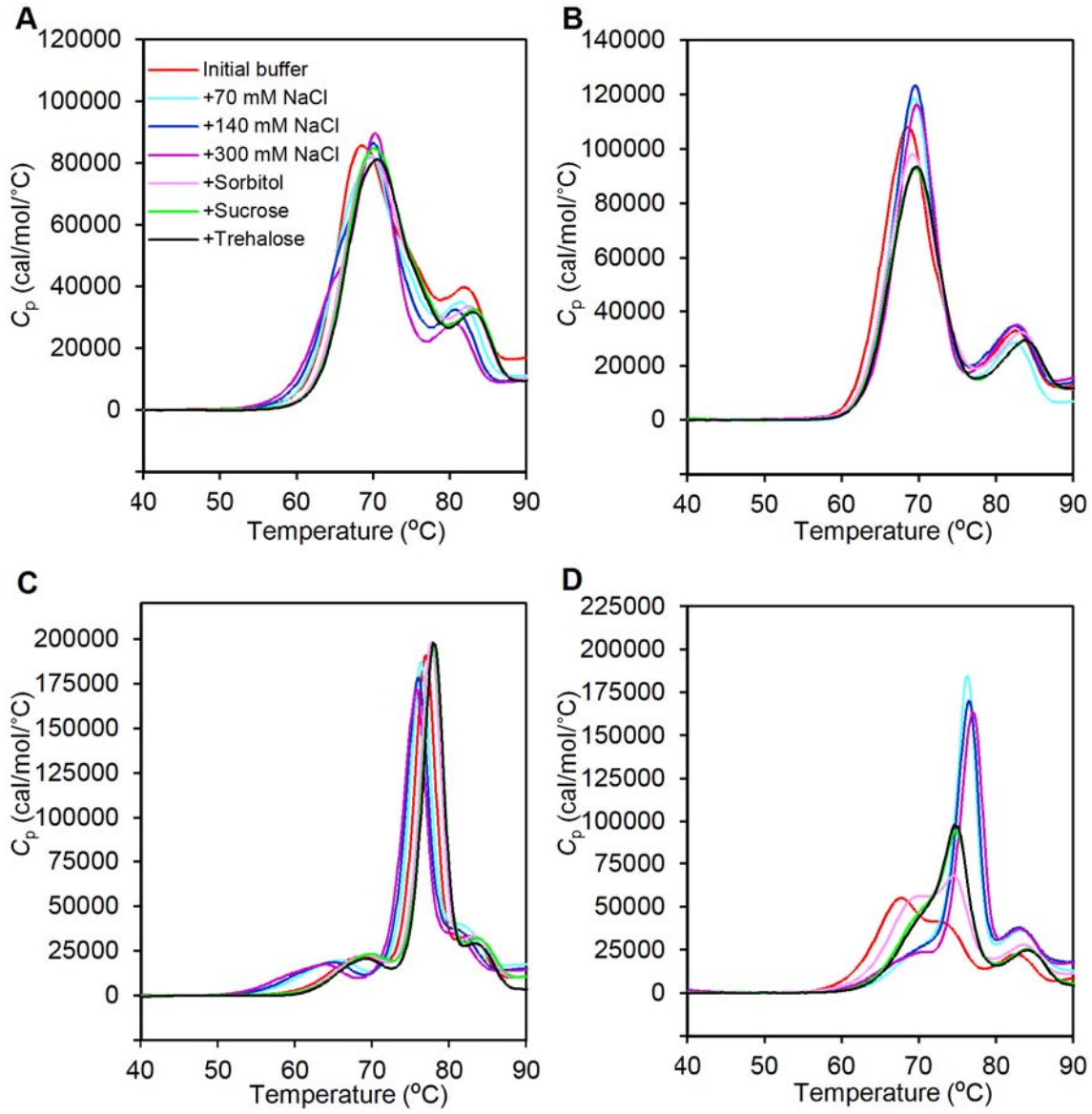

Figure 3.5. Thermal unfolding curves in different formulations

Thermal unfolding curves in formulations containing different concentrations of NaCl and different sugars were obtained using DSC for MAb-A at pH 5 (**A**), MAb-A at pH 7 (**B**), MAb-B at pH 5 (**C**), and MAb-B at pH 7 (**D**).

3.3.6 Electrostatic potential surfaces

The electrostatic potential surfaces of MAb-A and MAb-B were simulated as a function of ionic strength at pH 5 and pH 7, as shown in Fig. 3.6. The positive potential (+1 k_BT/e) and negative potential (-1 k_BT/e) isovalue surfaces are presented as blue and red areas, respectively. MAb-A at pH 5 and at an ionic strength of 40 mM had a positive potential surface over its structure except for the negative potential surface area around the CDR region (Fig. 3.6A). At pH 7 and an ionic strength of 40 mM, the negative potential surface increased slightly, whereas the positive potential surface decreased significantly and a negative potential surface appeared around the center of the molecule (Fig. 3.6C). In the case of MAb-B at pH 5 and an ionic strength of 10 mM, a large positive potential surface covered the entire structure and hardly any negative potential surface was observed (Fig. 3.6E). At pH 7, the positive potential surface decreased drastically, and small potential patches appeared around the center of the molecule (Fig. 3.6G). For all the MAbs, these distinct large potential surfaces observed at low ionic strength completely disappeared and many small potential surfaces appeared at an ionic strength of 310 mM (Figs. 3.6B, D, F, and H).

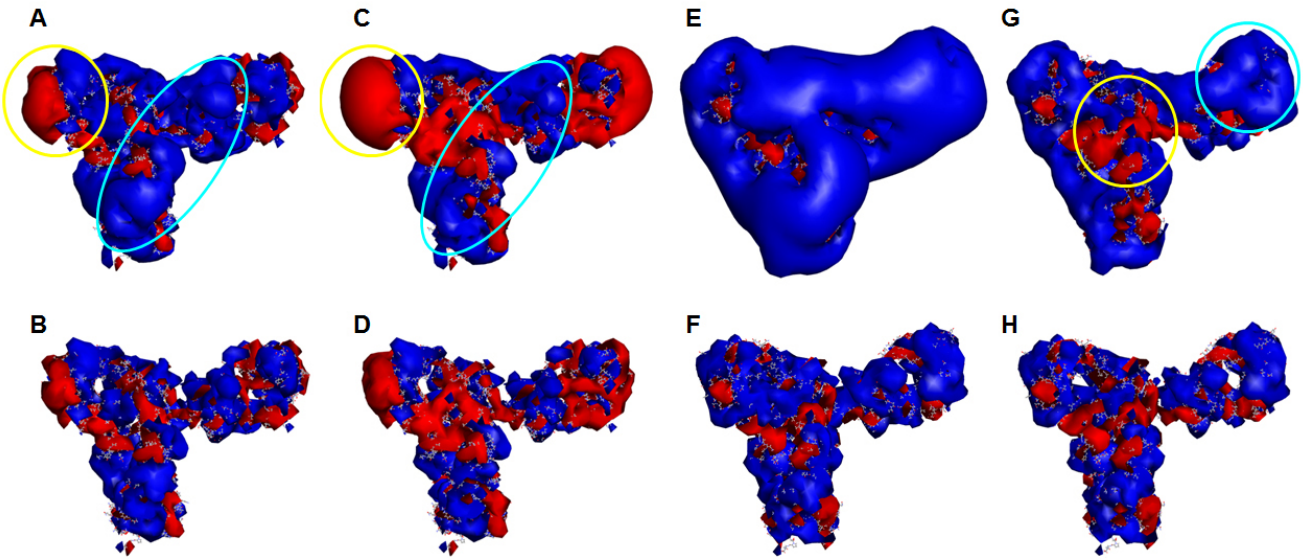

Figure. 3.6. Electrostatic potential surfaces of MAbs at different ionic strengths and pHs
A, **B**: MAb-A at pH 5; **C**, **D**: MAb-A at pH 7; **E**, **F**: MAb-B at pH 5; **G**, **H**: MAb-B at pH 7.
A, **C**, **E**, and **G** describe the electrostatic potential surface at the lowest ionic strength (40 mM ionic strength for MAb-A and 10 mM ionic strength for MAb-B), and **B**, **D**, **F**, and **H** describe those at an ionic strength of 310 mM. Isovalue surfaces are represented in blue and red as positive (+1 k_BT/e) and negative (-1 k_BT/e) charged surfaces, respectively.

3.4 Discussion

3.4.1 Relationship between colloidal stability and net charge

Under accelerated storage conditions at 40°C, at which the MAbs maintained their folded state (Fig. 3.5), the aggregation propensities were in quantitatively good agreement with the colloidal stability assessed from the values of B_2 (Figs. 3.1 and 3.4). We first tried to interpret these observations according to the DLVO theory, which accounts for the interaction between two identical molecules in solution. The DLVO theory states that the dispersity of a molecule is

determined by the sum of two major intermolecular forces, namely, charge–charge and van der Waals interactions. The van der Waals interactions are dispersive forces that are effective over shorter intermolecular distances than charge–charge interactions. The magnitude of intermolecular forces depends on the intermolecular distance between two molecules (Chari et al., 2009). For spherical colloidal particles, charge–charge and van der Waals interactions induce repulsive and attractive intermolecular interactions, respectively. Charge–charge interactions are long-range intermolecular interactions; they are inversely proportional to the intermolecular distance between two molecules and can be significant even at distances of 1.5–2.0 nm under conditions of low ionic strength (Chari et al., 2009). When the electrostatic repulsion is significantly greater than the van der Waals force, the molecules can stably disperse. Charge–charge interactions are directly related to the charge states on the surfaces of molecules and are affected by environmental conditions, such as the dielectric constants of the solvent and ionic solutes. We therefore determined the net charge to estimate the degree of electrostatic repulsion that enhances colloidal stability. In contrast to the recent report by Lehermayer et al. (2011) in which B_2 was shown to increase as the net charge increased, the correlation of net charge with B_2 holds in only a limited number of cases, and therefore, the aggregation propensity is not always predictable from the net charge (Figs. 3.3 and 3.4). The DLVO theory regards particles as spherical molecules with uniform charge distributions on their surfaces. In some cases, the localization of positive and negative charges are heterogeneous in proteins composed of multi-domains, such as MAbs. These uneven distributions of charges can induce attractive interactions even if the apparent net charge is positive. In MAb-A, the absolute values of the net charges were approximately +5 to +7 under low ionic strength at pH 5 and pH 7 (Fig. 3.3A). Increasing the NaCl concentration to 140 mM reduced the net charge to approximately +2 k_BT/e, which is one-third of that under low ionic strength. Contrary to the prediction based on the uniform charge distribution model, aggregation decreased as the NaCl concentration increased

(Figs. 3.4A and B). These trends in aggregation propensities as a function of the NaCl concentration were the inverse of the trends for the relationship to net charge. Thus, again, the net charge does not always reflect colloidal stability. Unexpectedly, the net charge was reduced by the addition of sugars. Cosolvents, including sugars, change the hydration state of proteins through a preferential hydration mechanism and/or preferential interaction between sugars and proteins (Liu et al., 1995, Timasheff, 1998, Kaushik et al., 2003), which might change the electrostatic state of MAbs.

3.4.2 Molecular origins of aggregation propensities

In the present study, the MAbs showed distinct dependencies of B_2 on pH or ionic strength, as shown in Figs. 3.1 and 3.2, indicating that colloidal stability was sensitive to pH and ionic strength. The interaction between two protein molecules can be described by B_{22}:

$$B_{22} = -\frac{1}{2}\frac{N_A}{M_W^2}\int\left(e^{-W_{22}/k_BT} - 1\right)\ 4\pi r^2 dr \tag{3.4}$$

,where T is the temperature, r is the center-to-center separation of the two solute molecules, N_A is Avogadro's number, and W_{22} is described as follows:

$$W_{22}(r) = W_{hs}(r) + W_{charge}(r) + W_{disp}(r) + W_{osm}(r) + W_{dip}(r) + W_{ass}(r) \tag{3.5}$$

,where W_{hs} represents the hard sphere potential, W_{charge} is the energetic potential comprising charge–charge interactions, W_{disp} is the dispersion (van der Waals) attractive potential, W_{osm} is the attractive potential resulting from the osmotic effect of high salt concentrations, W_{dip} represents the

interactions arising from the permanent and induced dipole moments of the molecules, and W_{ass} is the square-well interaction, which accounts for protein self-association. The square-well potential results from strong short-range interactions, such as hydrophobic interactions, hydrogen bonds, and ionic bonds (Curtis et al., 1998). This equation, Eq. 3.4, was originally proposed by McMillan and Mayer (1945), and theoretical and experimental studies address the contribution of each term to the overall potential (Curtis et al., 1998, Elcock and McGammon, 2001, Kumar et al., 2011). In Eq. 3.5 for W_{22}, W_{hs} and W_{charge} generate repulsive forces, while other potentials generate attractive forces. At concentrations of <10 mg/mL where B_2 was determined, the minimum average intermolecular distance between MAbs is 30 nm. At this concentration range, electrostatic repulsion (W_{charge}), which is a long-range interaction, is effective and the dominant contribution to W_{22} (Chari et al., 2009). The addition of salts suppresses electrostatic repulsion (W_{charge}), resulting in a reduction in colloidal stability. Aggregation and/or reductions in solubility are therefore promoted by increased salt concentrations. In our present study, MAb-B, MAb-C, and MAb-D demonstrated excellent colloidal stabilities at pH 5 with strong repulsive intermolecular interactions in the absence of NaCl as indicated by their high B_2 values [$B_2 > 40 \times 10^{-5}$ (mL mol)/g^2]. Significant suppression of repulsive forces was observed in the presence of 300 mM NaCl as apparent from the small B_2 values [$B_2 < 3 \times 10^{-5}$ (mL mol)/g^2]. Likewise, suppression of repulsive forces was observed in all MAbs at pH values resulting in positive B_2 values at low NaCl concentrations (Fig. 3.2). In these cases, W_{charge} contributes significantly to W_{22} as repulsive intermolecular interaction. The salt concentration in the formulation therefore requires minimization. Exceptionally, positive B_2 for MAb-D at pH 7, approximately 2×10^{-5} (mL mol)/g^2, was unchanged by the addition of NaCl (Fig. 3.2D). One possible explanation for the positive value of B_2 for MAb-D at pH 7, even under low ionic strength, is a contribution not from electrostatic repulsion but from the excluded volume as discussed later.

W_{hs} might potentially contribute to the repulsive forces represented by W_{22}. The contribution of W_{hs} by each MAb to B_{22} was estimated using Eq. 3.6, describing the excluded volume (Winzor et al., 2007):

$$B_{22} = \frac{16\pi N_A R_2^3}{3} + \frac{Z_2^2\left(1+2\kappa R_2\right)}{4I\left(1+\kappa R_2\right)^2} \qquad (3.6)$$

,where Z is the net charge, I is the ionic strength, and κ is the inverse screening length, calculated from the molar ionic strength as $3.27 \times 10^7\sqrt{I}$ (cm^{-1}). The estimated values were approximately 4–5 $\times 10^{-5}$ (mL mol)/g^2, with the assumption that MAbs are spheres with a diameter of 9 nm. The contribution of excluded volume to B_2 are less than one-eighth of B_2 values [40×10^{-5} (mL mol)/g^2] for the MAbs with higher colloidal stability, such as in the cases of MAb-B, MAb-C, and MAb-D at pH 5. This indicates that the electrostatic repulsion (W_{charge}) is dominant in influencing colloidal stability at the lowest ionic strength. In contrast, at high ionic strength, W_{charge} contributes little to the repulsive forces, and W_{hs}, the excluded volume potential, becomes dominant for positive B_2 values. Notably, MAb-A at pH 5 and pH 6, and MAb-B, MAb-C, and MAb-D at all pH values had similar B_2 values, $0 < B_2 < 3 \times 10^{-5}$ (mL mol)/g^2, in the presence of 300 mM NaCl which were close to those estimated from the excluded volume, 4–5 $\times 10^{-5}$ (mL mol)/g^2, (Fig. 3.2). Exceptionally, in MAb-A at pH 7, the B_2 values [6×10^{-5} (mL mol)/g^2] were slightly higher than those calculated from the excluded volume. This phenomenon could be explained by findings that anion binding generates repulsive interactions among protein molecules (Collins et al., 1997, Collins et al., 2004, Fesinmeyer et al., 2009). The marginally positive value of B_2 for MAb-A at pH 5 could also be attributed to binding of anions, which would mainly occur at positively charged patches on the MAb-A. Note the uneven charge distribution on the surface of MAb-A (Figs. 3.6A and C, also see discussion below). Considering the pI (6.7) of MAb-A, the total area of positively charged patches

on MAb-A at pH 7 is smaller than that at pH 5 (Figs. 3.6A and C); therefore, anion binding is less effective at pH 5 than at pH 7.

When B_2 is negative at the lowest ionic strength, like the cases of MAb-A at pH 5 and pH 7, and MAb-B at pH 7, according to Eq. 3.5, the possible contributions to attractive potentials are W_{disp}, W_{osm} W_{dip}, and W_{ass}. The osmotic attraction (W_{osm}) is not important at the low salt concentrations tested in the present study (Asakura and Oosawa, 1954, Asakura and Oosawa 1958, Curtis et al., 1998). Furthermore the dispersion force (W_{disp}) and the square-well interaction (W_{ass}) are short-range intermolecular interactions; therefore, they contribute little to attractive interactions at the concentrations used here. However, the dipole-related interaction (W_{dip}), which is effective over relatively long molecular distances, can play a dominant role in attractive interactions (Elcock et al., 2001). Note that increases in the NaCl concentration enhanced colloidal stability in some cases, such as that observed for MAb-A at all pH values, MAb-B and MAb-C at pH 7 and pH 8, and MAb-D at pH 8 (Fig. 3.2). Specifically, the stabilities of MAb solutions with negative B_2 values improved as the ionic strength increased. Such cases imply the presence of attractive dipolar electrostatic interactions that are progressively screened at higher salt concentrations. Salts, therefore, represent a two-edged sword, reducing or enhancing the colloidal stability depending on either repulsive or attractive intermolecular interaction.

3.4.3 Relationship between electrostatic interactions and electrostatic potential surfaces

The electrostatic potential surfaces simulated according to the Poisson–Boltzmann equation show uneven localizations of negative (-1 k_BT/e) and positive (+1 k_BT/e) potential surfaces, particularly for MAb-A at an ionic strength of 40 mM at pH 5. The positive potential surface

covered most of the molecules, with an exception around the F_V region, where a negative potential surface was observed (Fig. 3.6A). This uneven localization of negative and positive potential surfaces is consistent with the large negative B_2 value [-8×10^{-5} (mL mol)/g^2] of MAb-A at pH 5 under low salt conditions, suggesting the presence of dipolar attractive electrostatic interactions. Yadav et al. (2012) also suggested that uneven localizations of positive and negative potential surfaces were attributable to attractive interactions, resulting in viscosity enhancement. In contrast, MAb-B at pH 5 showed an evenly distributed electrostatic potential surface with the positive potential surface covering the entire structure, and hardly any negative potential surface was observed (Fig. 3.6E). The positive potential surface occupied a larger volume than the actual molecular size. This large positive potential surface is considered to contribute to strong repulsive intermolecular interactions. Indeed, the presence of strong repulsive interactions was indicated by the large positive B_2 values [$B_2 > 50 \times 10^{-5}$ (mL mol)/g^2], which require a large contribution from W_{charge}, as illustrated above, besides that from W_{hs} [5×10^{-5} (mL mol)/g^2] in Eq. 3.5.

The electrostatic potential surfaces at higher ionic strengths showed significant reductions in the large potential surfaces (Figs. 3.6B, D, F, and H). The large potential surfaces disappeared and small potential surfaces were distributed sparsely over the molecule. The volume occupied by the potential surface became as small as the molecular size, in contrast to those at low ionic strengths. These potential surfaces contributed to the small repulsive intermolecular interactions, as indicated by B_2. These findings support the observation that the dispersity was enhanced by increasing the salt concentration for MAb-A at pH 5. Uneven localization of large negative and positive potential surfaces should therefore be eliminated to prevent attractive electrostatic interactions.

In the case of humanized IgG_1, all MAbs have the same amino acid sequences and three-dimensional structures in a constant region: this provides a strong positive potential surface

around pH 5–6, which is a condition frequently used for MAb formulations. Designing the amino acid sequence in the variable region avoids negative potentials and is therefore a promising approach of generating stable MAbs with low aggregation propensities. It should be noted that the positive potential surfaces that are dominant at pH 5 weaken at pH 7, and then negative potential surfaces appear in the constant region, resulting in uneven localization of the potential surfaces. Consistently, the presence of attractive interactions was indicated by B_2 for both MAb-A and MAb-B at pH 7. The simulation of the electrostatic potential surfaces should therefore be conducted with consideration of the pH and ionic strength.

3.4.4 Effects of colloidal and conformational stabilities on aggregation of MAbs stored at 40°C

As shown in Fig. 3.7, linear correlations were observed between B_2 values and aggregation rates in the formulations containing different concentrations of NaCl, indicating that B_2 representing the colloidal stability well reflects the aggregation propensities for all the MAbs under accelerated storage condition at 40°C, which are normally used in stability tests. These results suggest that electrostatic interactions make major and quantitative contributions to the aggregation propensities of these MAbs and can therefore be predicted from the experimental estimates of B_2. It is important to note that aggregation was suppressed almost completely when B_2 was sufficiently positive; empirically $B_2 > 40 \times 10^{-5}$ (mL mol)/g^2.

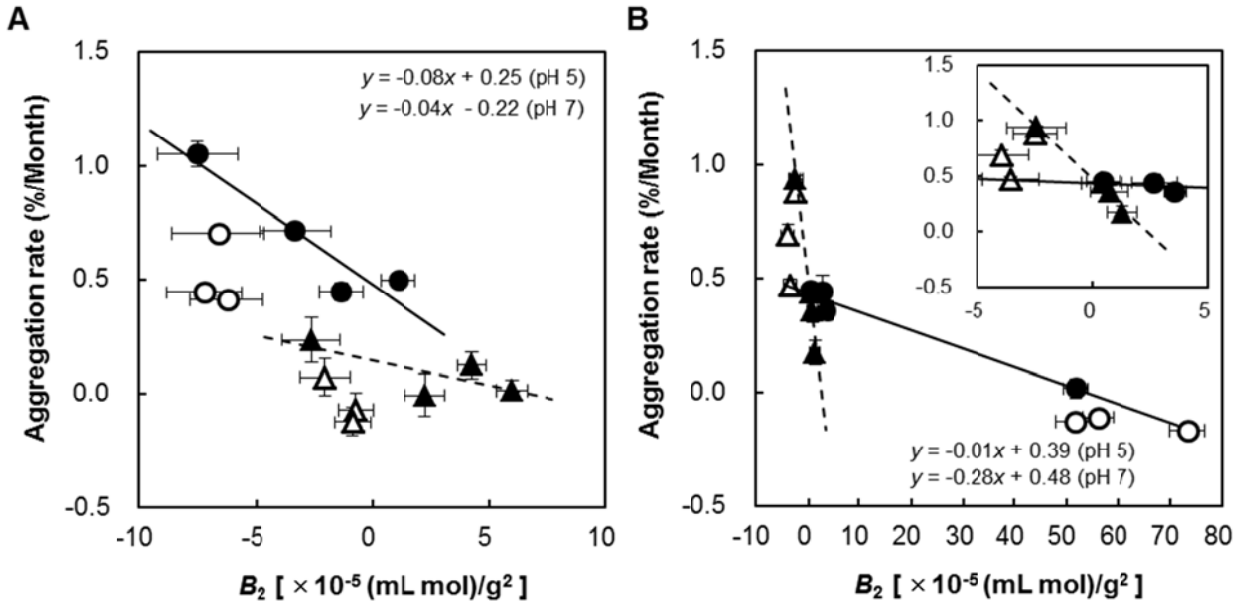

Figure 3.7. Correlation of B_2 with aggregation propensity for storage at 40°C

MAb-A (**A**) and MAb-B (**B**) at pH 5 (circles) and pH 7 (triangles); filled symbols represent formulations containing NaCl and open symbol represents formulations containing sugars. Linear regression was generated from formulations excluding those containing sugars. The correlation coefficients were R = -0.939 (MAb-A: pH 5), R = -0.719 (MAb-A: pH 7), R = -0.986 (MAb-B: pH 5), and R = -0.992 (MAb-B: pH 7). The error bars were estimated from three independent experiments performed under the same conditions.

The B_2 values for the formulations containing sugars also corresponded well with the aggregation propensities. The aggregation rates were, however, slightly lower than the values predicted from B_2 for MAb-A (open symbols, Fig. 3.7). This stabilization effect by sugars is attributed to factors other than colloidal stability. The different aggregation pathways related to conformational stability should be considered, particularly heat-induced aggregation resulting from structural and chemical perturbations. The T_{max} values determined from the formulations containing sugars were higher than those in the initial buffer for all MAbs (Table 3.3). These improvements in conformational stability contribute, in part, to the slight improvements in aggregation propensities

in the presence of sugars for MAb-A at pH 5 and pH 7, and MAb-B at pH 7. To evaluate the relationship between the enhancement of T_{max} and the degree of increase in conformational stability, we calculated ΔG_{FU} at 40°C ($\Delta G_{FU, 313.15K}$) using ΔH, ΔC_p, and T_{max} obtained from DSC, assuming that the unfolding of MAbs occurs in a two-state manner. This calculation provides only a rough estimate, because MAbs unfold through multiple intermediates, which is different from the two-state unfolding of small proteins we studied previously (Uchiyama et al., 2002). The 2K difference in the T_{max} values of MAb-A in initial buffer (T_{max} = 68.8°C) and that in the buffer containing trehalose (T_{max} = 70.8°C) at pH 5 corresponds to a difference in $\Delta G_{FU, 313.15K}$ ($\Delta\Delta G_{FU, 313.15K}$) of 1.6 kcal/mol, implying that the population of unfolded molecules in the initial buffer is 10-times higher than that in the buffer containing 10% trehalose. This may contribute to the difference in the aggregation propensity after 4 weeks of storage at 40°C. Consistent with our estimate above, Kaushik and Bhat reported stabilization of lysozyme by 2.22 kcal/mol with 1 M (34%) trehalose (Kaushik et al., 2003). It should be noted that in the present study, the heat capacity change upon unfolding (Fig. 3.5), ΔC_p, was decreased by the addition of sugars. A decrease in ΔC_p generally results in a shallower dependence of ΔG_{FU} on temperature (Kaushik et al., 2003); therefore, the addition of sugars may stabilize MAbs over a broad range of temperatures.

The T_{max} values for MAb-B at pH 5 were higher in the presence of sugars than those at the lowest ionic strength, whereas the stabilization effect was not observed in aggregation propensities. The T_{max} values of MAb-B at pH 5 were higher than those determined under other conditions, indicating superior conformational stability even in the absence of sugars. This may explain why the contribution of conformational stability was not significant for MAb-B at pH 5.

In Chapter 2 and the current chapter, B_2 was measured at 20°C using AUC-SE. As already mentioned, the value of B_2 at 20°C correlated significantly with aggregation propensities at 40°C (Fig. 3.7). This result is consistent with the findings that the B_2 values at 20°C show a linear

correlation with those determined for 40°C as shown in Fig. 3.8. The degree and type of intermolecular interactions are temperature-dependent, and the temperature dependencies of intermolecular interactions are influenced by the buffer components and proteins (Antipova et al., 1999, Valente et al., 2005, Burn et al. 2009). However, in contrast to a study which reported a dramatic change in B_2 induced by a conformational change due to increasing temperature (Burn et al. 2010b), the populations of MAbs in the unfolded state have similar B_2 values at 20°C and 40°C. Consequently, in the present study, the rank order and sign of B_2 values at two different temperatures are consistent with each other. Furthermore, aggregation rates at 40°C were in good agreement with those at 25°C (Fig. 3.9), confirming that determination of B_2 at 20°C accurately reflects the aggregation propensities at both temperatures.

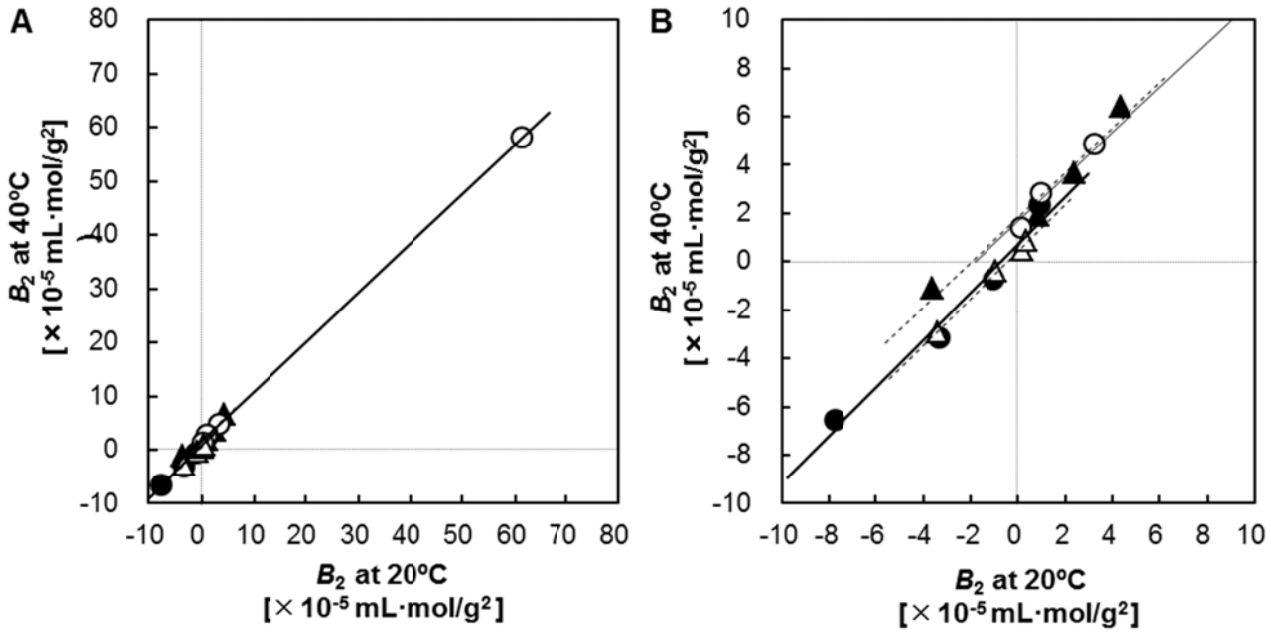

Figure 3.8. Correlation of B_2 at 20°C and 40°C

MAb-A at pH 5 (closed circle, solid line), MAb-A at pH 7 (closed triangle, dotted line), MAb-B at pH 5 (open circle, solid line), and MAb-B at pH 7 (open triangle, dotted line). The correlation coefficients are R = 0.987 (MAb-A: pH 5), R = 0.982 (MAb-A: pH 7), R = 1.000 (MAb-B: pH 5), and R = 0.998 (MAb-B: pH 7). **B** is an expanded figure of **A**.

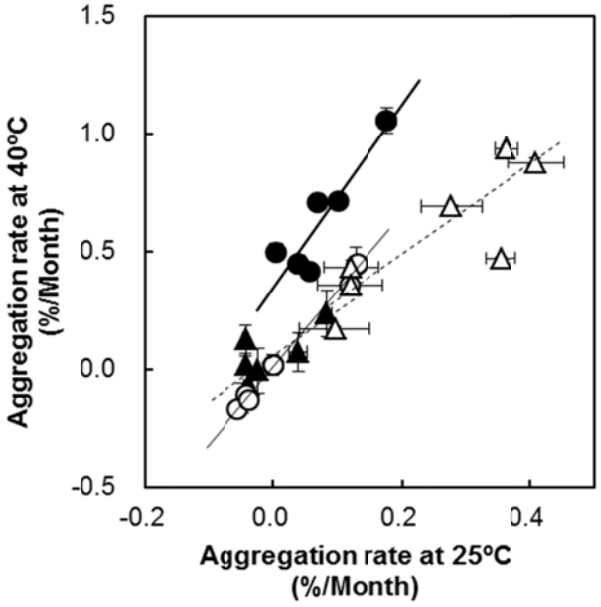

Figure 3.9. Correlation of aggregation rates at 25°C and 40°C

MAb-A at pH 5 (closed circle, solid line), MAb-A at pH 7 (closed triangle, dotted line), MAb-B at pH 5 (open circle, solid line), and MAb-B at pH 7 (open triangle, dotted line). The correlation coefficients were $R = 0.912$ (MAb-A: pH 5), $R = 0.749$ (MAb-A: pH 7), $R = 0.998$ (MAb-B: pH 5), and $R = 0.842$ (MAb-B: pH 7). The error bars were estimated from three independent experiments performed under the same conditions.

3.4.5 Effects of colloidal and conformational stabilities on aggregation during freeze-thaw cycles

Aggregation caused by freeze-thaw cycles is attributed to a combination of various stress factors such as cryo-concentration (Kueltzo et al., 2008), cold denaturation (Griko et al., 1998), generation of an ice–solution interface (Chang et al., 1996), solute crystallization (Izutsu et al., 1994), and shifts in pH (Murase et al., 1989). Cryo-concentration and solute crystallization can

potentially alter colloidal stability because of changes in the intermolecular distances between solutes and the ionic strength of the solution. In contrast, cold denaturation and adsorption to an ice–liquid interface alter the conformational stability by increasing the exposure of the hydrophobic residues buried in the proteins. Thus, aggregation under freeze-thaw stress needs to be assessed in terms of both conformational and colloidal stabilities.

The colloidal stability defined by B_2 failed to explain aggregation behaviors under freeze-thaw stress. This is evident for MAb-A at pH 5 and MAb-B at pH 7. Aggregation rates of MAb-A at pH 5 were effectively suppressed even in the presence of stronger attractive interactions (Fig. 3.4A and 3.10A). Similarly, significant suppression of aggregation was observed in the absence of NaCl in MAb-B at pH7, and B_2 was more attractive than those in the presence of NaCl (Fig. 3.4D and 3.10B). In contrast, the aggregation propensities of all MAbs were significantly improved by sugars, independent of B_2 values (open symbols, Fig. 3.10). Here, enhancements in T_{max} values were observed in the presence of sugars for MAb-A and MAb-B, which correlated qualitatively with aggregation propensities (Table 3.3). It should be noted that sugar suppressed the aggregation under freeze-thaw stress regardless of the NaCl concentration (Fig. 3.11).

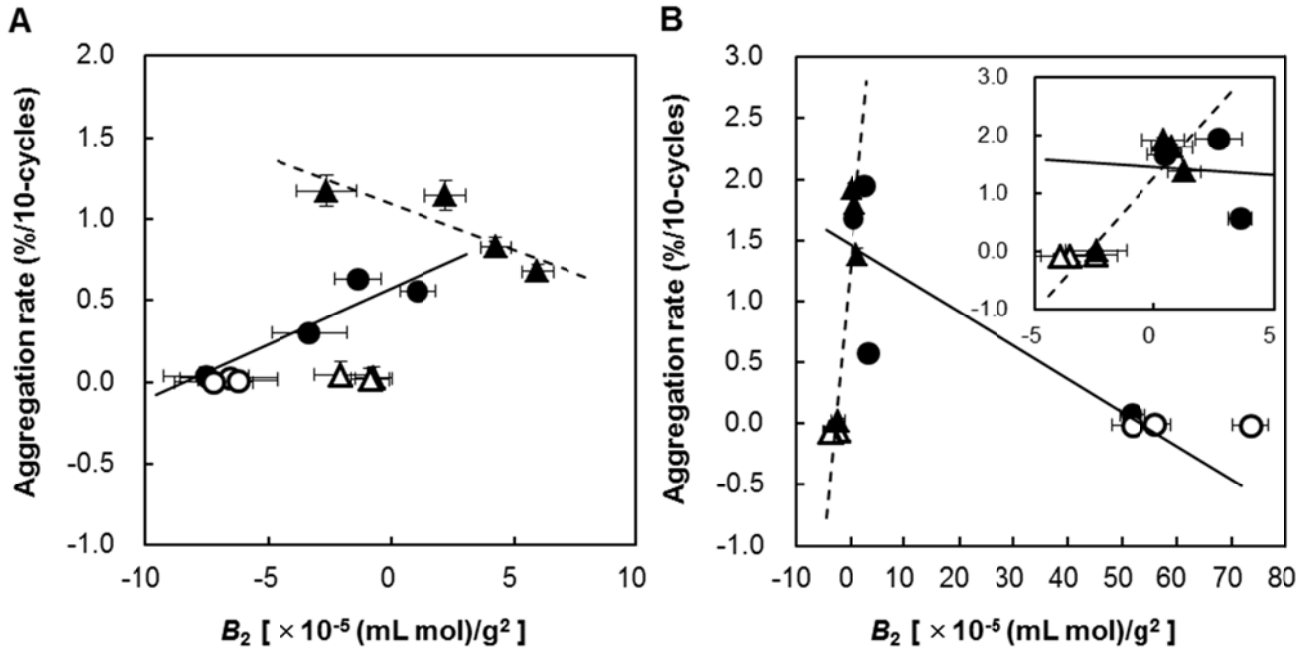

Figure 3.10. Correlation of B_2 with aggregation propensity under freeze-thaw cycles

MAb-A (**A**) and MAb-B (**B**) at pH 5 (circles) and pH 7 (triangles); filled symbols represent formulations containing NaCl and open symbols represent formulations containing sugars. The correlation coefficients from all formulations, excluding those containing sugars, were R = 0.921 (MAb-A: pH 5), R = -0.869 (MAb-A: pH 7), R = -0.765 (MAb-B: pH 5), and R = 0.882 (MAb-B: pH 7). The errors bars were estimated from three independent experiments performed under the same conditions.

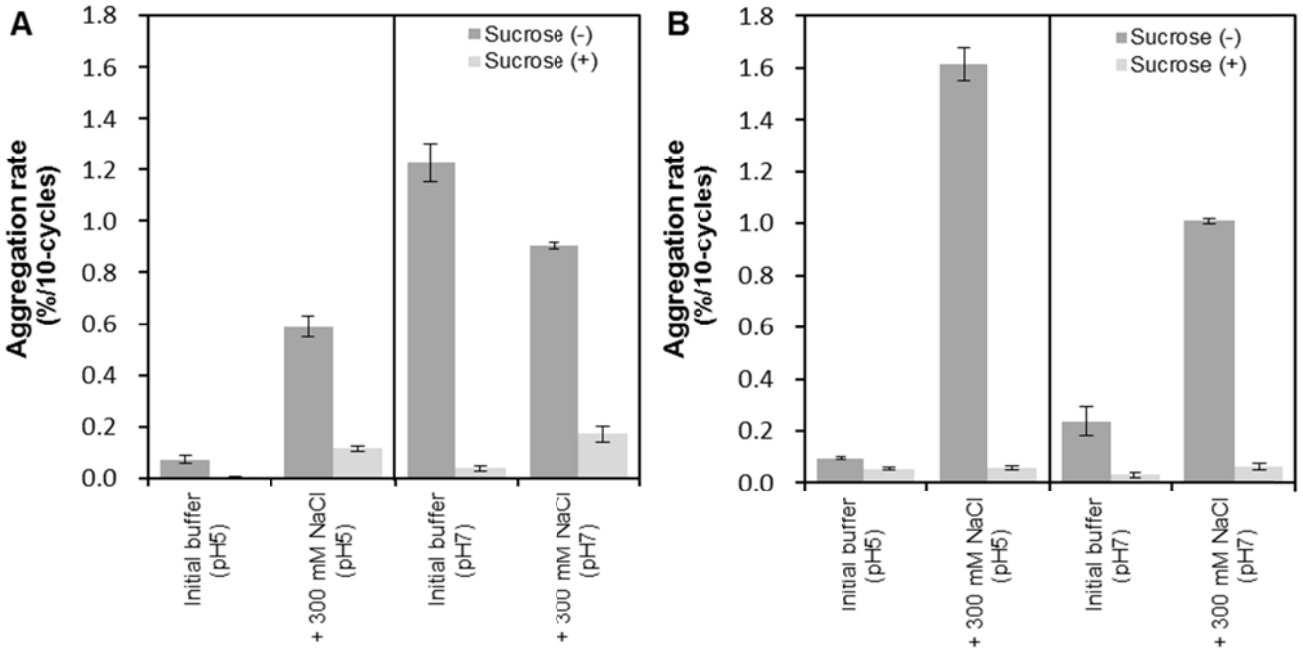

Figure 3.11. Effect of sugars on aggregation propensity under freeze-thaw stress

MAbs were degraded by 10 freeze-thaw cycles in the formulation containing 300 mM NaCl and/or 4% sucrose. The increases in the rate of aggregation were estimated from the increase in the population of aggregates obtained by SEC before and after freeze-thawing (**A**: MAb-A at pH 5 and pH 7; **B**: MAb-B at pH 5 and pH 7). The error bars were estimated from three independent experiments performed under the same conditions.

T_{max} reflects the conformational stability of the Fab domain of all MAbs (Welfle et al., 1999, Garber et al., 2007). The reductions in aggregation propensities in the presence of sugars were therefore attributed to enhanced conformational stability of the Fab domain. Preferentially excluded sugars stabilize protein conformations by localizing water molecules around the protein (Timasheff et al., 2002), resulting in a lower aggregation propensity. This stabilizing effect might play a major role on suppressing the unfolding at the liquid-ice interface boundary under freeze-thaw stress. Although the relationship between unfolding induced by an increase in temperature and those caused by contact with a hydrophobic interface was not fully elucidated here,

our results suggest that conformational stability correlates with aggregation under freeze-thaw stress. Unlike sugars, T_{max} values obtained from buffers containing different concentrations of NaCl did not show clear correlations with aggregation propensities (data not shown). Thus, the relationships of colloidal and conformational stabilities with aggregation under freeze-thaw stress in the presence of salts has not been clarified and requires further investigation.

3.5 Conclusion

In this chapter, in order to develop the optimization strategy for MAb formulation we evaluated colloidal and conformational stabilities of MAbs and then confirmed their relations to the aggregation behaviors. The colloidal stabilities were accurately assessed according to B_2 values obtained from AUC-SE. The net charge reflected the magnitude of the electrostatic interactions, although only partly correlated with the colloidal stability; as observed in this study, the electrostatic attraction and repulsion contributed oppositely to colloidal stability. Salts both stabilize and destabilize the MAbs, depending on the type of electrostatic interaction, i.e., repulsion or attraction. Exact evaluation of the intermolecular interactions is therefore of great importance for optimizing salts in formulations. The electrostatic potential surfaces showed that an uneven localization of potential surfaces contributed to attractive interactions, resulting in higher aggregation propensities. In contrast, the evenly distributed potential surface induced strong repulsive intermolecular interactions. Sugars did not have a significant influence on the colloidal stabilities but improved aggregation propensities at 40°C and under freeze-thaw stress mainly by improving the conformational stability of the Fab fragment. The colloidal and conformational stabilities therefore both contributed to aggregation to different degrees, depending on the stress

factors. In conclusion, assessment of colloidal stability at the lowest ionic strength is particularly effective for the formulation development. If necessary, salts are added to enhance the colloidal stability. Sugars further improve the aggregation propensities, in particular under freeze-thaw stress, by enhancing conformational stability. These behaviors are rationally predictable according to the potential surfaces of MAbs.

On the basis of the finding obtained in the present studies, we present pathways for aggregation and viscosity enhancement in Fig. 3.12. Colloidal stability relates to both aggregation (pathway I) and viscosity enhancement (pathway IV). Conformational stability relates to the aggregation pathways which is initiated by unfolding of the protein. Unfolding of the protein in the native state is induced by two major environmental factors as follows: a temperature increase (pathway II) and/or contact with a hydrophobic interface (pathway III). These multiple pathways, which are influenced by various stress factors, contribute with a different degree to aggregation. Both pathway I and II attributed to aggregation at the accelerated storage condition at 40°C with different degrees. On the other hand, pathway I is not attributed to aggregation under the freeze-thaw stress but pathway III is. Thus, aggregation propensity and viscosity need to be predicted on the consideration of stress factors.

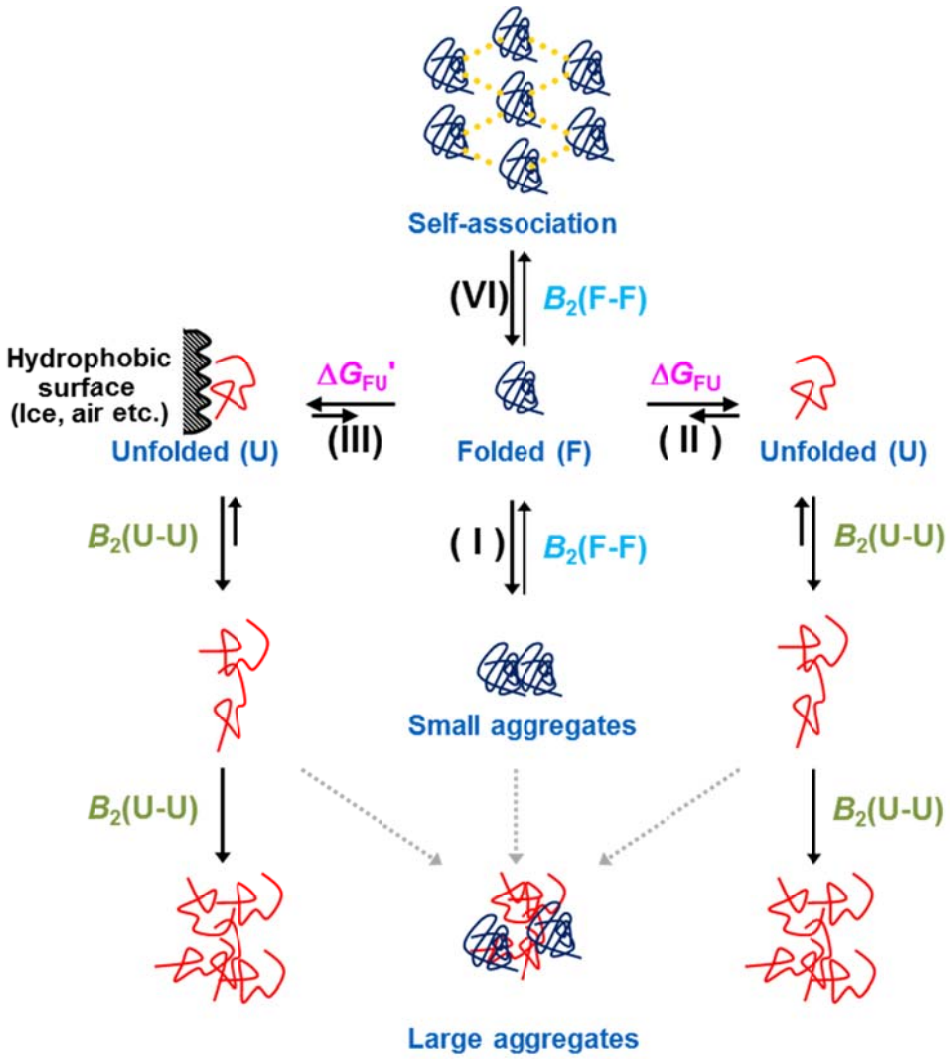

Figure 3.12. Model of viscosity enhancement and aggregation

B_2(F-F) is the second virial coefficient for MAbs in the folded state and B_2(U-U) is the second virial coefficient for MAbs in the unfolded state. ΔG_{FU} and $\Delta G_{FU}'$ are the free energy differences between MAbs in the folded and unfolded states induced by temperature increases or contact with hydrophobic interfaces, respectively.

Chapter 4
Novel strategy for formulation optimization of therapeutic MAbs

4.1 Introduction

As mentioned in Chapters 2 and 3, the solution pH, ionic strength and addition of sugars have significant impact on the physical properties, i.e., aggregation propensity and viscosity, of MAbs. Likewise, the concentration and kinds of surfactant and buffer components, and the concentration of MAb are also parameters, which are known to influence the physical properties of MAbs (Chi et al., 2003a, Bhambhani et al., 2012). Thus, tremendous efforts are necessary to evaluate all these parameters for optimization of MAb formulations. The conventional strategy for formulation optimization are direct assessments of long-term stability and viscosity, which are time consuming and require a large amount of samples. In contrast, prediction of the aggregation propensity and viscosity based on the indicators of colloidal and conformational stabilities allows rational screening of various parameters with small sample requirement.

In this chapter, we proposed a formulation strategy to predict the aggregation propensity and viscosity in terms of colloidal and conformational stabilities on the basis of our findings presented in Chapters 2 and 3. The advantage of our strategy was demonstrated by the comparison with the conventional strategies based on the direct assessments of long-term stability and viscosity in combination with a statistical approach, and based on *in-silico* prediction of aggregation propensities by using the IgG_1 structure model.

4.2 Results and discussion

4.2.1 Relationship between k_D from DLS and B_2 from AUC-SE

The value of k_D, which is obtained from the concentration dependence of the diffusion constant, D_m, is widely used to estimate the degree of intermolecular interactions (Zhang et al., 2003). The k_D is available from DLS in the high-throughput manner, however, poor correlation of k_D with aggregation propensity and viscosity are often observed. We therefore evaluated k_D as a indictor of colloidal stability of MAbs based on the relationship with B_2.

The k_D values of MAb-A and MAb-B in different formulations (Table 3.1) showed a linear relationship with those of B_2 obtained by AUC-SE (Fig. 4.1) in the range $B_2 < 10$ (mL mol)/g^2 showing a good correlation coefficient ($R = 0.95$), providing the following empirical equation:

$$k_D = 1.50 B_2 M_W - 12.4 \qquad (4.1)$$

The intercept of Eq. 4.1 has a larger negative value than that calculated from the previously proposed equation, $k_D = 1.06 A_2 M_W - 8.9$ (Lehermayr et al., 2011), where A_2 is the secondary virial coefficient estimated from light scattering. Winzor et al. (2007) reported that A_2 becomes smaller than B_2 because A_2 reflects the combined contributions of protein self-interactions and protein–buffer interactions due to thermodynamic nonideality. Theoretically, k_D is composed of a thermodynamic term, B_2, and a hydrodynamic term, $\xi_1 + \bar{\nu}$, as shown in the Eq. 2.4 where the frictional drag of the protein, ξ_1, increases with increasing protein solvation. The values of ξ_1 and $\bar{\nu}$ are positive, making a negative contribution to k_D as evidenced from the larger negative intercept in Eq. 4.1. In fact, k_D was negative in several cases in the present study, with AUC-SE giving positive values of B_2 (MAb-A at pH 5 with 300 mM NaCl, MAb-B, MAb-C, and MAb-D at pH 5 with NaCl > 70 mM, Table 3.1). Thus, the determination of the type of intermolecular interaction, i.e. repulsive or attractive, is difficult from k_D due to the contribution of the

hydrodynamic term. Therefore, the conversion of the k_D value according to Eq. 4.1 is necessary to properly estimate the intermolecular interaction. It should be noted that some exceptional relations between k_D and B_2 were observed. When B_2 exceeded 50×10^{-5} (mL mol)/g^2, the k_D values were smaller than those estimated from Eq. 4.1 as shown in Fig. 4.1 (open symbol). In addition, deviation from the linear relationship between B_2 and k_D was also observed in the pH dependence of MAb-C as mentioned in Section 2.4.1, where good correlation was observed between aggregation propensity and B_2 but not k_D (Fig. 2.8). These results suggest that a higher degree of hydration and/or conformational change increase the frictional drag of the MAb. In conclusion, although B_2 from AUC-SE is the most reliable approach, k_D can be used as an indicator of colloidal stability and is useful when high-throughput assay is required. However, the type of interaction needs to be determined according to Eq. 4.1. In addition, it should be kept in mind that k_D has a risk of misleading the intermolecular interaction. Therefore, B_2 from AUC-SE is recommended to estimate the colloidal stability when critical parameters such as pH and ionic strength which potentially change the colloidal stability dramatically.

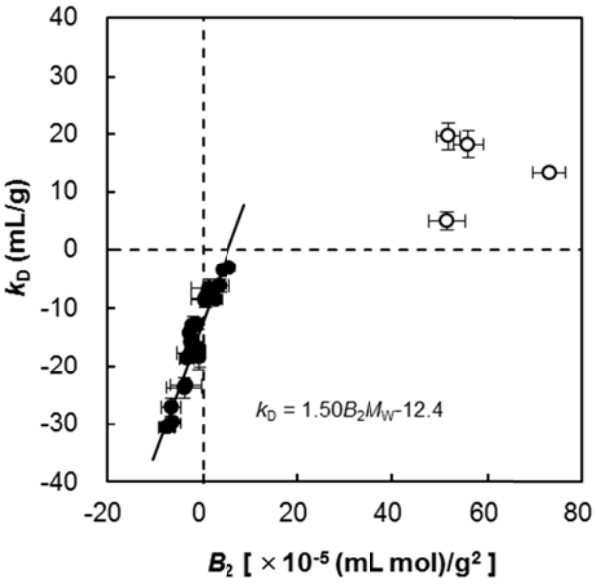

Figure 4.1. Correlation of B_2 with k_D for MAb-A and MAb-B

B_2 was obtained from AUC-SE and k_D was obtained from DLS. Regression lines were obtained from B_2 and k_D in different formulations at pH 5 and pH 7, except for those of MAb-B in the formulations without NaCl at pH 5 (○); these were eliminated for fitting to the regression line because of a deviation from the trend.

4.2.2 Novel strategy for formulation optimization

We suggest an effective strategy for the selection of optimum MAb formulations in Fig. 4.2 based on the finding of our studies. Colloidal stability correlates significantly with aggregation propensity under the storage at 40°C and is strongly influenced by changes in salt concentration, because electrostatic interactions have a large effect on colloidal stability. The contribution of electrostatic interaction to colloidal stability for individual MAb needs to be evaluated in the absence of salts and other excipients, because they potentially shield the electrostatic interaction. In

addition, solution pH drastically changes the electrostatic interaction depending on the pI of proteins. Furthermore, pH is known to change the physical properties of MAb. For example, higher pH accelerates the chemical degradation such as deamidation of asparagine residue. Low pH destabilizes the conformational stability of the Fc domain. The optimization of electrostatic interactions is therefore performed in terms of ionic strength and pH as a first step in the selection of the optimum formulation. Here, the formulation is selected to suppress electrostatic attraction and to enhance electrostatic repulsion.

In a practical experiment, B_2 is first measured at low ionic strength at acidic and neutral pHs. The solution with the pH providing the largest B_2 is selected. If B_2 is positive at the desired pH, salts should not be added, because their addition would lead to a reduction in colloidal stability by cancelling favorable electrostatic repulsions. If B_2 is negative at the desired pH, salts can be added to improve the colloidal stability by cancelling the electrostatic attractions. In the present study, MAb-B, MAb-C, and MAb-D at pH 5 are the preferred formulations and are characterized by large positive B_2 values [$B_2 > 40 \times 10^{-5}$ (mL mol)/g^2]. The second step is the selection of sugars to improve the conformational stability. Basically, sugars are added to improve the freeze-thaw stability. In the experiment, T_{max}, which reflects T_m of the Fab fragment, measurements using DSC are performed in selected formulations containing various sugars. All sugars that we tested slightly differed in their ability to improve stability, therefore the sugars providing the highest T_{max} would be the first choice. The third step, is the further optimization of other parameters such as concentrations of salt, sugar and surfactant and solution pH based on B_2. In formulation development, restrictions in osmolality are often required, depending on the dosage form. In this step, the k_D can be used as an alternative indicator in case the higher throughput analysis is required. However, the negative contribution from hydrodynamic terms should be taken into account. The k_D should not be evaluated as a single value but as trends of values as a function of screening

parameters to avoid an incorrect assessment. In case an abnormal trend is observed, the AUC-SE should be conducted for conformation. As a final step, assessment of stability is performed by the directly measurements of the aggregation propensity.

In summary, the optimum formulation is selected according to the following steps (Fig. 4.2): [1] Assessment of pH and ionic strength on the basis of colloidal stability, [2] selection of sugar on the basis of conformational stability, [3] optimization of formulation on the basis of colloidal stability, and [4] assessment of stability and viscosity by direct measurement in the selected formulation. This approach proposed here could reduce the burden of direct stability assessment which is time consuming and requires a large amount of samples. In practice, an optimum formulation for MAb-A can be predicted according to this strategy. The B_2 value for MAb-A was larger at pH 7 than at pH 5 in the presence of low concentrations of NaCl. The B_2 value was negative even at pH 7, indicating the presence of attractive intermolecular interactions. A formulation containing salts is therefore selected. Moreover, sugars are added to improve the freeze-thaw stability and to enhance conformational stability, providing a higher T_{max}. The selected formulation is at pH 7 and contains salts and sugars. The concentrations and types of salts and sugars are optimized in the third or final step. The tentative formulation is the same as the formulation providing the lowest aggregation propensities under the storage at 40°C and under freeze-thaw stress. For MAb-B, a larger B_2 is obtained at pH 5. The B_2 value is positive at pH 5; therefore, only sugars are added. The selected formulation is at pH 5, containing sugars but not salts. This formulation is also the same as that providing the lowest aggregation propensities for storage at 40°C and under freeze-thaw stress.

MAb-A and MAb-B represent typical types of MAbs, and specifically, MAb-A and MAb-B have unevenly and evenly distributed electrostatic potential surfaces, respectively. MAb-A showed higher colloidal stability in the presence of salts, whereas the trend for MAb-B was the opposite.

Our strategy for optimization is applicable to both types of MAbs and can be generalized. This strategy can be applied to highly concentrated MAb solution because the B_2 obtained at a low concentration of less than 10 mg/mL correlated well with aggregation propensity and viscosity at a high concentration of more than 100 mg/mL as shown in Chapter 2.

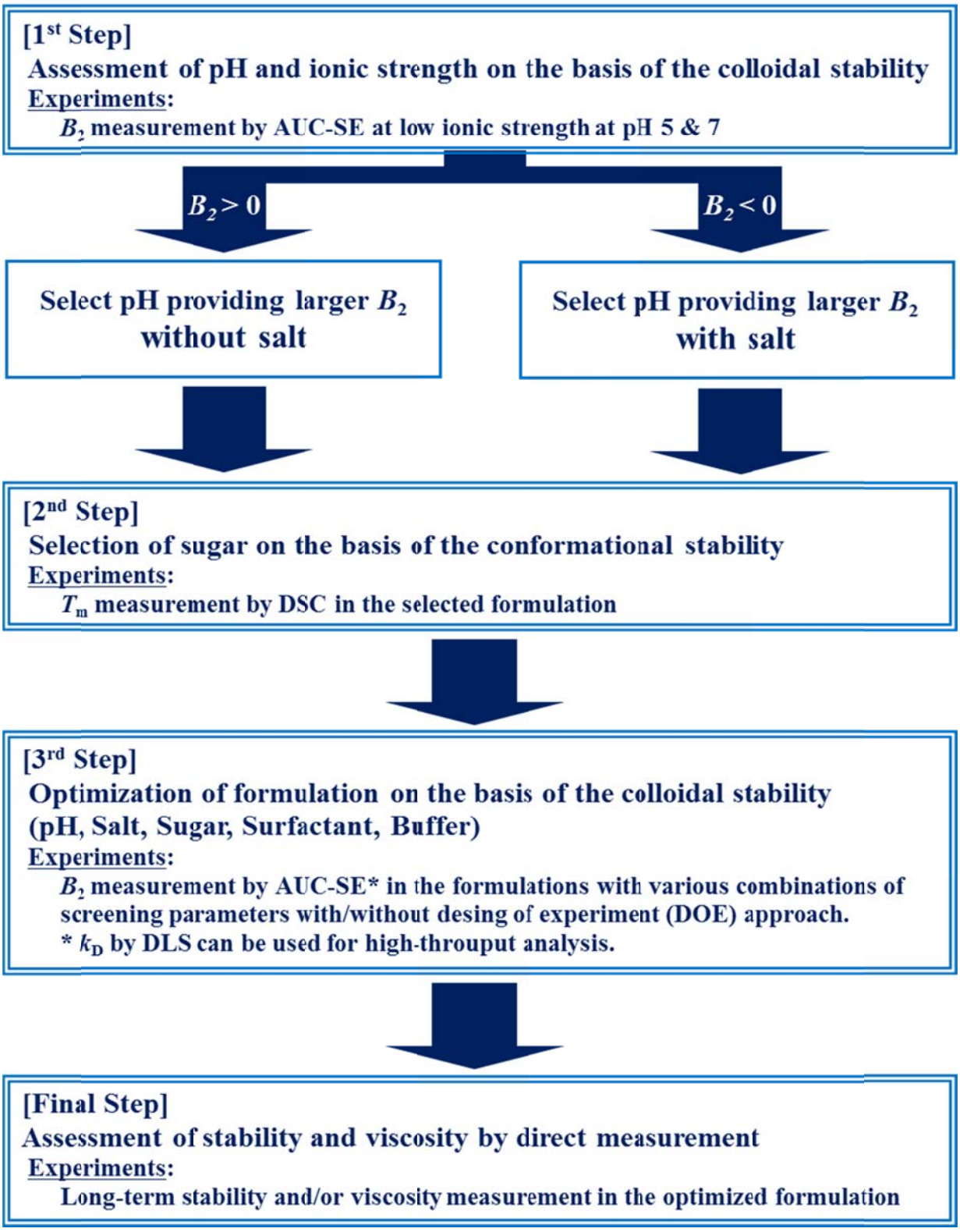

Figure 4.2. Proposed strategy for formulation optimization

4.2.3 Comparison of the proposed strategy to conventional strategy in combination with design of experiment (DOE)

As mentioned previously, various parameters including type and concentration of salt, sugar, surfactant, other excipients, and pH have to be evaluated to optimize the formulation of therapeutic MAbs (Chi et al., 2003a, Bhambhani et al., 2012). The conventional strategy for formulation optimization has been based on the direct assessments of long-term stability and viscosity, which generally requires a large amount of samples and longer assay time. Therefore, an experiment using the conventional strategy has been planned for efficient collection of data and a quick approach to optimum formulation according to the design of the experiment (DOE) which is a commonly used statistical approach to reduce the points for required measurements. Nevertheless, the optimization of formulation by the conventional strategy still requires a large amount of samples and long assessment time, and remains as a bottleneck in the development of therapeutic MAbs.

In this section, we compared our proposed strategy based on the indicators for colloidal and conformational stabilities to the conventional strategy with a DOE approach. Table 4.1 shows the estimated amount of samples and time required for each strategy. The standard screening parameters for formulation optimization are shown in Table 4.2. Herein, the types of sugar, pH and concentrations of NaCl and sugar are selected as parameters. Practically, more parameters such as the concentration of MAb and buffer species, type and concentration of surfactant are required (Chi et al., 2003a, Bhambhani et al., 2012). Ideally, all conditions should be evaluated, however the number of conditions, 147, is too extensive to be evaluated. Therefore, the experimental design for formulation optimization was simulated based on the DOE approach with statistical data processing software JMP 8.0.1 (SAS Institute Japan, Tokyo, Japan). Twenty-one conditions are recommended for evaluating the parameters in Table 4.2 with the restriction that osmolarity be more than 280 mOsm/kg as shown in Table 4.3. The amount of samples required for the conventional strategy

with the DOE approach is approximately 1.5 g in the case of 100 mg/mL MAb solution. Herein, the required assessment time is 1.5 months. On the other hand, steps 1 to 3 of our proposed strategy requires 30 mg of MAb and 1 week as shown in Table 4.4. Obviously, our proposed strategy dramatically reduces the sample requirement and shortens the assessment time. In practice, the additional stability study is performed with a selected range of conditions as the final step both in the conventional and the proposed strategies to confirm the optimized formulation. It should be noted that the preparation of high concentrated MAbs is another problem in the conventional strategy as mentioned in Chapter 2. Therefore, the prediction of aggregation propensity and viscosity based on the indicators of colloidal and conformational stabilities from the MAb solutions at a low concentration is an effective strategy for the formulation development of highly concentrated MAb solution.

Table 4.1 Required amount and time for analysis

Analysis		Volume (μL)	Concentration (mg/mL)	Repetition	Amount (mg)	Time
Conventional strategy	Stability	100	20	3	6	1.5 Months
		100	100	3	30	1.5 Months
	Viscosity	150	100	3	45	20 samples/Day
Proposed strategy	AUC-SE	60	1, 5, 10	2	2	7 samples/Day
	DLS	15	2, 4, 6, 8, 10	3	2	100~ samples/Day
	DSC	500	1	1	0.5	10 samples/2 h

Required amounts were calculated by multiplication of volume, repetition and concentration.
Required time for stability testing is estimated at 1-month for storage at an accelerated condition of 40°C and 0.5-month for assay

Table 4.2 Standard screening parameters for formulation optimization

Sugar	Sugar conc. (mM)	NaCl conc. (mM)	pH
Sorbitol	0	0	4.5
Sucrose	150	150	5.0
Trehalose	300	300	5.5
-	-	-	6.0
-	-	-	6.5
-	-	-	7.0
-	-	-	7.5

Table 4.3 Experimental protocol based on DOE

Sugar	Sugar conc. (mM)	NaCl conc. (mM)	pH
Sorbitol	0	300	4.5
Sorbitol	150	300	5.0
Sorbitol	300	150	5.5
Sorbitol	0	150	6.0
Sorbitol	300	0	6.5
Sorbitol	150	75	7.0
Sorbitol	300	0	7.5
Sucrose	150	150	4.5
Sucrose	300	0	5.0
Sucrose	300	0	5.5
Sucrose	300	300	6.0
Sucrose	0	150	6.5
Sucrose	0	300	7.0
Sucrose	150	150	7.5
Trehalose	300	0	4.5
Trehalose	0	150	5.0
Trehalose	150	300	5.5
Trehalose	150	75	6.0
Trehalose	300	300	6.5
Trehalose	300	150	7.0
Trehalose	0	300	7.5

The experimental protocol was generated by statistical data processing software JMP 8.0.1.

Table 4.4 Sample amount and analysis time for formulation optimization

	Step	Indicator	Number of sample	Amount (mg)	Time
1	Optimization of pH and salts	B_2 (AUC-SE)	2	4	1 Day
2	Selection of sugars	T_m (DSC)	4	2	1 Day
3	Further optimization of excipients	B_2 (AUC-SE)	12 (27)	24 (54)	4 Days (8 Days)
		k_D (DLS)		24 (54)	1 Day (1 Day)
4	Direct stability assessment	Stability/Viscosity	--	--	1.5 Months

The number of samples for step 3 was generated according to DOE by JMP from three pHs, and concentrations of sugar and NaCl with the restriction in the osmotic ration to be more than 280 mOsm/kg. The maximum estimations without DOE are shown in parentheses.

4.2.4 Comparison with the *in-silico* approach using an IgG_1 structure model

Engineering of the amino acid sequence in CDR regions has been attempted to generate aggregation resistant MAbs based on the higher order structure model obtained from *in-silico* simulation (Escamilla et al., 2004, Wang et al., 2009, Wu et al., 2010b). There are several structural properties which are potentially prone to aggregation such as β-sheet rich structures and hydrophobic patches. The statistical *in-silico* approaches for the prediction of such aggregation prone structures have been proposed. Recently, some numerical parameters generated from *in-silico* simulation have been used for high-throughput prediction of aggregation propensity of proteins (Spassov et al., 2008, Lauer et al., 2012). Spatial aggregation propensity (SAP), is one of these parameters. SAP is a measure of the local hydrophobicity of surface patches which is considered to be responsible for hydrophobic interaction, and is defined as Eq. 4.2.

$$\mathrm{SAP} = \sum \left[\left(\frac{\text{SAA of side chain atoms within radius R}}{\text{SAA of side chain atoms of fully exposed residue}} \right) \times \text{residue hydrophobicity} \right] \qquad (4.2)$$

,where SAA is the solvent accessible area. SAA of the side chain of fully exposed residue is obtained by calculating the SAA of the side chain of an amino acid residue, X, of tripeptide "Alanine-X-Alanine" in fully extended conformation. Residue hydrophobicity is obtained from the hydrophobicity scale of Black and Mould (1991). The scale is normalized such that glycine has a hydrophobicity of zero, the most hydrophobic residue (i.e., Phenylalanine) has a value of 0.5, and the least hydrophobic residue (i.e., Arginine) has a value of –0.5. The SAP score is determined by the sum of all positive SAP values of the atoms in the Fab domain. SAP scores for MAb-A, MAb-B, MAb-C and MAb-D were calculated by using Discovery Studio ver. 3.5 (Accelrys Inc.).

Developability Index (DI) is the other parameter to predict the aggregation propensity. The higher DI value means the higher aggregation propensities. DI is calculated according to the following equation where the contribution of electrostatic interactions to aggregation in addition to

that of hydrophobic interaction (SAP) is incorporated.

$$\mathrm{DI} = \mathrm{SAP} - \beta \times e^2 \qquad (4.3)$$

,where weighting factor, β, determines the relative importance of SAP and net charge, and e is the total net charge. For the calculation of DI in the present study, the constant value of 0.05, which is experimentally estimated from MAbs in the previous study (Lauer et al., 2012), was used for β to compare with the aggregation propensities of MAb-A, MAb-B, MAb-C and MAb-D in different formulations. Total net charges at given pH and ionic strength were calculated from the pKa of individual residues of the protein molecule (Bashford and Karplus, 1991) by using Discovery Studio ver. 3.5 (Accelrys Inc.).

4.2.4.1 Evaluation of spatial aggregation propensity (SAP)

SAP distributions on the surfaces and SAP scores of MAb-A, MAb-B, MAb-C and MAb-D are shown in Fig. 4.3 and Table 4.5, respectively. Only single SAP scores are available from each MAb regardless the formulation according to Eq. 4.2. All MAbs showed almost comparable SAP distributions with an exception that MAb-B and MAb-D have higher SAP regions on the tips of Fab when compared to those of MAb-A and MAb-C (Fig. 4.3). SAP scores become larger in the rank order of MAb-A < MAb-B < MAb-C < MAb-D. The same rank order of the aggregation propensities was observed only in the formulation containing 300 mM NaCl at pH 5 (Table 4.5 and Fig. 4.4), while a good correlation was not observed in the other formulations. Thus, overall correlation between SAP scores and aggregation propensities is unsatisfactory and we could not find the general rule for prediction of aggregation propensities on the basis of SAP.

Theoretically SAP is estimated based only on the hydrophobicity of the protein surface,

whereas, electrostatic properties of a protein are not taken into consideration. However, as the present study showed, aggregation propensities of each MAb are highly dependent on the NaCl concentration and pH, indicating that electrostatic interactions play an important role on the aggregation propensities of MAbs. The better correlation observed in the formulation containing 300 mM NaCl at pH 5 might be attributed to the shielding effect of salt which cancels the contribution of electrostatic interaction to aggregation, although poor correlation was confirmed in other solution conditions. These results indicate that prediction of the aggregation propensity based on the sole hydrophobicity has the risk of a misleading or wrong prediction. The contribution of electrostatic interactions to aggregation has to be incorporated.

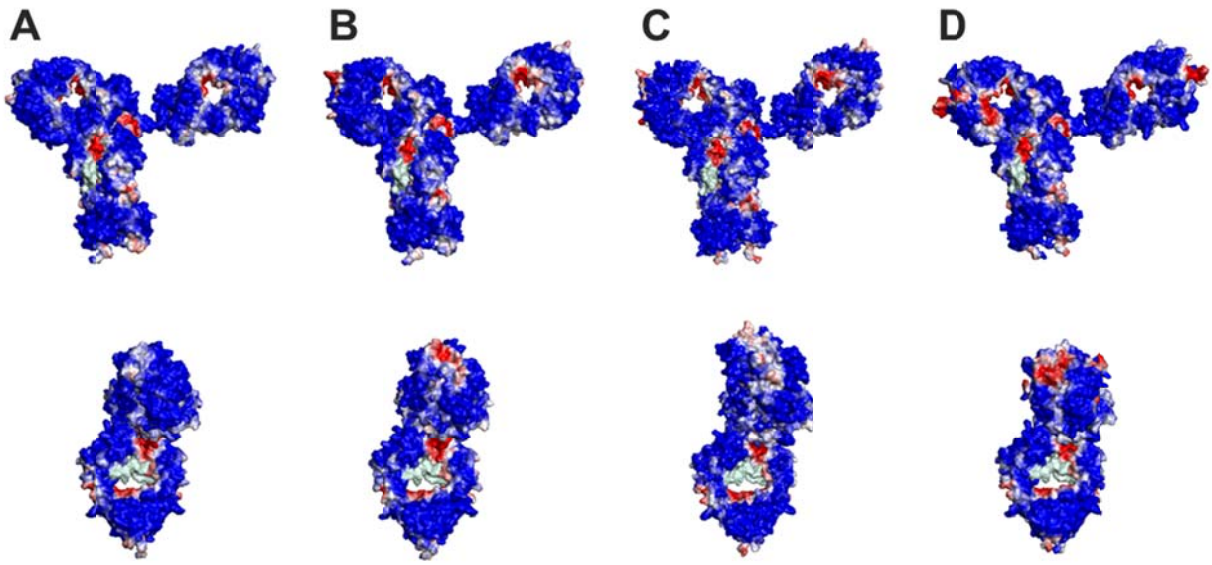

Figure. 4.3. Spatial aggregation propensities (SAP)

SAPs for MAb-A (**A**), MAb-B (**B**), MAb-C (**C**) and MAb-D (**D**) were obtained based on the full-length IgG_1 model structures by using Discovery Studio®. Higher SAP surfaces are represented in red and lower surfaces are presented in blue, respectively.

Table 4.5: Spatial aggregation propensity (SAP) score

	pH	Formulation	SAP score	Aggregation rate	
				40ºC (%/Month)	Freeze-thaw (%/10-cycles)
MAb-A	5	Initial buffer	298.4	1.06±0.06	0.04±0.01
		300mM NaCl		0.50±0.04	0.56±0.02
	7	Initial buffer		0.24±0.10	1.17±0.07
		300mM NaCl		0.02±0.04	0.68±0.02
MAb-B	5	Initial buffer	310.9	0.02±0.04	0.07±0.01
		300mM NaCl		0.45±0.02	1.68±0.18
	7	Initial buffer		0.94±0.02	0.02±0.02
		300mM NaCl		0.17±0.05	1.38±0.04
MAb-C	5	Initial buffer	314.6	0.18±0.01	0.15±0.01
		300mM NaCl		0.76±0.01	1.15±0.08
	7	Initial buffer		2.06±0.22	0.29±0.02
		300mM NaCl		1.06±0.02	0.92±0.04
MAb-D	5	Initial buffer	369.8	0.29±0.00	0.09±0.01
		300mM NaCl		0.92±0.01	1.01±0.09
	7	Initial buffer		0.93±0.01	0.12±0.01
		300mM NaCl		0.57±0.02	1.26±0.03

SAP scores were calculated by Discovery Studio®. Aggregation rates were obtained from the SEC analysis.

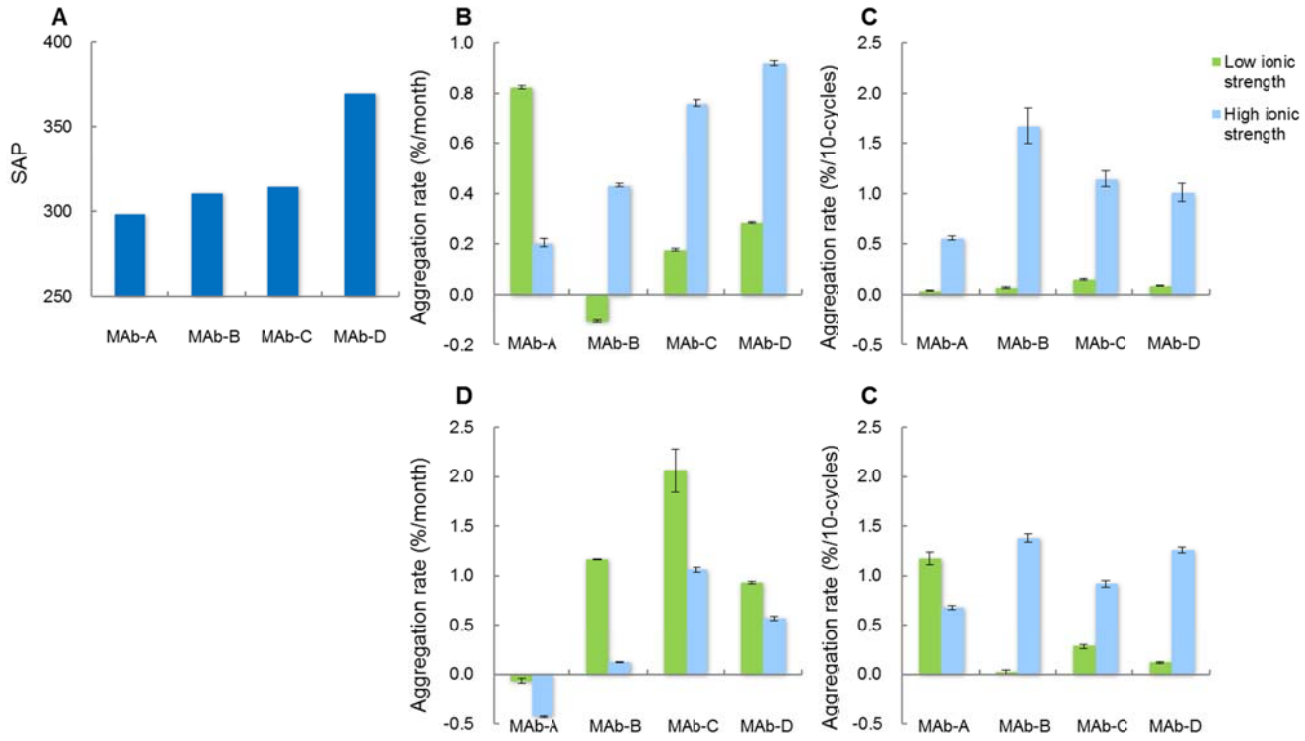

Figure 4.4. Relation of SAP score with aggregation propensity

SAP scores for four MAbs were obtained based on the full-length IgG_1 model structures by using Discovery Studio® (**A**). Aggregation rates were evaluated at 40°C (**B**: pH5, **D**: pH7) and under freeze-thaw stress (**C**: pH5, **E**: pH7) at low ionic strength (30 mM NaCl for MAb-A and 10 mM NaCl for MAb-B, MAb-C and MAb-D) and high ionic strength (300 mM NaCl for all MAbs) based on the SEC analysis.

4.2.4.2 Evaluation of developability index (DI)

As described previously, the higher DI value implies the higher aggregation propensities. DI values for MAb-A, MAb-B, MAb-C and MAb-D in the formulations containing different NaCl conditions are shown in Table 4.6. The trends of DI value and aggregation propensity among four MAbs are shown in Fig 4.5. The trends of DI value are qualitatively comparable regardless pH and ionic strength, where the rank order of DI is MAb-B < MAb-A < MAb-C < MAb-D. On the other

hand, the rank orders of actual aggregation propensities among four MAbs changed depending on the pH and ionic strength. They obviously have no clear correlation with that of DI. It should be noted that all MAbs provided larger DI values at low ionic strength than at high ionic strength, indicating that the aggregation is accelerated at lower ionic strength. Whereas opposite trends of aggregation rates were observed in MAb-B, MAb-C and MAb-D at pH 5 at 40°C, and MAb-A at pH5, and MAb-B, MAb-C and MAb-D at pH 7 under freeze-thaw stress. Furthermore, the significant correlation between DI and aggregation propensity are not found when DI values are plotted against the aggregation propensities for all MAbs in the four different NaCl concentrations at pH 5 and pH 7 (Fig. 4.6). Herein, the higher DI values do not indicate the higher aggregation propensities. Thus, we concluded that employment of DI for the prediction of aggregation propensities can be used only for MAbs under limited circumstances.

These poor correlations between DI and aggregation propensities can be explained in terms of the type of electrostatic interactions, i.e. repulsive or attractive. According to Eq. 4.3, electrostatic interactions attribute to only stabilization of protein. However, as we mentioned in Chapter 3, electrostatic interactions attribute not only to stabilization but also to destabilization. In the case where the electrostatic attraction is present, the larger net charge accelerates aggregation, whereas the larger net charge provides smaller DI values. Thus, DI according to Eq. 4.3 misleads aggregation propensities. Therefore, not only the total net charge but also the distribution of charges have to be incorporated for appropriate prediction of the aggregation propensity. However, to our knowledge, it remains difficult to generate numerical parameters reflecting the uneven or even distribution of surface potential by *in-silico* approaches. In addition, it should be noted that the effect of ionic strength on the calculated net charge used for DI estimation is different from that on the measured net charge. Normally, the net charge decreased as ionic strength increased as shown in Fig. 3.3 resulting in suppression of electrostatic interaction. Whereas the calculated net

charge increased as ionic strength increased (Table 4.6), indicating that the calculated net charge did not reflect the shielding effect of salts. Thus, two aspects from the electrostatic interactions need to be taken into account in order to estimate accurate DI. First, the types of electrostatic interaction need to be consideredon the basis of the charge distribution on the surface of protein. Second, the shielding effect to electrostatic interaction by increased ionic strength needs to be incorporated.

The other possible cause of poor correlation is the fact that SAP represents only the hydrophobicity of MAb in the folded state. As shown in Chapter 3, the conformational stability contributes to aggregation propensities at 40°C and under freeze-thaw stress, indicating that hydrophobicity in an unfolded state is more important to predict the aggregation propensity. In addition, the relative importance of SAP and net charge, which is represented as β in Eq. 4.3, is dependent on the formulation and type of MAb (Lauer et al., 2012), making the prediction of aggregation propensities more difficult.

To estimate the relative importance of SAP and net charge, the β were calculated from the actual stability data at 40°C according to the following equations.

$$\beta = -\frac{k_{\text{agg}} C - \text{SAP}}{e^2} \tag{4.4}$$

$$\frac{dC_M}{dt} = -k_{\text{agg}} \text{C}_M^2 \tag{4.5}$$

,where C is a weighting factor, C_{M} is the concentration of non-aggregated MAb, k_{agg} is the aggregation rate constant. A constant value of 50,000 is used for C, which was obtained by fitting the stability data of six different MAbs at 40°C into Eq. 4.4 (Laue TM, et al., 2012). The β values are variable (Table 4.6), indicating that relative contribution of electrostatic and hydrophobic interactions are dependent on the pH, ionic strength and MAbs. Thus, the DI may not be suitable for comparison of MAbs in the different formulations.

In conclusion, DI and SAP still need further improvements for prediction of aggregation propensities. In particular, the proper estimation of electrostatic interaction needs to be incorporated. On the contrary, our proposed strategy allows researchers to appropriately evaluate the impacts of electrostatic interactions and conformational changes. Therefore, our suggested procedure has more advantages than *in-silico* approaches for prediction of aggregation propensities.

Table 4.6: Developability Index

	pH	Formulation	SAP score	DI	Net charge	Aggregation rate		β (40ºC)
						40ºC (%/Month)	Freeze-thaw (%/10-cycles)	
MAb-A	5	Initial buffer	298.4	230	37	1.06±0.06	0.04±0.01	0.19
		70 mM NaCl		218	40	0.72±0.02	0.30±0.01	0.17
		140 mM NaCl		202	44	0.45±0.04	0.63±0.02	0.15
		300 mM NaCl		183	48	0.50±0.04	0.56±0.02	0.12
	7	Initial buffer		295	8	0.24±0.10	1.17±0.07	4.72
		70 mM NaCl		295	8	-0.01±0.09	1.14±0.03	4.98
		140 mM NaCl		295	8	0.13±0.06	0.83±0.01	5.01
		300 mM NaCl		294	9	0.02±0.04	0.68±0.02	3.96
MAb-B	5	Initial buffer	310.9	223	42	0.02±0.04	0.07±0.01	0.18
		70 mM NaCl		181	51	0.36±0.01	0.57±0.05	0.12
		140 mM NaCl		160	55	0.44±0.08	1.94±0.01	0.10
		300 mM NaCl		137	59	0.45±0.02	1.68±0.18	0.09
	7	Initial buffer		284	23	0.94±0.02	0.02±0.02	0.56
		70 mM NaCl		274	27	0.43±0.04	1.92±0.07	0.42
		140 mM NaCl		272	28	0.36±0.05	1.81±0.03	0.39
		300 mM NaCl		266	30	0.17±0.05	1.38±0.04	0.34
MAb-C	5	Initial buffer	314.6	239	39	0.18±0.01	0.15±0.01	0.21
		300 mM NaCl		152	57	0.76±0.01	1.15±0.08	0.09
	7	Initial buffer		297	19	2.06±0.22	0.29±0.02	0.81
		300 mM NaCl		286	24	1.06±0.02	0.92±0.04	0.53
MAb-D	5	Initial buffer	369.8	282	42	0.29±0.00	0.09±0.01	0.21
		300 mM NaCl		178	62	0.92±0.01	1.01±0.09	0.09
	7	Initial buffer		350	20	0.93±0.01	0.12±0.01	0.90
		300 mM NaCl		336	26	0.57±0.02	1.26±0.03	0.54

SAP scores and DI values were calculated by Discovery Studio®, in which β of 0.05 was used for conditions. Aggregation rates were obtained from the SEC analysis. β values were calculated from aggregation rates at 40°C, SAP and net charge according to Eqs. 4.4 and 4.5 where *C* of 50000 was used.

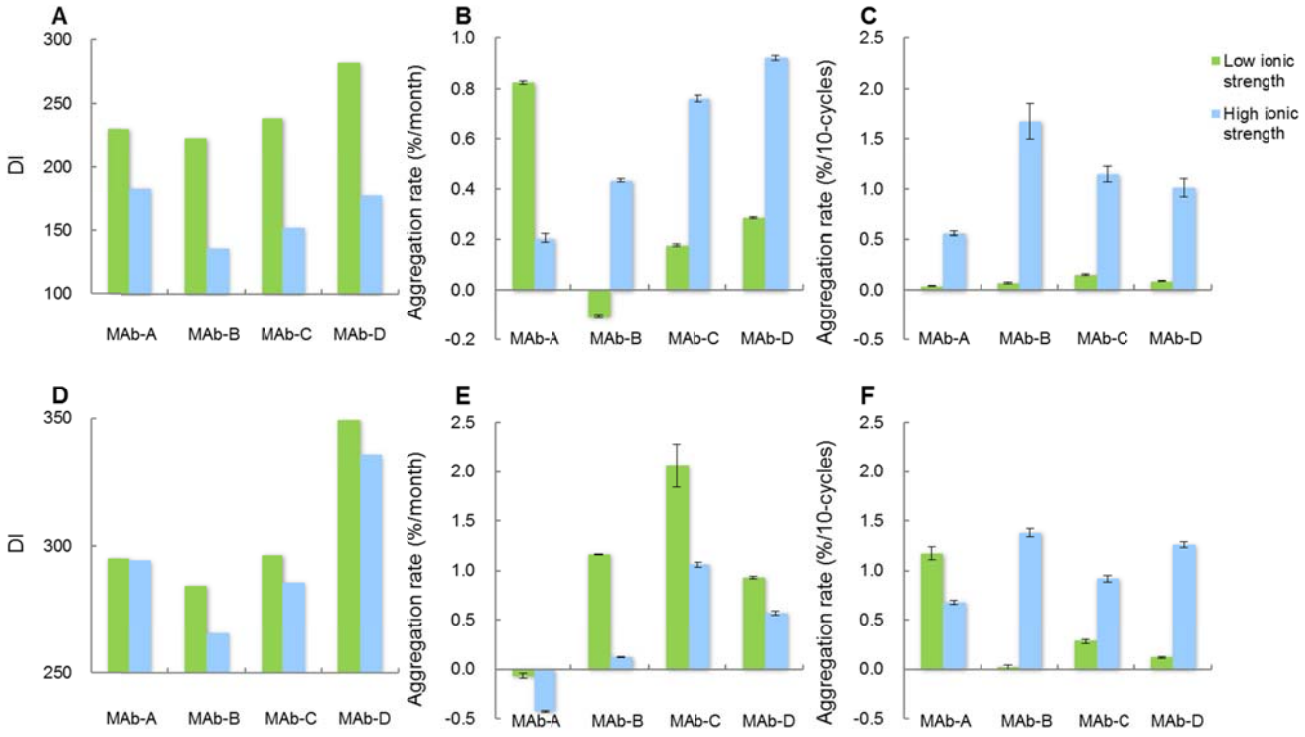

Figure 4.5. Relation of DI with aggregation propensity

DI values for four MAbs were obtained based on the full-length IgG_1 model structures by using Discovery Studio® at low (40 mM for MAb-A and 10 mM for MAb-B, MAb-C and MAb-D) and high ionic strength (310 mM for all MAbs). Aggregation rates were evaluated at 40°C (**B**: pH5, **E**: pH7) and under freeze-thaw stress (**C**: pH5, **F**: pH7) at low ionic strength (30 mM NaCl for MAb-A and 10 mM NaCl for MAb-B, MAb-C and MAb-D) and high ionic strength (300 mM NaCl for all MAbs) based on the SEC analysis.

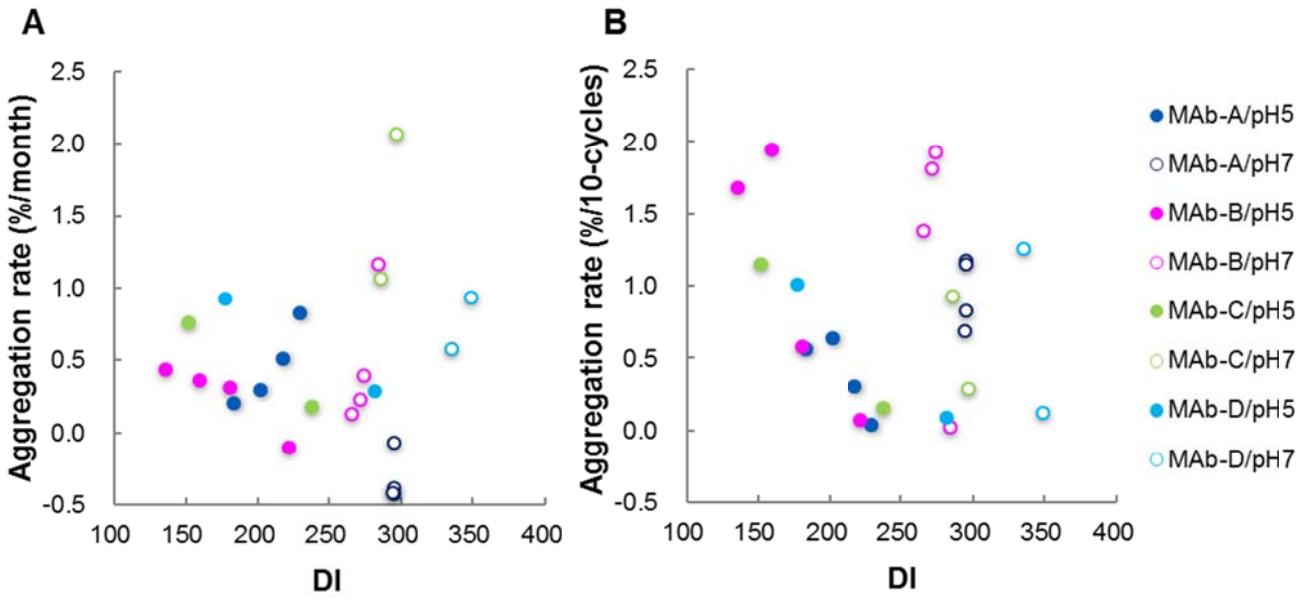

Figure 4.6. Relation of DI with aggregation propensity

DI values for four MAbs were obtained based on the full-length IgG_1 model structures by using Discovery Studio®. Aggregation rates were evaluated at 40°C (**A**) and under freeze-thaw stress (**B**) based on the SEC analysis.

4.3 Conclusions

We suggest a novel strategy for formulation optimization of MAbs based on the indicators for the colloidal and conformational stabilities. The estimated optimum formulations for MAb-A and MAb-B according to the proposed general strategy were in good agreement with aggregation propensity observed at the accelerated condition of 40°C and under freeze-thaw stress. In addition, our strategy has a great advantage in terms of the sample amount and assay time required for assessment compared to the conventional strategy based on the direct assessments of long-term stability and viscosity in combination with the DOE approach. We also evaluated the *in-silico* approach, however a consistent correlation between *in-silico* parameters, SAP and DI, and

aggregation propensity were not found. Thus, our proposed strategy for formulation optimization in terms of colloidal and conformational stabilities enables the reduction of resources and development time for therapeutic MAbs.

Chapter 5
General conclusions

We demonstrated the presence of multiple pathways for aggregation and that for viscosity enhancement of the MAbs in terms of colloidal and conformational stabilities, and suggested the models for aggregation and viscosity enhancement. We focused on the B_2 obtained from AUC-SE and found that B_2 is an effective indicator of the viscosity and aggregation propensity of the MAb solutions. Based on findings in the present studies, we proposed the novel strategy for formulation optimization that is generally applicable for the different MAbs. Our strategy dramatically saved the sample and evaluation time compared to those based on direct assessments of long-term stability and viscosity. Thus, our proposed strategy for formulation optimization in terms of colloidal and conformational stabilities enables the reduction of resources and development time for therapeutic MAbs.

References

Alford JR, Kendrick BS, Carpenter JF, Randolph TW. Measurement of the second osmotic virial coefficient for protein solutions exhibiting monomer-dimer equilibrium. Anal Biochem. 2008;377:128-133.

Alford JR, Kwok SC, Roberts JN, Wuttke DS, Kendrick BS, Carpenter JF, and Randolph TW. High concentration formulations of recombinant human Interleukin-1 receptor antagonist: I. Physical characterization. J Pharm Sci. 2008;97:3035-3050.

Antipova AS, Semenova MG, Belyakova LE. Effect of sucrose on the thermodynamic properties of ovalbumin and sodium caseinate in bulk solution and at air–water interface. Colloids Surf B Biointerface. 1999;12:261-270.

Asakura S, Oosawa F. On interaction between two bodies immersed in a solution of macromolecules. J Chem Phys. 1954;22:1255-1256.

Asakura S, Oosawa F. Interaction between particles suspended in solutions of macromolecules. J Polym Sci. 1958;33:183-192.

Attri AK, Minton AP. New methods for measuring macromolecular interactions in solution via static light scattering: basic methodology and application to nonassociating and self-associating proteins. Anal Biochem. 2005;337:103-110.

Barrett BS, Markham AP, Esfandiary R, Picking WL, Picking WD, Joshi SB, Middaugh CR. Formulation and immunogenicity studies of type III secretion system needle antigens as vaccine candidates. J Pharm Sci. 2010;99:4488-4496.

Bashfold D, Karplus M. Multiple-site titration curves of proteins: An analysis of exact and approximate methods for their calculations. J Phys Chem. 1991:95;9556-9561.

Bender NK, Heilig CE, Droll B, Wohlgemuth J, Armbruster F-P, Heilig B. Immunogenicity, efficacy and adverse events of adalimumab in RA patients. Rheumatol Int 2007:27;269-274.

Bhambhani A, Kissmann JM, Joshi SB, Vokin DB, Kashi RS, Middaugh. Formulation design and high-throughput excipient selection based on structural integrity and conformational stability of dilute and highly concentrated IgG_1 monoclonal antibody solutions. J Pharm Sci. 2012;101:1120-1135.

Biro CE, Garcia G, The antigenicity of aggregated and aggregate-free human gamma-globulin for rabbits. Immunology 1965;8: 411-419.

Black SD, Mould DR. Development of hydrophobicity parameters to analyze proteins which bear post or cotranslational modifications. Anal Biochem. 1991;193:72-82.

Burn VL, Friess W, Schultz-Fademrecht T, Muehlau S, Garidel P. Lysozyme-lysozyme self-interactions as assessed by the osmotic second virial coefficient: Impact for physical protein stabilization. Biotechnol J. 2009;4:1305-1319.

Burn VL, Friess W, Bassarab S, Garidel P. Correlation of protein-protein interactions as assessed by affinity chromatography with colloidal protein stability: A case study with lysozyme. Pharm Develop Technol. 2010;15:421-430.

Brun VL, Friess W, Bassarab S, Mühlau S, Garidel P. A critical evaluation of self-interaction chromatography as a predictive tool for the assessment of protein-protein interactions in protein formulation development: A case study of a therapeutic monoclonal antibody. Eur J Pharm Biopharm. 2010;75:16-25.

Carpenter JF, Randolph TW, Jiskoot W, Crommelin DJA, Middaugh CR, Winter G, Fan YX, Kirshner S, Verthelyi D, Kozlowski S, Clouse KA, Swann PG, Rosenberg A, Cherney B. Overlooking subvisible particles in therapeutic protein products: Gap that may compromise product quality. J Pharm Sci. 2009;98:1201-1205.

Chang BS, Kendrick BS, Carpenter JF. Surface-induced denaturation of proteins during freezing and its inhibition by surfactants. J Pharm Sci. 1996;85:1325–30.

Chari R, Jerath K, Badkar AV, Kalonia DS. Long- and short-range electrostatic interactions affect the rheology of highly concentrated antibody solutions. Pharm Res. 2009;26:2607-2618.

Chase SF, Laue TM. The determination of protein valence by capillary electrophoresis. P/ACE Setter 2008;12:1-5.

Chi EY, Krishnan S, Randolph TW, Carpenter JF. Physical stability of proteins in aqueous solution: Mechanism and driving forces in nonnative protein aggregation. Pharm Res. 2003;20:1325-1336.

Chi EY, Krishnan S, Kendrick BS, Chang BS, Carpenter JF, Randolph TW. Roles of conformational stability and colloidal stability in the aggregation of recombinant human granulocyte colony-stimulating factor. Protein Sci. 2003;12:903-913.

Chou DK, Krishnamurthy R, Manning MC, Randolph TW, Carpenter JF. Physical stability of albinterferon-α_{2b} in aqueous solution: Effects of conformational stability and colloidal stability on aggregation. J Pharm Sci. 2012:101;2702-2719.

Claman HN. Tolerance to a protein antigen in adult mice and the effect of nonspecific factors. J Immunol. 1963;91: 833-839.

Collins KD. Charge density-dependent strength of hydration and biological structure. Biphys J. 1997:72;65-76.

Collins KD. Ions from the Hofmeister series and osmolytes: effects on proteins in solution and in the crystallization process. Methods. 2004:34:300-311.

Curtis RA, Prausnitz JM, Blanch HW. Protein-protein and protein-salt interactions in aqueous protein solutions containing concentrated electrolytes. Biotech Bioeng. 1998;57:11-21.

Deszczynski M, Harding SE, Winzor DJ. Negative second virial coefficients as predictors of protein crystal growth: Evidence from sedimentation equilibrium studies that refutes the designation of those light scattering parameters as osmotic virial coefficients. Biophys Chem. 2006;120:106-113.

Durant JA, Chen C, Laue TM, Moody TP, Allison SA. Use of T4 lysozyme charge mutants to examine electrophoretic models. Biophys Chem. 2002;101-102:593-609.

Elcock AH, McCammon JA. Calculation of weak protein-protein interactions: The pH dependence of the second virial coefficient. Biophys J. 2001;80:613-625.

Engelsman J, Garidel P, Smulders R, Koll H, Smith B, Bassarab S, Seidl A, Hainzl O, Jiskoot W. Strategies for the assessment of protein aggregates in pharmaceutical biotech product development. Pharm Res. 2011;28:920-933.

European Medicines Agency (EMA). Guideline on immunogenicity assessment of biotechnology-derived therapeutic proteins. 2007.

Fernandez-Escamilla AM, Rousseau F, Schymkowitz J, Serrano L. Prediction of sequence-dependent and mutational effects on the aggregation of peptides and proteins. Nat Biotechnol. 2004;10:1302-6.

Fesinmeyer, RM, Hogan S, Saluja A, Brych SR, Kras E, Narhi LO, Brems DN, Gokarn YR. Effect of Ions on Agitation- and Temperature-Induced Aggregation Reactions of Antibodies. Pharm Res. 2009;26:903-913.

Filipe V, Jiskoot W, Basmeleh AH, Halim A, Schellekens H, Filipe V. Immunogenicity of different stressed IgG monoclonal antibody formulations in immune tolerant transgenic mice. MAbs. 2012;4:740-752.

Food and Drug Administration (FDA), Immunogenicity assessment for therapeutic protein products. Guidance for Industry (draft guidance). 2013.

Fradkin AH, Carpenter JF, Randolph TW. Immunogenicity of aggregates of recombinant human growth hormone in mouse models. J Pharm Sci. 2009; 98:3247-3264.

Fradkin AH, Carpenter JF, Randolph TW. Glass particles as an adjuvant: a model for adverse immunogenicity of therapeutic proteins. J Pharm Sci. 2011; 100:4953-4964.

Frost RA, Caroline D. Diffusion of polystyrene in a theta mixed solvent (Benzene-2-Propanol) by Photon-correlation spectroscopy. Macromolecules 1976; 10:616–618.

Fujita H. Mathematical theory of sedimentation analysis. New York. Academic press. 1962:246-247.

Gamble CN. The role of soluble aggregates in the primary immune response of mice to human gamma globulin. Int Arch Allergy Appl Immunol. 1966;30:446-455.

Garber E, Demarest SJ. A broad range of Fab stabilities within a host of therapeutic IgGs. Biochem Biophys Res Commun. 2007;355:751-757.

Goldberg DS, Bishop SM, Shah AU, Sathish HA. Formulation development of therapeutic monoclonal antibodies using high-throughput fluorescence and static light scattering techniques: Role of conformational stability and colloidal stability. J Pharm Sci. 2011;100:1306–15.

Gokarn YR, Fesinmeyer RM, Saluja A, Cao S, Dankberg J, Goetze A, Rammele Jr RL, Narhi LO, Brems DN. Ion-specific modulation of protein interactions: Anion-induced, reversible oligomerization of a fusion protein. Protein Sci. 2009;18:169-179.

Griko YV, Privalov PL, Sturtevant JM, Venyaminov SY. Cold denaturation of staphylococcal nuclease. Proc Natl Acad Sci USA.1988;85:3343–3347.

Guo Z, Chen A, Nassar RA, Helk B, Mueller C, Tang Y, Gupta K, Klibanov AM. Structure-activity relationship for hydrophobic salts as viscosity-lowering excipients for concentrated solutions of monoclonal antibodies. Pharm Res. 2012;29:3102-3109

Harding SE, Rowe AJ, Horton JC. Analytical Ultracentrifugation in Biochemistry and Polymer Science. London: Royal Society of Chemistry; 1992:90-125.

Harn N, Allan C, Oliver C, Middaugh CR. Highly concentrated monoclonal antibody solutions: Direct analysis of physical structure and thermal stability. J Pharm Sci. 2007;96:532-546.

Hawe A, Kasper JC, Friess W, Jiskoot W. Structural properties of monoclonal antibody aggregates induced by freeze-thawing and thermal stress. Eur J Pharm Sci. 2009;38:79-87.

Hermeling S, Crommelin DJ, Schellekens H, Jiskoot W. Structure-immunogenicity relationships of therapeutic proteins. Pharm Res. 2004;21:897-903.

Hermeling S, Aranha L, Damen JM, Slijper M, Schellekens H, Crommelin DJ, Jiskoot W. Structural characterization and immunogenicity in wild-type and immune tolerant mice of degraded recombinant human interferon alpha2b. Pharm Res. 2005;22:1997-2006.

Hermeling S, Schellekens H, Maas C, Gebbink MF, Crommelin DJ, Jiskoot W. Antibody response to aggregated human interferon alpha2b in wild-type and transgenic immune tolerant mice depends on type and level of aggregation. J Pharm Sci. 2006;95:1084-1096.

Holde KE, Johnson C, Ho PS. Principles of physical biochemistry. Upper Saddle River: Pearson Education; 2006.

Hopp TP. Immunogenicity of a synthetic HBsAg peptide: enhancement by conjugation to a fatty acid carrier. Mol Immunol.1984;21:13-16.

Izutsu K, Yoshioka S, Terao T. Effect of mannitol crystallinity on the stabilization of enzymes during freeze-drying. Chem Pharm Bull. 1994;42:5–8.

Jachimska B, Wasilewska M, Adamczyk Z. Characterization of globular protein solutions by dynamic light scattering, electrophoretic mobility, and viscosity measurements. Langmuir 2008;24:6866-6872.

Jacobs SA, Teplyakov A, Gilliland GL, Feng Y. Structure-based engineering of a monoclonal antibody for improved solubility. Protein Eng Des Sel. 2010;23:643-651.

Jiménez M, Rivas G, Minton AP. Quantitative characterization of weak self-association in concentrated solutions of immunoglobulin G via the measurement of sedimentation equilibrium and osmotic pressure. Biochemistry 2007;46:8373-8378.

Joubert MK, Hokom M, Eakin C, Zhow L, Deshpande M, Baker MP, Goletz TJ, Kwewin BA, Chirmule N, Narhi LO, Jawa V. Highly aggregated antibody therapeutics can enhance the in vitro innate and late-stage T-cell immune responses. J Biol Chem. 2012;287:25266-25279.

Kamerzell TJ, Kanai S, Liu J, Shire SJ, Wang YJ. Increasing IgG concentration modulates the conformational heterogeneity and bonding network that influence solution properties. J Phys Chem. 2009;113:6109-6118.

Kanai S, Liu J, Patapoff TW, Shire SJ. Reversible self-association of a concentrated monoclonal antibody solution mediated by Fab-Fab interaction that impacts solution viscosity. J Pharm Sci. 2008;97:4219-4227.

Kaushik JK, Bhat R. Why is trehalose an exceptional protein stabilizer? J Biol. Chem. 2003;278:26458-26465.

Kittiworakarn J, Lecoq A, Moine G, Thai R, Lajeunesse E, Drevet P, Vidaud C, Ménez A, Léonetti M. HIV-1 Tat raises an adjuvant-free humoral immune response controlled by its core region and its ability to form cysteine mediated oligomers. J Bio Chem. 2006;281: 3105-3115.

Kueltzo LA, Wang W, Randolph TW, Carpenter JF. Effects of solution conditions, processing

parameters, and container materials on aggregation of a monoclonal antibody during freeze-thawing. J Pharm Sci. 2008;97:1801-1812.

Kumar V, Dixit N, Zhou L, Fraunhofer W. Impact of short range hydrophobic interactions and long range electrostatic forces on the aggregation kinetics of a monoclonal antibody and a dual-variable domain immunoglobulin at low and high concentrations. Int J Pharm. 2011;421:82-93.

Laue TM, Shah BD, Ridgeway TM, Pelletier SL. Analytical Ultracentrifugation in Biochemistry and Polymer Science. London: Royal Society of Chemistry; 1992:90-125.

Laue TM, Agrawal NJ, Chennamsetty N, Egodage K, Helk B, Trout BL. Developability index: A rapid in silico tool for the screening of antibody aggregation propensity. J Pharm Sci. 2012;101:102-115.

Lehermayr C, Mahler HC, Mäder K, Fischer S. Assessment of net charge and protein-protein interactions of different monoclonal antibodies. J. Pharm. Sci. 2011;100:2551-2562.

Liu J, Nguyen MDH, Andya JD, Shire SJ. Reversible self-association increases the viscosity of a concentrated monoclonal antibody in aqueous solution. J Pharm Sci. 2005;94:1928-1940.

Liu Y, Bolen DW. The peptide backbone plays a dominant role in protein stabilization by naturally occurring osmolytes. Biochemistry. 1995;34:12884-12891.

Mahler HC, Friess W, Grauschopf U, Kiese S. Protein aggregation: Pathways, induction factors and analysis. J Pharm Sci. 2009;98:2909-2934.

Man N, Cartwright AJ, Andrews KM, Morris GE. Treatment of human muscle creatine kinase with glutaraldehyde preferentially increases the immunogenicity of the native conformation and permits production of high-affinity monoclonal antibodies which recognize two distinct surface epitopes. J Immunol. Methods 1989;125:251-259.

Matzinger, P. The danger model. A renewed sense of self. Science 2002;296:301-305.

Matzinger, P. Friendly and dangerous signals: is the tissue in control? Nat. Immunol. 2007;8:11-13.

McGown EL, Hafeman DG. Multichannel pipettor performance verified by measuring pathlength of reagent dispensed into a microplate. Anal Biochem. 1998;258:155-157.

McMillan Jr. WG, Mayer JE. The statistical thermodynamics of multicomponent systems. J. Chem. Phys. 1945;13: 276-305.

Minton AP. The influence of macromolecular crowding and macromolecular confinement on biochemical reactions in physiological media. J Biol Chem. 2001;276:10577-10580.

Minton AP. Influence of macromolecular crowding upon the stability and state of association of proteins: Predictions and observations. J Pharm Sci. 2005;94:1668-1675.

Moody TP, Kingsbury JS, Durant JA, Wilson TJ, Chase SF, Laue TM. Valence and anion binding of bovine ribonuclease A between pH 6 and 8. Anal Biochem. 2005;336:243-252.

Moore WV, Leppert P. Role of aggregated human growth hormone (hGH) in development of antibodies to hGH. J Clin Endocrinol Metab. 1980;51:691-697.

Murase N, Franks F. Salt precipitation during the freeze-concentration of phosphate buffer solutions. Biophys Chem. 1989;34:293-300.

Narayanan J, Liu XY. Protein interactions in undersaturated and supersaturated solutions: A study using light and X-ray scattering. Biophys J. 2003;84:523-532.

Neal BL, Asthagiri D, Lenhoff AM. Molecular origins of osmotic second virial coefficients of proteins. Biophys J. 1998;75:2469-2477.

Nishi H, Miyajima M, Nakagami H, Noda M, Uchiyama S, Fukui K. Phase separation of an IgG_1 antibody solution under a low ionic strength condition. Pharm Res. 2010;27:1348-1360.

Nishi H, Miyajima M, Wakiyama N, Kubota K, Hasegawa J, Uchiyama S, Fukui K. Fc domain mediated self-association of an IgG_1 monoclonal antibody under a low ionic strength condition. J. Biosci Bioeng. 2011;112:326-332.

Peces R, de la Torre M, Alcázar R, Urra JM. Antibodies against recombinant human erythropoietin in a patient with erythropoietin-resistant anemia. N Engl J Med. 1996;335:523-524.

Prummer O. Treatment-induced antibodies to interleukin-2. Biotherapy 1997;10:15-24.

Reichert JM, Rosensweig CJ, Faden LB, Dewitz MC. Monoclonal antibody successes in the clinic. Nat Biotechnol. 2005;23:1073-1078.

Reichlin M, Nisonoff A, Margoliash E. Immunological activity of cytochrome c. 3. Enhancement of antibody detection and immune response initiation by cytochrome c polymers. J Biol Chem. 1970;245:947-954.

Rifkin RA, Maggio ET, Dike S, Kerr DA, Levy M. n-Dodecyl-beta-D-maltoside inhibits aggregation of human interferon-beta-1b and reduces its immunogenicity. J Neuroimmune Pharmacol. 2011; 6:158-162.

Rosenberg AS. Effects of protein aggregates: an immunologic perspective. AAPS J. 2006;8:E501-507.

Rudra JS, Tripathi PK, Hildeman DA, Jung JP, Collier JH. Immune responses to coiled coil supramolecular biomaterials. Biomaterials 2010;31:8475-8483.

Saito S, Hasegawa J, Kobayashi N, Kishi N, Uchiyama S and Fukui K. Behavior of Monoclonal Antibodies: Relation Between the Second Virial Coefficient (B_2) at Low Concentrations and Aggregation Propensity and Viscosity at High Concentrations. Pharm Res. 2012;29:397-410.

Sahin E, Grillo AO, Perkins MD, Roberts CJ. Comparative effects of pH and ionic strength on protein-protein interactions, unfolding, and aggregation for IgG_1 antibodies. J Pharm Sci. 2010;99:4830-4848.

Salinas BA, Sathish HA, Bishop SM, Harn N, Carpenter JF, Randolph TW. Understanding and modulating opalescence and viscosity in a monoclonal antibody formulation. J Pham Sci. 2010;99:82-93.

Saluja A, Badkar AV, Zeng DL, Kalonia DS. Ultrasonic rheology of a monoclonal antibody (IgG_2) solution: Implications for physical stability of proteins in high concentration formulations. J Pharm Sci. 2007;96:3181-3195.

Saluja A, Badkar AV, Zeng DL, Nema S, Kalonia DS. Ultrasonic storage modules as a novel parameter for analyzing protein-protein interactions in high protein concentration solutions: Correlation with static and dynamic light scattering measurements. Biophys J. 2007;92:234-244.

Saluja A, Kalonia DS. Nature and consequences of protein-protein interactions in high protein concentration solutions. Int J Pharm. 2008;358:1-15.

Saluja A, Fesinmeyer M, Hogan S, Brems DN, Gokarn YR. Diffusion and sedimentation interaction parameters for measuring the second virial coefficient and their utility as predictors of protein aggregation. Biophys J. 2010;99:2657-2665.

Sauerborn M, Brinks V, Jiskoot W, Schellekens H. Immunological mechanism underlying the immune response to recombinant human protein therapeutics. Trends Pharmacol Sci. 2010;31:53-59.

Seidl A, Hainzl O, Richter M, Fischer R, Böhm S, Deutel B, Hartinger M, Windisch J, Casadevall N, London GM, Macdougall I. Tungsten-induced denaturation and aggregation of epoetin alfa during primary packaging as a cause of immunogenicity. Pharm Res. 2011;29:1454-1467.

Shire SJ, Shahrokh Z, Liu J. Challenges in the development of high protein concentration formulations. J Pharm Sci. 2004;93:1390-1402.

Singh SK, Afonina N, Awwad M, Bechtold-Peters K, Blue JT, Chou D, Cromwell M, Krause HJ, Mahler HC, Meyer BK, Narhi L, Nesta DP, Spitznagel T. An industry perspective on the monitoring of subvisible particles as a quality attribute for protein therapeutics. J Pharm Sci.

2010;99:3302-3321.

Singh SK. Impact of product-related factors on immunogenicity. J Pharm Sci. 2011;100:354-387.

Spassov VZ, Yan L. A fast and accurate computational approach to protein ionization. Protein Sci. 2008;17:1955-1970.

Sule SV, Cheung JK, Antochshuk V, Bhalla AS, Narasimhan C, Blaisdell S, Shameem M, Tessier PM. Solution pH that minimizes self-association of three monoclonal antibodies is strongly dependent on ionic strength. Mol. Pharmaceutics 2012;9:744-751.

Tessier PM, Lenhoff AM, Sandler SI. Rapid measurement of protein osmotic second virial coefficients by self-interaction chromatography. Biophys J. 2002;82:1620-1631.

Thakkar SV, Joshi SB, Jones ME, Sathish HA, Bishop SM, Volkin DB, Middaugh CR. Excipients differently influence the conformational stability and pretransition dynamics of two IgG_1 monoclonal antibodies. J Pharm Sci. 2012;101:3062-3077.

Timasheff SN. Control of Protein Stability and Reactions by Weakly Interacting Cosolvents: The Simplicity of the Complicated. Adv. Protein Chem. 1998;51:355-432.

Timasheff SN. Protein hydration, thermodynamic binding, and preferential hydration. Biochemistry. 2002;41:13473-13482.

Treuheit MJ, Kosky AA, Brems DN. Inverse relationship of protein concentration and aggregation. Pharm Res. 2002;19:511-516.

Uchiyama S, Hasegawa J, Tanimoto Y, Moriguchi H, Mizutani M, Igarashi Y, Sambongi Y, Kobayashi Y. Thermodynamic characterization of variants of mesophilic cytochrome c and its thermophilic counterpart. Protein Eng Des Sel. 2002;15:455-461.

Valente JJ. Payne RW, Manning MC, Wilson WW, Henry CS. Colloidal behavior of proteins: effects of the second virial coefficient on solubility, crystallization and aggregation of proteins in aqueous solution. Curr Pharm Biotechnol. 2005;6:427-436.

Van Beers MM, Jiskoot W, Schellekens H. On the role of aggregates in the immunogenicity of recombinant human interferon beta in patients with multiple sclerosis. J Interferon Cytokine Res. 2010; 30:767-775.

Van Beers MM, Sauerborn M, Gilli F, Brinks V, Schellekens H, Jiskoot W. Oxidized and aggregated recombinant human interferon beta is immunogenic in human interferon beta transgenic mice. Pharm. Res. 2011;28: 2393-2402.

Vermeer AWP, Norde W. The Thermal Stability of Immunoglobulin: Unfolding and Aggregation of

a Multi-Domain Protein. Biophys J. 2000;78:394-404.

Verwey EJW, Overbeck JTK. Theory of stability of lyophobic colloids. 1948. Elsevier, Amsterdam.

Vos Q, Lees A, Wu ZQ, Snapper CM, Mond JJ. B-cell activation by T-cell-independent type 2 antigens as an integral part of the humoral immune response to pathogenic microorganisms. Immunol Rev. 2000;176:154-170.

Wang W, Singh SK, Li N, Toler MR, King KR, Nema S. Immunogenicity of protein aggregates-Concerns and realities. Int J Pharm. 2012;431:1-11.

Wang X, Das TK, Singh SK, Kumar S. Potential aggregation prone regions in biotherapeutics: A survey of commercial monoclonal antibodies. MAbs. 2009;3:254-267.

Weldon WC, Wang BZ, Martin MP, Koutsonanos DG, Skountzou I, Compans RW. Enhanced immunogenicity of stabilized trimeric soluble influenza hemagglutinin. PLoS One 2010;5:e12466.

Welfle K, Misselwitz R, Hausdorf G, Höhne W, Welfle H. Conformation, pH-induced conformational changes, and thermal unfolding of anti-p24 (HIV-1) monoclonal antibody CB4-1 and its Fab and Fc fragments. Biochem Biophys Acta. 1999;1431:120-131

Winzor DJ, Deszczynski M, Harding SE, Wills PR. Nonequivalence of second virial coefficients from sedimentation equilibrium and static light scattering studies of protein solutions. Biophys Chem. 2007;128:46-55.

Wright JK, Tschopp J, Jaton JC, Engel J. Dimeric, trimeric and tetrameric complexes of immunogloblin G fix complement. Biochem J. 1980;187:775-780.

Wu SJ, Luo J, O'Neil KT, Kang J, Lacy ER, Canziani G, Baker A, Huang M, Tang QM, Raju TS, Nezlin R. Interactions between immunoglobulin G molecules. Immunol Lett. 2010;132:1-5.

Wu SJ, Luo J, O'Neil KT, Kang J, Lacy ER, Canziani G, Baker A, Huang M, Tang QM, Raju TS, Jacobs SA, Teplyakov A, Gilliland GL, Feng Y. Structure-based engineering of a monoclonal antibody for improved solubility. Protein Eng Des Sel. 2010;23:643-651.

Yadav S, Liu J, Shire SJ, Kalonia DS. Specific interactions in high concentration antibody solutions resulting in high viscosity. J Pharm Sci. 2010;99:1152-1168.

Yadav S, Shire SJ, Kalonia DS. Factors affecting the viscosity in high concentration solutions of different monoclonal antibodies. J Pharm Sci. 2010;99:4812-4829.

Yadav S, Sreedhara A, Kanai S, Liu J, Lien Samantha, Lowman H, Kalonia DS, Shire SJ. Establishing a link between amino acid sequence and self-associating and viscoelastic behavior of two closely related monoclonal antibodies. Pharm Res. 2011;28:1750-1764.

Yadav S, Laue TM, Kalonia DS, Singh SN and Shire SJ. The influence of charge distribution on self-association and viscosity behavior of monoclonal antibody solutions. Mol. Pharmaceutics 2012;9:791-802.

Yamakawa H. Concentration dependence of the frictional coefficient of polymers in solution. 1962, 36:2995-3001.

Yang X, Wyatt R, Sodroski J. Improved elicitation of neutralizing antibodies against primary human immunodeficiency viruses by soluble stabilized envelope glycoprotein trimers. J Virol. 2001;75: 1165-1171.

Zhang J, Liu XY. Effect of protein-protein interactions on protein aggregation kinetics. J Chem Phys. 2003;119:10972-10976.

Zhang A, Singh SK, Shirts MR, Kumar S, Fernandez EJ. Distinct aggregation mechanisms of monoclonal antibody under thermal and freeze-thaw stresses revealed by hydrogen exchange. Pharm Res. 2012;29:236-250.

Zhao HL, Xue C, Wang Y, Sun B, Yao XQ, Liu ZM. Elimination of the free sulfhydryl group in the human serum albumin (HSA) moiety of human interferon-alpha2b and HSA fusion protein increases its stability against mechanical and thermal stresses. Eur J Pharm Biopharm. 2009;72: 405-411.

List of publications

1. Saito S, Hasegawa J, Kobayashi N, Kishi N, Uchiyama S and Fukui K.
   Behavior of Monoclonal Antibodies: Relation Between the Second Virial Coefficient (B_2) at Low Concentrations and Aggregation Propensity and Viscosity at High Concentrations.
   Pharm Res. 2012;29:397-410

2. Saito S, Hasegawa J, Kobayashi N, Tomitsuka T, Uchiyama S and Fukui K.
   Effects of Ionic Strength and Sugars on the Aggregation Propensity of Monoclonal Antibodies: Influence of Colloidal and Conformational Stabilities.
   Pharm Res. 2013;30:1263-1280

Acknowledgements

First and foremost I would like to thank my graduate supervisor, Professor Kiichi Fukui and Assistant Professor Susumu Uchiyama. I appreciate all their contributions of time, encouragement and discussions during the course of my work. The author also thanks Professors, Shigenori Kanaya and Takuya Nihira for critical readings of the thesis and insightful suggestions for my research.

I also would like to express my gratitude to Dr. Toshiaki Tomitsuka, Dr. Naoyuki Kishi and Naoki Kobayashi who gave me the opportunity for this study, to Dr. Jun Hasegawa for helpful advice, and to all my colleagues in Group V of Biologics Technology Research Laboratories, Daiichi-Sankyo Co. Ltd. for supporting me during this study.

Lastly, I would like to thank all members of Fukui Laboratory, many of my colleagues and my family for all their support and encouragement.

It would not have been possible to complete this doctor thesis without help from those who have been very helpful to me. To only some of whom it was possible to give particular mention here.

Shuntaro Saito
Osaka University
Daiichi Sankyo Co., Ltd.
July 2013